

Effect of DNA damage on microtubule dynamics

A thesis

submitted in partial fulfilment of the requirements

Of the degree of
Doctor of Philosophy

By

Aishwarya Venkataravi

20152001



**INDIAN INSTITUTE OF SCIENCE EDUCATION AND
RESEARCH PUNE**

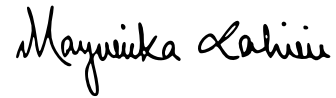
2022

CERTIFICATE

Certified that the work incorporated in the thesis entitled “Effect of DNA damage on microtubule dynamics” submitted by Aishwarya Venkataravi was carried out by the candidate, under my supervision. The work presented here or any part of it has not been included in any other thesis submitted previously for the award of any degree or diploma from any other University or Institution.

10 December 2022

Date



(Dr. Mayurika Lahiri)

Signature of the supervisor

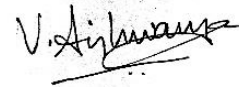
DECLARATION

I declare that this written submission represents my idea in my own words and where others' ideas have been included; I have adequately cited and referenced the original sources. I also declare that I have adhered to all principles of academic honesty and integrity and have not misrepresented or fabricated or falsified any idea/data/fact/source in my submission. I understand that violation of the above will be cause for disciplinary action by the institute and can also evoke penal action from the sources which have thus, not been properly cited or from whom proper permission has not been taken when needed.

The work reported in this thesis is the original work done by me under the guidance of Dr. Mayurika Lahiri.

10 December 2022

Date



(Aishwarya Venkataravi)

Signature of the student

DEDICATION

To my parents,
who always believed in my passion for science and encouraged
me to pursue my dreams

ACKNOWLEDGEMENTS

My PhD journey was a rollercoaster ride that taught me how to do research and be a better person. People who have accompanied me through this journey or been a part of it will always have a special place in my heart. Without them, my journey wouldn't have been complete.

Firstly, I would like to thank my PhD supervisor, Dr Mayurika Lahiri, for trusting me with a project which pushed us into uncharted territories. This endeavour would not have been possible without her constant support and guidance. Words cannot express my gratitude to Dr Aurnab Ghose for his invaluable guidance, which pushed the project in the right direction. I am also grateful for the valuable suggestions and feedback from Dr Thomas Pucadyil during RAC meetings. I would like to express my special thanks to Dr Richa Rikhy for enthusiastically helping me with microscopy and image analysis.

I am also grateful to the generosity of several scientists whose timely help with reagents made this project possible. I would like to thank Dr Carsten Janke (Institut Curie, Paris) for providing us with the Tubulin PTM antibodies; Dr Jomon Joseph for providing us with the acetylated tubulin antibody; Dr Frank Perez (Institut Curie, Paris) for providing us with the RUSH constructs and Dr Richa Rikhy and Dr Aurnab Ghose for the GalT and EB3 constructs.

I would like to thank CSIR, India, for providing me with the fellowship that helped me sustain my life in Pune. I would also like to thank IISER Pune for the infrastructure and facilities needed for my research.

I would be remiss in not mentioning the help provided by the technicians and non-academic staff, which helped with the smooth functioning of the department. I would like to thank Vijay Vittal and Dr Santosh Poddar of the IISER microscopy facility for their help with image acquisition and analysis. I would also like to thank the biology admin staff, Kalpesh and Piyush, for help with the procurement of lab reagents. I cannot count the times Vijay had to rush to the microscopy facility when the system was down or Kalpesh had to

run to the cell culture when the incubator CO₂ was low. I loved sharing my experience working in the covid testing centre with Kalpesh and Piyush.

During my PhD journey, the lab was like a second home, and the present and past ML lab members ensured a conducive environment for work. I would like to thank Libi and Ashiq for being my friends and mentors and for why I chose ML Lab. Dr Rupa Raman Mishra 'the postdoc' and Vaishali, for their unconditional love and support. Their constant encouragement and wise guidance got me through the most challenging years of my PhD. I have had the great opportunity to share my journey with excellent contemporaries- Abhijith, Rintu and Virender- who created a favourable lab environment which nurtured good science. I am grateful to have worked with outstanding undergraduate students with whom I had the most fun. The time I spent with – Kezia, Faseela, Shrinal and Rose will forever remain in my memories. I will forever cherish the unconditional love and adoration I received from Apurva and Tathagata. I would like to thank the current lab members – Anisha, Ben and Madhu for adding fresh insight to the science we do in the lab.

Last but not least, I would like to thank- Shivang, Raveena and Rochelle for making the final lap memorable. I will miss discussing science, gossiping and partying with them. I would also like to thank present and past AG and ABH lab members for treating me like their own.

A senior once said PhD is a mostly long lonely journey and be grateful if you make friends along the way, and I did. I could not have undertaken this journey without the support from two of my best friends, Yamini and Snehal. I thank them for being with me through my ups and downs. Thanks, is a small word to describe my gratitude for you two. And yet thanks, Yamini, for being 'my person' for 7 years! You have played various roles in my life – a friend, a wise counsellor, a brilliant researcher with whom I could discuss anything under the sun and a fellow plant mom. Thank you, Snehal, for being a wonderful friend and my support system in our short time together.

Lastly, I'm incredibly grateful to the iPhD 2015 biology batch for making the journey with me. I wouldn't do it with anyone else.

SYNOPSIS

Title: Effect of DNA damage on microtubule dynamics

Name: Aishwarya Venkataravi

Registration number: 20152001

Name of the thesis advisor: Mayurika Lahiri

Date of registration: 1st August 2017

Indian Institute of Science Education and Research (IISER), Pune, India

Introduction

Faithful propagation of genetic material is the prime objective of all life forms. However, DNA is exposed to several endogenous and environmental insults that result in damaging the DNA. This damage if not repaired leads to a mutation which leads to disease. Nature has evolved a well-coordinated mechanism called DNA damage response to combat this threat. DNA damage response (DDR) involves detecting the damage, signalling its presence and recruiting proteins to repair the damaged DNA (Jackson et al., 2009).

DDR is mainly orchestrated by a group of PI3K-like proteins that include ATM, ATR and DNA-PK. Upon DNA damage, these proteins are activated which mediate cell cycle arrest, activate DNA repair and transcriptionally regulate proteins involved in DDR (Bartek et al., 2007; Patil et al., 2013). DDR is initiated by sensor proteins which detect the aberrant DNA and phosphorylate the transducers (ATM, ATR and DNA-PK) which lead to activation of proteins

such as CHK1 and CHK2, which results in cell cycle arrest, apoptosis, transcription halt and DNA repair (Marechal et al., 2013)

Studies pertaining to the DDR are majorly restricted to processes occurring inside the nucleus of the cell. The effect of DNA damage on cytoplasmic organelles is not well studied. Farber-Katz et al. in their 2014 study have highlighted the role of DNA damage-induced Golgi dispersal in cell survival (Farber-Katz et al., 2014). They showed that activation of the DNA-PK/GOLPH3/MYO18A pathway is essential for the survival of the cell post DNA damage. Depletion of GOLPH3 or MYO18A using shRNA mediated knockdown results in apoptosis of the cell in response to DNA damage and overexpression of GOLPH3 results in resistance to cell death by DNA damaging agents. It is suggested that there exists critical cargo whose trafficking from Golgi to the plasma membrane is vital for the cell survival post DNA damage. However, the cargo and the pathway remain to be identified.

Studies from our lab further explored this effect of DNA damage by showing that DNA alkylating agent MNU resulted in activation of DNA-PK and Golgi dispersal leading to the transformation of breast epithelial cells (Anandi et al., 2017). In addition to Golgi dispersal, a dramatic reorganisation of cytoskeleton resulting in a parallel array of microtubules and loss of actin stress fibres was observed. This project focuses on answering the questions – How and why does DNA damage lead to reorganisation of the cytoskeleton? Is there a functional relationship between Golgi dispersal and the reorganisation of microtubules? Furthermore, to characterise other phenotypes of the cell, which might be a secondary action of the cytoskeletal rearrangement.

This study falls at the juncture of DNA damage response and regulation of the cytoskeleton. Therefore, this study unlocks several questions, expanding our understanding of cellular response to genotoxic stress and improving our regulation of Golgi- microtubule association.

Objective

1. To characterise the microtubule and actin phenotypes post DNA damage
 - 1.1 To characterise changes in microtubule and actin dynamics post DNA damage
 - 1.2 To identify changes in tubulin post-translational modifications post DNA damage
2. To elucidate the mechanism by which DNA damage leads to reorganisation of the cytoskeleton
 - 2.1 To check if activation of DNA-PK and Golgi dispersal play a role in DNA damage-induced microtubule stabilisation
 - 2.2 To identify whether there is a functional association between microtubule rearrangement and Golgi dispersal upon DNA damage
3. To determine the functional relevance of rearrangement of cytoskeleton post DNA damage
 - 3.1 To determine whether changes in microtubule dynamics lead to impaired intracellular trafficking
 - 3.2 To determine whether the cytoskeletal rearrangement plays a role in migration and invasion following DNA damage

Results

DNA damage leads to microtubules stabilisation

To evaluate the effect of DNA damage on the cytoskeleton, we resorted to immunostaining MCF10A cells for microtubule and actin post DNA damage. It was observed that both components of cytoskeleton were significantly reorganised 48 hours post-induction of DNA damage. The usual radial microtubule array was observed to have attained a more parallel arrangement post DNA damage. The rearrangement of the microtubule network was quantified using the directionality tool. It was also observed that there was a change in cell shape and size, which might be due to the reorganisation of the underlying cytoskeleton. Monitoring EB3 showed that, in cells treated with DNA damaging agents were slower than control cells. It was also observed that these microtubules exhibited a longer lifetime, longer length and reduced growth speed. Treatment with nocodazole revealed the presence of a subset of hyper stable microtubules in cells with DNA damage. Changes in tubulin post-translational modifications and interaction with MAPs are known to regulate microtubule dynamics. To address this, we checked for changes in tubulin PTMs following DNA damage, by immunostaining. Here we found that while there was no change in tubulin polyglutamylation, there was an increase in acetylation α -tubulin post DNA damage. We also went on to test whether DNA damage led to change in microtubule dynamics using another cell line.

Similar to MCF10A, HEK293 showed Golgi dispersal and microtubule stabilization following treatment with a DNA damaging agent.

DNA damage led to an increase in Golgi derived microtubules through activation of DNA-PK and Golgi dispersal

To decipher the mechanism by which DNA damage might lead to changes in microtubule dynamics, we checked for activation of DNA-PK and Golgi dispersal. Since Golgi has a close association with microtubules, we proposed that changes in microtubule dynamics might be through changes in Golgi (Chabin-Brion et al., 2001; Zhu et al., 2013). Activation of DNA-PK (T2609) and Golgi dispersal was detected 48h post NEU treatment. To characterise the time course of these changes, we stained for phospho-DNA-PK and Golgi after time points indicated in respectively. Inhibition of DNA-PK with a small molecule inhibitor, DMNB following MNU treatment showed a reversal of the Golgi dispersal and to some extent, the transformation phenotype (Anandi et al., 2017). DMNB was used to check for the involvement of DNAPK in Golgi dispersal and microtubule rearrangement post-NEU and UV treatment. A reduction in nocodazole resistant microtubules, as well as acetylated tubulin, was observed after treatment with DMNB. This proves that the activation of DNA-PK is necessary for both Golgi and microtubule phenotypes post DNA damage.

To investigate if microtubule stabilization occurs due to disruption of Golgi structure and increase Golgi derived microtubules, we sought to check for changes in microtubule dynamics post Latrunculin A (LatA) treatment. Farber-Katz and group, in their 2014 study, proved that the F-actin is required for

DNA-damage-induced Golgi dispersal (Farber-Katz et al., 2014). Upon treatment with LatA (250nM) for 6h a reduction in the levels of acetylated tubulin and as well as nocodazole resistant microtubules was observed. These results suggests that reorganisation of Golgi is leading to microtubule stabilisation. Further, it was observed that acetylated microtubules were closely associated with the dispersed Golgi elements, which indicates that they might be Golgi nucleated. Nocodazole washout assay was performed to determine changes in the nucleation of microtubules at Golgi. An increase in microtubule nucleation at Golgi was observed 10mins post washout.

DNA damage led to mislocalisation of cell-cell junction and polarity proteins through impaired intracellular trafficking

Faber-Katz et al. and previous studies have shown that DNA damage leads to aberrant Golgi structure and function. We wanted to check if treatment with DNA damaging agent leads to impaired intracellular trafficking, which leads to changes in cell polarity. RUSH assay with ManII (α -Mannosidase II) tagged with EGFP and GPI (Glycosylphosphatidylinositol) anchored EGFP as reporters were used to test for defects in intracellular trafficking from ER-Golgi and Golgi to plasma membrane, respectively (Boncompain et al., 2012; Boncompain et al., 2014). A delay in trafficking was observed in cells post DNA damage when compared to untreated cells. Further, immunostaining cells with E-cadherin, β -catenin and α 3-integrin revealed mislocalisation of these proteins in the cytoplasm. Diffused staining at the junctions as well as punctate structures throughout the cytoplasm was seen in NEU treated cells as compared to a clean junctional localisation in untreated cells. This

suggests impaired intracellular trafficking leading to mislocalisation of proteins destined to the plasma membrane.

Conclusion

Taken together, the results from this study along with previous studies from lab and others, we propose a model by which DNA damage leads to microtubule stabilisation through an increase in Golgi derived microtubules. We propose that these stable microtubules deregulate intracellular trafficking resulting in changes in cell polarity (Figure1). This study is thus the first to demonstrate the link between Golgi dispersal and microtubule reorganisation orchestrating changes in cell polarity.

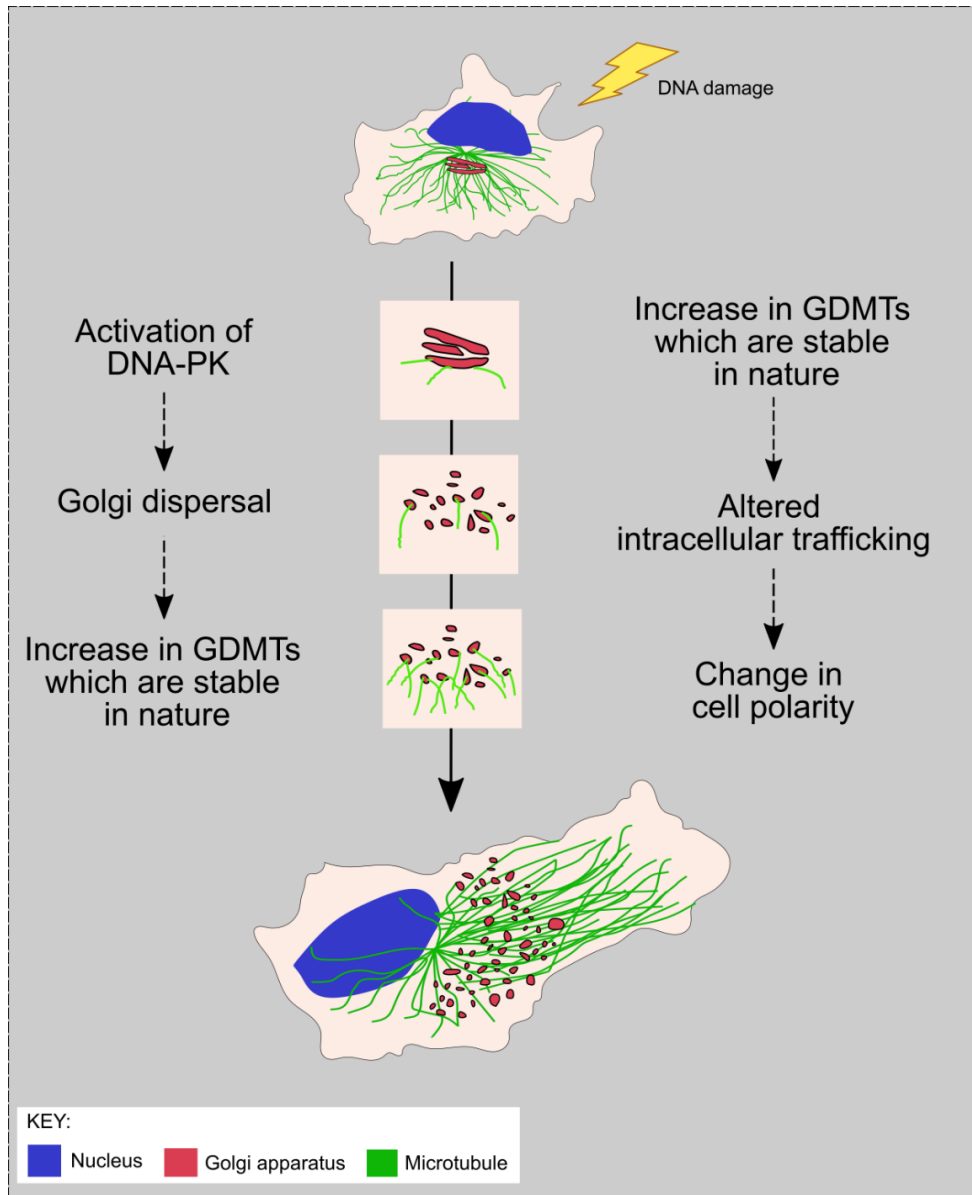


Figure1- Schematic representation of the proposed model. the DNA damage leads to Golgi dispersal through the DNA-PK-GOLPH3-MYO18A axis. Golgi dispersal leads to an increase in GDMTs. Due to the difference in dynamics of GDMTs, the trafficking of proteins to the membrane gets altered, leading to the mislocalisation of polarity proteins. We hypothesise that this is the mechanism through which DNA damage might lead to transformation

References

- Anandi, L., Chakravarty, V., Ashiq, K.A., Bodakuntla, S., and Lahiri, M. (2017). DNA-dependent protein kinase plays a central role in transformation of breast epithelial cells following alkylation damage. *J Cell Sci* 130, 3749-3763.
- Bartek, J., and Lukas, J. (2007). DNA damage checkpoints: from initiation to recovery or adaptation. *Curr Opin Cell Biol* 19, 238-245.
- Boncompain, G., Divoux, S., Gareil, N., de Forges, H., Lescure, A., Latreche, L., Mercanti, V., Jollivet, F., Raposo, G., and Perez, F. (2012). Synchronization of secretory protein traffic in populations of cells. *Nat Methods* 9, 493-498.
- Boncompain, G., and Perez, F. (2014). Synchronization of secretory cargos trafficking in populations of cells. *Methods in molecular biology* 1174, 211-223.
- Chabin-Brion, K., Marceiller, J., Perez, F., Settegrana, C., Drechou, A., Durand, G., and Pous, C. (2001). The Golgi complex is a microtubule-organizing organelle. *Mol Biol Cell* 12, 2047-2060.
- Farber-Katz, S.E., Dippold, H.C., Buschman, M.D., Peterman, M.C., Xing, M., Noakes, C.J., Tat, J., Ng, M.M., Rahajeng, J., Cowan, D.M., *et al.* (2014). DNA damage triggers Golgi dispersal via DNA-PK and GOLPH3. *Cell* 156, 413-427.
- Jackson, S.P., and Bartek, J. (2009). The DNA-damage response in human biology and disease. *Nature* 461, 1071-1078.
- Marechal, A., and Zou, L. (2013). DNA damage sensing by the ATM and ATR kinases. *Cold Spring Harb Perspect Biol* 5.

Patil, M., Pabla, N., and Dong, Z. (2013). Checkpoint kinase 1 in DNA damage response and cell cycle regulation. *Cell Mol Life Sci* *70*, 4009-4021.

Zhu, X., and Kaverina, I. (2013). Golgi as an MTOC: making microtubules for its own good. *Histochemistry and cell biology* *140*, 361-367.

TABLE OF CONTENTS

CERTIFICATE	ii
DECLARATION	iii
DEDICATION.....	iv
ACKNOWLEDGEMENTS	v
SYNOPSIS	viii
TABLE OF FIGURES.....	3
ABBREVIATIONS	12
ABSTRACT.....	13
I. Introduction.....	14
1.1 Microtubules	15
1.1.1 Regulation of microtubule dynamics	15
1.1.2 Asymmetry in microtubule dynamics and cell polarisation:	26
1.2 DNA Damage Response:.....	30
1.2.1 DNA repair pathways:	31
1.2.2 Microtubule and genome maintenance:	32
1.2.3 Effect of DNA damage on Golgi morphology:.....	33
II. Materials and Methods	36
2.1 Cell line and culturing methods.....	37
2.2 Immunofluorescence	37
2.3 Microtubule regrowth assay	38
2.4 EB3 dynamics.....	38
2.5 Quantitative analysis.....	39
2.6 Wound healing assay	40
2.7 RUSH assay	41
2.8 Reagents table.....	42
III. DNA damage leads to microtubule stabilisation.....	44
3.1 Background.....	45
3.2 Results.....	47
3.2.1 DNA damage leads to the reorganisation of the microtubule network.....	47
3.2.2 DNA damage leads to an increase in tubulin acetylation	55
3.3 Summary and discussion.....	59

IV. DNA damage leads to microtubule stabilisation through activation of DNA-PK and Golgi dispersal.....	62
1.3 Background.....	63
1.4 Results.....	64
1.4.1 DNA damage-induced microtubule stabilisation is preceded by activation of DNA-PK and dispersal of Golgi	64
1.4.2 DNA damage leads to microtubule stabilisation in HEK293 cells	68
1.4.3 Activation of DNA-PK and Golgi dispersal is required for microtubule stabilisation post DNA damage	71
1.4.4 DNA damage leads to an increase in Golgi-derived microtubules	75
1.5 Summary and discussion.....	83
V. DNA damage leads to impaired intracellular trafficking	87
1.6 Background.....	88
1.7 Results.....	89
1.7.1 DNA damage does not lead alter collective cell migration.....	89
1.7.2 DNA damage led to mislocalisation of cell-cell junction and polarity proteins through impaired intracellular trafficking.	90
1.7.3 DNA damage leads to a permanent change in microtubule dynamics.....	96
1.8 Summary and discussion.....	101
VI. Discussion and Future perspectives	102
1.9 Conclusion	103
1.10 Microtubule stabilisation as a cell stress response	105
1.11 Microtubules, Golgi-derived microtubules and cancer	107
VII. BIBLIOGRAPHY	110
VIII. PUBLICATIONS	124

TABLE OF FIGURES

Figure1- Schematic representation of the proposed model. the DNA damage leads to Golgi dispersal through the DNA-PK-GOLPH3-MYO18A axis. Golgi dispersal leads to an increase in GDMTs. Due to the difference in dynamics of GDMTs, the trafficking of proteins to the membrane gets altered, leading to the mislocalisation of polarity proteins. We hypothesise that this is the mechanism through which DNA damage might lead to transformation..... xv

Figure I-1: Model of γ -TuRC assembly and microtubule nucleation. γ -TuRC is an assembly of γ -TuSCs. γ -TuSC is composed of GCP2 and GCP3 along with two molecules of γ -tubulin. γ -TuSC-like complexes have GCP2 and GCP3, or both replaced with other GCPs such as GCP4, 5 and GCP6. This model of microtubule nucleation is called template nucleation model. (Teixido-Travesa et al., 2012). 16

Figure I-2: Microtubule organisation at Golgi. GM130, localised to cis-Golgi recruits AKAP450. AKAP450 recruits CDK5RAP2 and its homolog myomegalin(MMG) which attract γ -TuRC which nucleates microtubules. CLASP1/2 promotes microtubule nucleation, and CAMSAP2 stabilises the minus end of the nucleated microtubule. (Wu and Akhmanova, 2017). 18

Figure I-3 Tubulin PTMs and their modifying enzymes. a. Schematic representation of α and β tubulin dimer and their associated modifications. b. Schematic of enzymes catalysing the generation and removal of each tubulin PTM (Janke and Bulinski, 2011).22

Figure I-4- Schematic is representing the mechanism of Golgi dispersal upon DNA damage. DNA damage activates DNA-PK, which phosphorylates GOLPH3. Phosphorylation of GOLPH3 strengthens its interaction with MYO18A-F-Actin, which exerts a tensile force on the Golgi leading to Golgi dispersal. 34

Figure III-1- Schematic represents the Golgi dispersal mechanism upon DNA damage. DNA damage activates DNA-PK, which phosphorylates GOLPH3. Phosphorylation of GOLPH3 strengthens its interaction with MYO18A-F-Actin, which exerts a tensile force on the Golgi, leading to Golgi dispersal ((Buschman et al., 2015))......46

Figure III-2- MNU induced DNA damage leads to reorganisation of the cytoskeleton. (a) Treatment with MNU leads to rearrangement of microtubule cytoskeleton from a mesh-like to a more parallel arrangement and loss of actin stress fibres (N=3, n=145). (b and c) Quantification of microtubule phenotype (N=3, n=30). The quantification of microtubule dynamics using EB3-GFP constructs shows that MNU slows down microtubule dynamics. d. represents a few microtubule tracks of cells, treated with and without MNU, labelled with EB3-GFP; e, f and g show the graphs corresponding to microtubule lifetime, length and speed measured by tracking EB3 comets (N=3, n=120, 25 tracks per cell) . Asterisks indicate Mann-Whitney U test significance values; **** p < 0.0001.....48

Figure III-3- NEU induced DNA damage leads to reorganisation of the cytoskeleton. (a) Treatment with NEU leads to rearrangement of microtubule cytoskeleton from a mesh-like to a more parallel arrangement and loss of actin stress fibres (N=3, n=140). (b and c) Quantification of microtubule phenotype (N=3, n=30). Quantifying microtubule dynamics using EB3-GFP constructs shows that NEU slows down microtubule dynamics. d. represents a few microtubule tracks of cells, treated with and without MNU, labelled with EB3-GFP; e, f and g show the graphs corresponding to microtubule lifetime, length and speed measured by tracking EB3 comets (N=3, n=120, 25 tracks per cell). Asterisks indicate Mann-Whitney U test significance values; **** p < 0.0001, ** p < 0.01.....50

Figure III-4- UV induced DNA damage leads to reorganisation of the cytoskeleton. (a) Treatment with UV leads to rearrangement of microtubule cytoskeleton from a mesh-like to a more parallel

arrangement and loss of actin stress fibres (N=3, n=130). (b and c) Quantification of microtubule phenotype (N=3, n=30). Quantifying microtubule dynamics using EB3-GFP constructs shows that UV slows down microtubule dynamics. d. represents a few microtubule tracks of cells, treated with and without MNU, labelled with EB3-GFP; e, f and g show the graphs corresponding to microtubule lifetime, length and speed measured by tracking EB3 comets (N=3, n=120, 25 tracks per cell). Asterisks indicate Mann-Whitney U test significance values; **** p < 0.0001.....51

Figure III-5- DNA damage leads to an increase in area and elongation of the cell. Quantification of cell area (d.), circularity (e) and aspect ratio (f.) (N=3, n=160). Asterisks indicate Mann-Whitney U test significance values; **** p < 0.0001; *** p< 0.001; ** p< 0.0152

Figure III-6- Treatment with nocodazole reveals a subset of microtubules (a.) in MNU-treated cells, which are resistant to depolymerisation (N=3, n=140). Shown in b. are binary images of the subset of microtubules, quantified in c. using a ridge detection tool. Similarly, (d.) shows binary images of nocodazole-resistant microtubules in NEU and UV-treated cells (N=3, n=130), quantified in (e.). Asterisks indicate Mann-Whitney U test significance values; **** p < 0.000154

Figure III-7- MCF10A cells treated with and without NEU have poly glutamylation (GT335) shows an enrichment on nocodazole stable microtubules. GT335 is labelled in magenta, α -tubulin in yellow and nucleus in cyan.....56

Figure III-8- MCF10A cells treated with and without NEU have very little poly glutamylation (PolyE) but show an enrichment after nocodazole stable microtubules. PolyE is labelled in yellow, α -tubulin in magenta and nucleus in cyan.....57

Figure III-9- DNA damage leads to increased α -tubulin acetylation at K40. Shown in a. are cells with and without DNA damage, stained for α -tubulin K40 acetylation and α -tubulin after treatment with nocodazole (2.5mg/mL,

20mins). The nocodazole-resistant microtubules were enriched with acetylation. (b.) An increase in K40 acetylation can be observed upon treatment with NEU (2mM, 48h) and UV (10J/m², 48h), which is quantified in c. Asterisks indicate Mann-Whitney U test significance values; * p < 0.05.....58

Figure III-10- Schematic summarising the results of this chapter. DNA damage leads to microtubule stabilisation. EB3 assay shows that microtubules in cells treated with a DNA damaging agent have lower speed, higher displacement and longer lifetime. A subset of microtubules remain intact upon nocodazole treatment post DNA damage. Increase in tubulin acetylation was observed upon DNA damage.....59

Figure IV-1: MCF10A cells treated with NEU (2mM) and UV (10J/m²) show activation of DNA-PK and Golgi dispersal. a. and c. represent cells stained for pDNAPK (yellow and nucleus (blue), post-NEU and UV treatments, respectively. e. and g. show plots for quantification of same. b. and d. represent cells stained for Golgi (yellow) and nucleus (cyan), post-NEU and UV treatments, respectively. f. and h. show plots for quantification of same. Asterisks indicate Mann-Whitney U test significance values; **** p < 0.0001.65

Figure IV-2: Activation of DNAPK and Golgi dispersal precedes microtubule stabilisation. Post-NEU treatment DNAPK gets phosphorylated at T2609 at 10mins and remains active till 48hrs. Shown in a. are representative images of a few selected time points after treatment with NEU(2mM). b. depicts quantification of the number of pDNAPK foci per nucleus. Asterisks indicate Kruskal-Wallis test significance values; **** p < 0.0001, ns – Non-significant. Golgi starts to disperse 4h post DNA damage, as shown in c. and d. Asterisks indicate Kruskal-Wallis test significance values; **** p < 0.0001, **p< 0.01.....66

Figure IV-3-Appearance of nocodazole-resistant microtubules starts at 18h after NEU treatment. Shown in a. are binary images of tubulin and nucleus (in grey) of select timepoints post-NEU treatment. b. shows the

quantification of the same using a ridge detection tool. Asterisks indicate Kruskal-Wallis test significance values; **** $p < 0.0001$, * $p < 0.05$ and ns – Non-significant. c. An increase in tubulin acetylation was observed after Golgi dispersal at 18h. d. is the quantification of the same. Asterisks indicate Kruskal-Wallis test significance values; **** $p < 0.0001$, * $p < 0.05$ and ns – Non-significant 67

Figure IV-4: HEK293 cells treated with different doses of NEU and stained with pDNA-PK(T2609). a. Activation of DNA-PK can be observed by the presence of foci (green) in the nucleus stained with Hoechst 33258 (blue). b. depicts quantification of the number of pDNAPK foci per nucleus. Asterisks indicate Mann-Whitney U test significance values; **** $p < 0.0001$ 68

Figure IV-5: DNA damage leads to microtubule Golgi dispersal and microtubule stabilisation in HEK293 cells. a. shows cells stained with Golgi (yellow) and nucleus (cyan) post-treatment with NEU (0.5mM, 48h) and UV (10J/m², 48h). b. shows the quantification of dispersal of Golgi. Treatment with nocodazole reveals a subset of microtubules in cells with DNA damage, which resist depolymerisation. Shown in c. are binary images of the subset of microtubules and the nucleus, quantified in (d.) using ImageJ ridge detection tool. e. HEK293 cells treated with NEU (0.5mM, 48h) and UV (10J/m²) stained for α -tubulin(magenta), acetylated-Tubulin(yellow), and Hoechst 33258(cyan) show an increase in tubulin acetylation post DNA damage. f. plot represents quantification of acetylated tubulin. Asterisks indicate Mann-Whitney U test significance values; **** $p < 0.0001$; *** $p < 0.001$ 70

Figure IV-6- DNA damage-induced microtubule stabilisation is through activation of DNA-PK. (a) inhibition of DNAPK and reversal of golgi upon treatment with 25mM DMNB for 24h, quantified in c and d. After NEU treatment, treatment with DMNB also reduces acetylated tubulin (b) and nocodazole-resistant microtubules (f), which are quantified in e and g, respectively. Asterisks indicate Kruskal-Wallis test significance values; **** $p < 0.0001$, ** $p < 0.01$ and ns – Non-significant..... 72

Figure IV-7- DNA damage-induced microtubule stabilisation is through golgi dispersal. (a) Depolymerisation of F-actin by LatA (250nM, 6h) leads to compaction of the dispersed golgi fragments, quantified in (b). Treatment with LatA after NEU treatment leads to a reduction of acetylated tubulin (b) and nocodazole-resistant microtubules (f), which are quantified in e and g, respectively. Asterisks indicate Kruskal-Wallis test significance values; **** p < 0.0001, ***p< 0.001, **p< 0.01 and ns – Non-significant74

Figure IV-8- Acetylated microtubules are associated with Golgi elements. The image shows cells with and without NEU (2mM) treatment stained for acetylated tubulin (green), Golgi (red) and nucleus (blue).75

Figure IV-9- Maximum intensity project images of cells expressing EB3-GFP (green) and GalT (red).76

Figure IV-10- Standardisation of nocodazole dose. Images show MCF10A cells with and without NEU treatment incubated with three concentrations of nocodazole (2.5 mg/ml, 5 mg/ml and 10 mg/ml) and incubated for 20mins, 60mins, 2h and 3h, stained for α-tubulin (magenta) and nucleus (cyan).....77

Figure IV-11- NEU induced DNA damage leads to an increase in Golgi-derived microtubules. Nocodazole washout assay was performed to determine changes in the nucleation of microtubules at Golgi. Cells were treated with 2.5mg/mL for 3h, then washed with cold PBS and supplemented with fresh media. Microtubules were allowed to recover at 37°C and fixed and stained for microtubules and Golgi. a. An increase in microtubule (magenta) nucleation at Golgi (yellow) was observed 10mins post nocodazole washout, which was quantified (b.) by manually counting the number of nucleation sites. Asterisks indicate Mann-Whitney U test significance values; **** p < 0.0001.78

Figure IV-12- Nocodazole washout assay. a. Schematic shows the experimental timeline. The cells were treated with nocodazole for 3h and washout out. The cells were fixed at the indicated time points after washout. As seen in b., the microtubules (magenta) start to repolymerise

but stop recovering at 20mins. Depolymerized microtubules were observed at 30 and 60min timepoints.80

Figure IV-13- MCF10A cells treated with nocodazole (2.5 mg/ml, 20mins) followed by nocodazole removal. The cells were then supplemented with fresh media, and the microtubules were allowed to recover at 37°C. Cells were fixed at time points during the recovery and stained for tubulin (green) and nucleus (blue).81

Figure IV-14- Recovery after cold shock. a. Schematic shows the experimental timeline. The cells were incubated on ice for 30mins and then shifted to room temperature. The cells were fixed at the indicated time points. b. It can be observed that the microtubules recover, and the microtubule (magenta) array is complete by 20mins. It is to be noted that the golgi (yellow) does not reassemble in NEU-treated cells, while it reassembles in untreated cells.82

Figure IV-15- DNA-PK activation and Golgi dispersal precede microtubule stabilisation. a. following induction of DNA damage, DNA-PK activation occurs around 10mins, followed by Golgi dispersal, which occurs around 4h. Microtubule stabilisation occurs from 18h onwards. b. inhibition of activation of DNA-PK (using DMNB) and Golgi dispersal (using LatA) led to a reversal of DNA damage-induced microtubule stabilisation.84

Figure IV-16- DNA damage leads to an increase in Golgi-derived microtubules. Upon treatment with a DNA damaging agent, the intact Golgi (a.) disperses (b.) in a DNA-PK-dependent manner which leads to an increase in Golgi-derived microtubules (c.) which constitute the stable subset of microtubules which are parallel.85

Figure V-1- DNA damage does not lead to change in collective cell migration. a. representative images of wound in a confluent monolayer of the cells with and without MNU treatment. Percentage wound closure has been quantified in b. Asterisks indicate Mann-Whitney U test significance values; ns- non-significant.90

Figure V-2- DNA damage led to altered ER-Golgi trafficking. (a) delayed trafficking of ManII-GFP to golgi apparatus was observed upon induction DNA damage which has been quantified in (c). Graph represents percentage of cells showing GFP signal in ER(yellow), Golgi (blue) or both (green) at the indicated timepoints post biotin addition.92

Figure V-3- DNA damage led to altered ER-Golgi trafficking. An impaired trafficking of GPI anchored EGFP was also observed (a) which has been quantified in (b). Each point in the graph represents mean±sem with the asterisks indicating two-way ANOVA test significance value of $p < 0.0001$93

Figure V-4- Mis-localization of E-cadherin, β -Catenin and $\alpha 3$ -Integrin post DNA damage. Immunostaining NEU treated cells for a. E-cadherin, b. β -Catenin, and c. $\alpha 3$ -Integrin showed an altered localisation of the cell-cell junction proteins. A pronounced distribution of the proteins in the cytoplasm (white arrow) and a diffused staining (green arrow) at the junctions was observed. The cytoplasmic proteins has been quantified by measuring CTCF and plotted in (d-f). Asterisks indicate Mann-Whitney U test significance values; **** $p < 0.0001$95

Figure V-5- Long-time course experiment shows activation of DNA-PK till day 9. Images showing pDNA-PK(T2609) foci (yellow) against nucleus (blue). The foci have been quantified per day (b-d). Asterisks indicate Mann-Whitney U test significance values; **** $p < 0.0001$ 97

Figure V-6- Long-time course experiment shows activation of Golgi dispersal till day 9. Images showing Golgi (yellow) against nucleus (cyan). The Golgi area has been quantified per day (b-d). Asterisks indicate Mann-Whitney U test significance values; **** $p < 0.0001$ 98

Figure V-7- Long-time course experiment shows increase tubulin acetylation till day 9. Images showing acetylated tubulin (yellow) against nucleus (cyan). Tubulin acetylation has been quantified per day (b-d). Asterisks indicate Mann-Whitney U test significance values; **** $p < 0.0001$; *** $p < 0.001$; ** $p < 0.01$ 99

Figure V-8- Long-time course experiment shows presence of nocodazole resistant microtubules till day 9. (a) Images showing binary images of nocodazole resistant microtubules. The nocodazole resistant microtubules have been quantified per day (b-d). Asterisks indicate Mann-Whitney U test significance values; **** $p < 0.0001$ 100

Figure VI-1- DNA damage leads to Golgi dispersal through the DNA-PK-GOLPH3-MYO18A axis. Golgi dispersal leads to an increase in GDMTs. Due to the difference in dynamics of GDMTs, the trafficking of proteins to the membrane gets altered, leading to the mislocalisation of polarity proteins. We hypothesise that this is the mechanism through which DNA damage might lead to transformation. 104

ABREVIATIONS

acTub	Acetylated α -tubulin
CTCF	Corrected total cell fluorescence
DDR	DNA damage response
DMEM	Dulbecco's Modified Eagle Medium
DMNB	4,5-Dimethoxy-2-nitrobenzaldehyde
DMSO	Dimethyl sulfoxide
DNA-PK	DNA dependent protein kinase
DPBS	Dulbecco's phosphate-buffered saline
DSB	Double Strand Breaks
EGF	Epidermal Growth Factor
EMT	Epithelial to Mesenchymal Transition
FAK	Focal adhesion kinase
GalT	Galtase T
GDMT	Golgi-derived microtubules
GM130	Golgi matrix protein 130
GPI	Glycosylphosphatidylinositol
L-15	Leibovitz's Medium
LatA	Latrunculin A
ManII	Manosidase II
MAP	Microtubule associated proteins
MNU	N-nitroso-N-methylurea
MT	Microtubule
NEU	N-ethyl N-nitrosourea
NHEJ	Non-homologous end joining
PBS	Phosphate buffer saline
PFA	Paraformaldehyde
PTM	Post translational modification
RUSH	Retention using a selective hook
SSB	Single stranded break

ABSTRACT

Cells are constantly exposed to DNA damaging agents. In response to DNA damage, cells trigger processes such as cell cycle arrest, increased transcription of DNA repair genes leading to DNA repair. Although the nuclear effects of DNA damage are well studied, little is known regarding the impact of DNA damage on cytoplasmic organelles. Farber-Katz et al. for the first time demonstrated that DNA damage triggers a dramatic reorganisation of the Golgi apparatus that resulted in its dispersal throughout the cytoplasm. In our study, we report DNA damage leads to aberrant Golgi structure and function accompanied by reorganisation of the microtubule network. Characterisation of the microtubule dynamics showed the presence of a stable pool of microtubules that were resistant to depolymerisation by nocodazole and were enriched in acetylated tubulin. Monitoring microtubule dynamics by using a plus-TIP marker further confirmed that microtubules were stabilised. Inhibition of DNA-PK leads to the reversal of microtubule reorganisation, suggesting that alteration of microtubule organisation occurs via the activation of DNA-PK. Investigation of the functional association between Golgi dispersal and microtubule stability revealed that the Golgi elements were distributed along the acetylated microtubules. Interestingly, reversal of Golgi morphology by depolymerising F-actin led to reversal of microtubule stability. An increase in Golgi derived microtubule post DNA damage was observed which implies that the stable microtubules originate from Golgi. We propose that these stable microtubules deregulate intracellular trafficking resulting in changes in cell polarity. This study is thus the first to demonstrate the link between Golgi dispersal and microtubule reorganisation orchestrating changes in cell polarity.

CHAPTER I

Introduction

1.1 Microtubules

Microtubules are polymers composed of heterodimers of α - and β -tubulin (Nogales et al., 1998). The heterodimers polymerise lengthwise into protofilaments. Thirteen such filaments assemble into a hollow tubule which forms the microtubule filament (Li et al., 2002). Microtubules participate in several cellular functions such as cell division, motility and intracellular transport in association with motor proteins. Numerous post-translational modifications decorate the microtubule surface, which provides a mechanism for functional specialisation.

1.1.1 Regulation of microtubule dynamics

1.1.1.1 Microtubule nucleation:

The tubulin heterodimer polymerises *in vitro* when a critical concentration is reached. However, in the cell, tubulin rarely polymerises spontaneously but requires a nucleating factor. Early electron microscopy images showed different subcellular structures from which microtubules originated and called them "microtubule nucleating centres" abbreviated as MTOC.

Centrosome:

Centrosome, a non-membranous organelle with a pair of centrioles, is the best-studied MTOC. The minus end of the microtubule is anchored at the MTOC. The MTOC is characterised by the presence of γ -tubulin, the third type of tubulin, which is known for its proficiency to nucleate microtubules (Kollman et al., 2011). γ -tubulin along with Spc97 (GCP2) and Spc98 (GCP3) forms the γ -tubulin ring complex (γ -TuRC) which is observed to have a 13-fold symmetry that acts as a scaffold for

microtubule nucleation(Kollman et al., 2010; Murphy et al., 2001)(**Figure I-1**). It is believed that the 13-fold symmetry of the γ - TuRC restricts the MT assemble in a 13-fold symmetry *in vivo*, unlike *in vitro* where the MTs assemble in a 14-fold symmetry(Moritz et al., 2000). Centrosomal microtubules are arranged radially and are well-known for their role in segregation of chromosome during cell division.

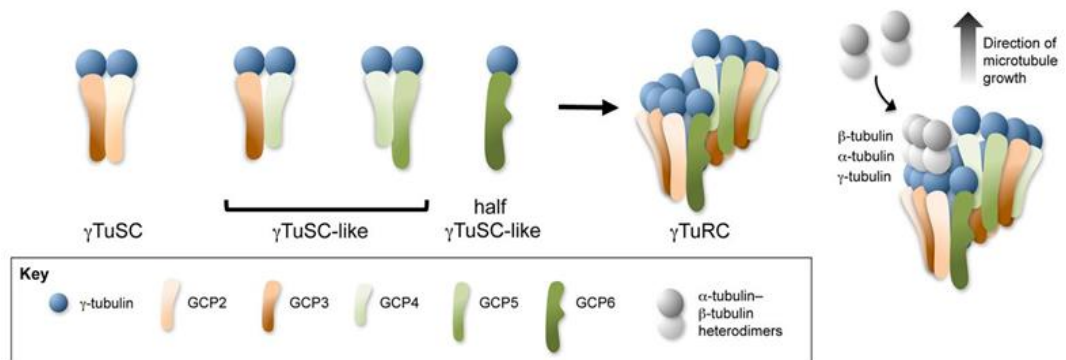


Figure I-1: Model of γ -TuRC assembly and microtubule nucleation. γ -TuRC is an assembly of γ -TuSCs. γ -TuSC is composed of GCP2 and GCP3 along with two molecules of γ -tubulin. γ -TuSC-like complexes have GCP2 and GCP3, or both replaced with other GCPs such as GCP4, 5 and GCP6. This model of microtubule nucleation is called template nucleation model. (Teixido-Travesa et al., 2012).

Golgi Apparatus:

The role of Golgi as a microtubule organising centre has gained importance since a decade. Cells have a significant proportion of their microtubules nucleated at the Golgi and represents the second primary MTOC in mammalian cells. Christian Poüs group found the first evidence of microtubule nucleation at Golgi in 2001(Chabin-Brion et al., 2001). They showed that placing isolated Golgi membranes in a

solution of tubulin resulted in the formation of microtubules attached to the Golgi vesicles(Chabin-Brion et al., 2001). The molecular mechanism of microtubule organisation at Golgi was deciphered recently(Wu et al., 2016)(**Figure I-2**). GM130 anchors AKAP450, a scaffolding protein, at the cis-Golgi(Rivero et al., 2009). AKAP450 is responsible for recruiting microtubule nucleating factors such as CDK5RAP2 and MMG on the Golgi membrane. CDK5RAP2 and MMG attract γ -TuRC, which nucleates microtubules at the Golgi membrane(Roubin et al., 2013; Wang et al., 2010). CAMSAP2 binds and stabilises the newly nucleated MT and gets affixed onto the AKAP450-CDK5RAP2/MMG complex(Jiang et al., 2014). Golgi anchored microtubules are thought to play a role in maintaining Golgi structure during polarised cell movement and cancer cell invasion(Kodani and Sutterlin, 2009; Thyberg and Moskalewski, 1999; Vinogradova et al., 2012; Wu et al., 2016; Zhu and Kaverina, 2013).

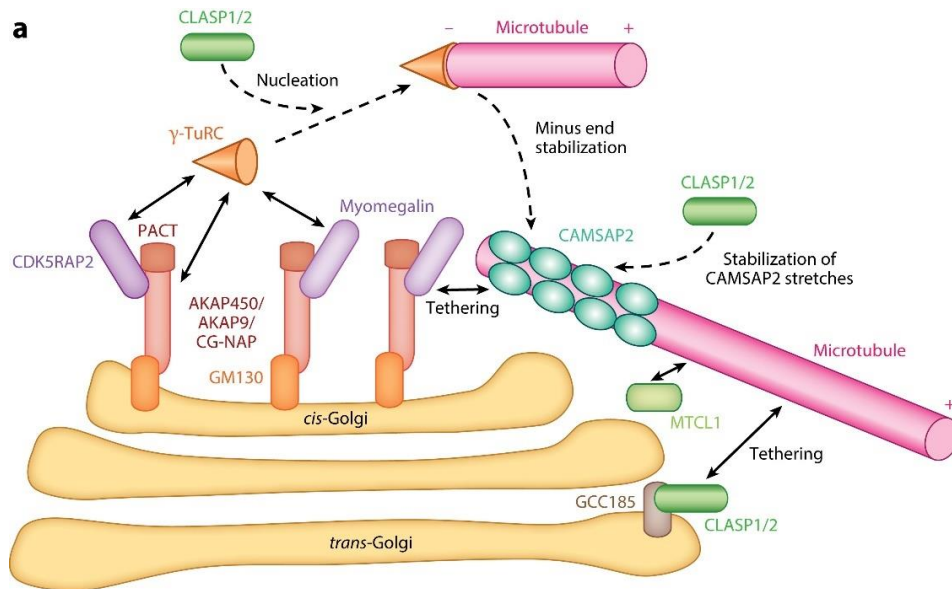


Figure I-2: Microtubule organisation at Golgi. GM130, localised to cis-Golgi recruits AKAP450. AKAP450 recruits CDK5RAP2 and its homolog myomegalin (MMG) which attract γ -TuRC which nucleates microtubules. CLASP1/2 promotes microtubule nucleation, and CAMSAP2 stabilises the minus end of the nucleated microtubule. (Wu and Akhmanova, 2017).

Nuclear membrane:

Plants cells and specific highly differentiated cell such as in muscle cells, microtubules are organised at the nuclear membrane (Bugnard et al., 2005; Masoud et al., 2013). The mechanism of microtubule nucleation at the nuclear membrane is not well established. It is proposed that plant-specific nuclear transmembrane proteins help anchor γ -TuRC to the nuclear envelope, which leads to microtubule nucleation. In muscle cells, the LINC (linker of nucleoskeleton and cytoskeleton) complexes are thought to associate with γ -tubulin and

pericentrin along with ninein which functions as the MTOC (Kim et al., 2015; Tassin et al., 1985)

Chromatin and Kinetochores:

Chromatin nucleates microtubule during mitosis, which generates a gradient of Ran-GTP that activates spindle assembly factors such as TPX2 (Clarke and Zhang, 2008). TPX2 activates Aurora A, which in turn activates NEDD1, which is essential for Chromatin-mediated nucleation of microtubules (Luders et al., 2006; Pinyol et al., 2013; Scrofani et al., 2015).

1.1.1.2 Regulation of microtubule function by tubulin PTMs and MAPs:

Microtubules are essential for a variety of critical functions in the cell. They are necessary for maintaining cell polarity, cell shape and intracellular transport. They play a significant role in proper segregation of chromosomes during mitosis and meiosis, and they form a part of the axonemal structures such as cilia and flagella. Despite the various structures formed and its varied functions, microtubules are always assembled from the heterodimer of α - and β - tubulin, which raises the question of how they can perform so many different functions. Three major factors contribute to the heterogeneity of microtubule function- i) the gene encoded isotypes of α - and β - tubulin incorporated into the microtubule, ii) the post-translational modification (PTMs) of tubulin and iii) interactions with several microtubule-associated proteins (MAPs). It is to be noted that all three of the factors mentioned above can influence each other. The tubulin isotypes differ in the type, and specific MAPs recognise the extent of post-translational modification and specific

post-translational modifications. This section focuses on a few PTMs of tubulin (Figure I-3) and also discuss a few MAPs.

Tubulin Post-translational modifications:

- *Acetylation:*

Tubulin acetylation is often associated with long-lived microtubules. It is still a debate on whether acetylated microtubules are stable because they are acetylated, or they are acetylated because they are stable. Cryo-EM structures demonstrate that acetylated microtubules are more flexible, making them more resistant to mechanical stress (Howes et al., 2014; Xu et al., 2017). Tubulin acetylation has been linked to cell adhesion, migration and intracellular transport (Castro-Castro et al., 2012; Deakin and Turner, 2014; Reed et al., 2006). Studies have shown that acetylation of tubulin is increased in metastatic breast cancer and promote microtentacle formation and invasion (Boggs et al., 2015). Tubulin acetylation has also been implicated in kinesin-1 based transport (Reed et al., 2006)

- *Detyrosination:*

Detyrosination is the removal of the C-terminal Tyr residue which exposes the penultimate Glu residue (Fig2a). Detyrosinated tubulin (Detyr-tubulin) is used as a marker for long-lived microtubules but, as in case of acetylated microtubules, the mechanism was long debated (Khawaja et al., 1988; Kreis, 1987). It was recently discovered that detyrosination protects the microtubules from depolymerisation induced by kinesin-13-type motor proteins like MCAK, thus increasing

their longevity(Peris et al., 2009; Sirajuddin et al., 2014). Tyrosination status of the microtubules also regulates the binding of +TIPs like CLIP170 or p150/glued(Bieling et al., 2008; Peris et al., 2006). Detyrtubulin is enriched in microtubule protrusions that help in the reattachment of circulating tumour cells (Whipple et al., 2007). The carboxypeptidase catalysing detyrosination of α -tubulin is unidentified, but the enzyme catalysing the reverse reaction has been identified to be catalysed by tubulin tyrosine ligase(Boggs et al.)(**Figure I-3**)(Raybin and Flavin, 1975)

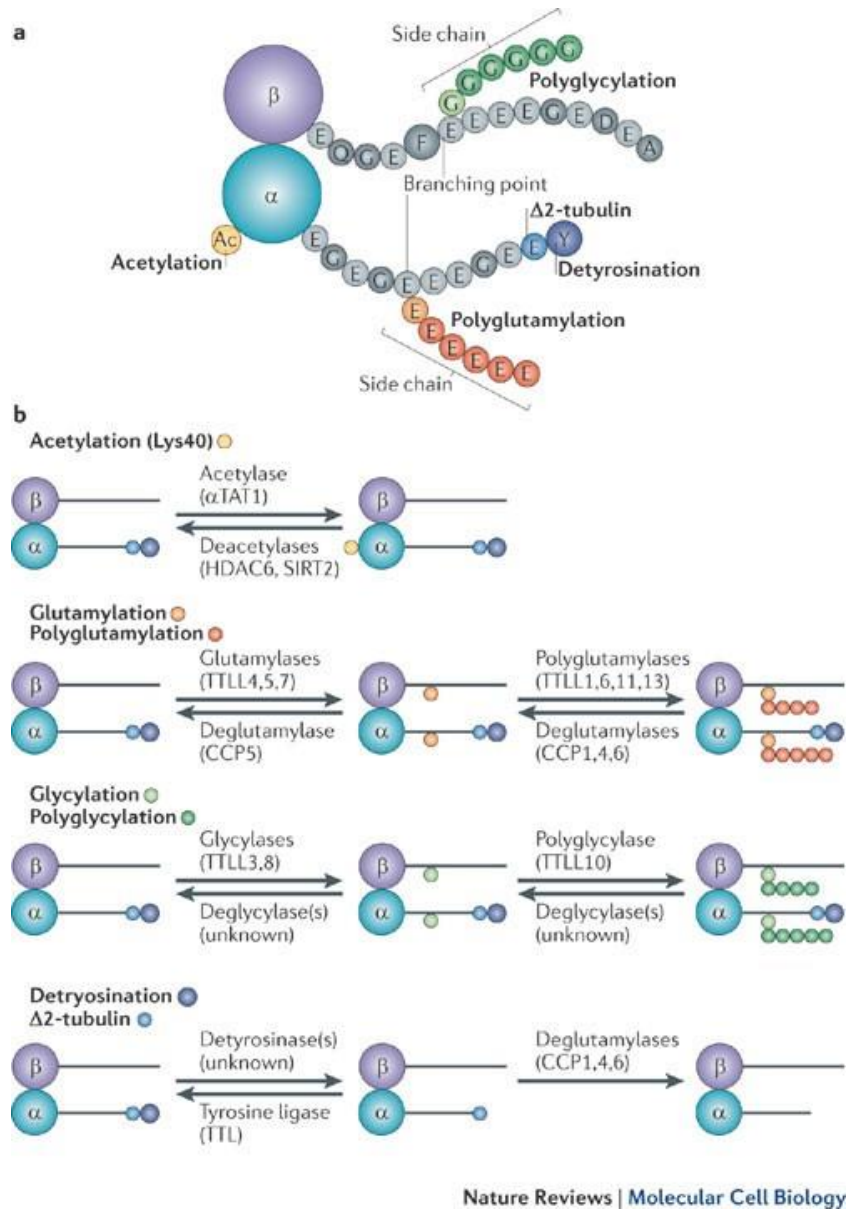


Figure I-3 Tubulin PTMs and their modifying enzymes. **a.** Schematic representation of α and β tubulin dimer and their associated modifications. **b.** Schematic of enzymes catalysing the generation and removal of each tubulin PTM (Janke and Bulinski, 2011).

- *Δ2-tubulin:*

Δ2-tubulin is formed by further removal of the penultimate Glu residue(Fig2a). Unlike detyr, this modification is irreversible, and it is associated with long-lived microtubules as it locks the microtubules in the detyrosinated state(Paturle-Lafanechere et al., 1994). Δ2-tubulin requires a previously detyrosinated microtubule and hence is dependent on the tyrosination/detyrosination cycle which is governed by the TTL class of enzymes. It has been shown that the absence of TTL results in accumulation of Δ2-tubulin in mice(Erck et al., 2005). High levels of Δ2-tubulin have also been observed in tumour samples and have been thought to contribute to aggressiveness and invasiveness of cancer by a yet unknown mechanism(Mialhe et al., 2001). The removal of the penultimate Glu residue is catalysed by Cytosolic carboxypeptidases(CCPs) (Figure I-3). CCPs also catalyse the removal of the polyglutamylation from the tubulin.

- *Polyglutamylation:*

Polyglutamylation refers to the addition of multiple glutamate residues to the γ -carboxyl groups of the glutamate residues in a protein(Fig2a). Glutamylation reactions are catalysed by the TTL- like a family of proteins(TTLL). Nine of these glutamylases exist, and they each have an intrinsic preference towards one isotype of tubulin (either α / β)(van Dijk et al., 2007). The reverse reaction is catalysed by the CCPs (Figure I-3). Thus, changes in Δ2-tubulin levels can also result in concomitant changes in Detyr-tubulin or polyglutamylation depending on whether TTL or CCPs govern the first change. It would be

interesting to see how a small change in levels of one enzyme can result in global changes in the microtubule dynamics.

Microtubule regulatory proteins:

Microtubule-associated proteins (MAPs) help remodel the microtubules by altering its dynamics. They modulate microtubule growth, stabilise or destabilise microtubules and enable interaction with other cellular organelles.

Mechanochemical ATPases popularly known as motor proteins such as kinesins and dyneins use microtubules as tracks for intracellular transport.

- *Microtubule Stabilising proteins:*

Proteins of the MAP2/Tau family are best known for their microtubules stabilising activity. These include Tau, MAP2(A, B, C) and MAP4. MAP2 and Tau are found in neurons, whereas MAP4 is present in other tissues but is generally not found in neurons. They stabilise microtubules by either promoting polymerisation or preventing their depolymerisation. Tau was shown to bind at the hydrophobic pocket at the interphase between the heterodimers. There is increasing evidence which suggests that MAP2/Tau family of proteins perform other functions such as binding to microfilaments, recruitment of signalling proteins and regulation of intracellular transport. Studies involving motor proteins moving along microtubules with decorated with stretches of Tau show that dynein reverses its direction and kinesin dissociates from the microtubule once they hit a patch of Tau. Other MAPs such as STOP (Stable tubulin only proteins) are associated with cold-stable microtubules. Tektin family of proteins have been studied

for their ability to crosslink and stabilise microtubules in axonemal structures like cilia and flagella.

- *Microtubule-Severing Proteins and Disassembly Promoters:*

Microtubule severing proteins cut the microtubule into smaller fragments creating new minus- and plus-ends which allows for the reorganisation of microtubules without complete disassembly of the microtubule. These severing proteins belong to three classes of microtubule severing proteins, katanin, spastin and fidgetin. On the surface, it appears that this severing action is to catalyse rapid depolymerisation of a subset of microtubules. Some of the short fragments of microtubules act as a scaffold for the growth of new microtubules. Spastin plays a role in axonal transport and maintenance of ER morphology. Spastin and katanin also play a role in cytokinesis. All three severing proteins contribute to the chromosome segregation and add to the process of Pacman-flux. Pacman-flux is the mechanism of chromosomal segregation in which the plus-end of the microtubules is actively depolymerised by the chromosomes (Pacman) while being pulled towards the spindle pole due to poleward movement of the tubulin subunits driven by minus-end depolymerisation (flux). Studies have shown that Fidgetin and Spastin play a role in the minus end depolymerisation while katanin is responsible for stimulating the plus end depolymerisation.

Microtubule disassembly act by two mechanisms- either by sequestering tubulin dimers or by binding to the microtubule and directly depolymerising them. Stathmin acts by the sequestering the

tubulin dimers, thereby decreasing the tubulin pool for polymerisation and increasing the frequency of spontaneous depolymerisation. On the other hand, two classes of kinesins – kinesin-13 (MCAK) and kinesin-8, bind directly to the microtubule ends and actively depolymerise the microtubules.

- *Microtubule plus-end tracking proteins:*

+TIPS are specialised MAPs which bind to the growing plus end of the microtubules. End Binding (King et al.) proteins form the core components of the +TIP networks as they autonomously track the growing end of the microtubules without the need of any binding proteins. CLIP-170 is the first +TIP protein which promotes MT rescue and has anti catastrophe property. Other +TIPs such as APC, MACF and CLASP are involved in stabilising microtubules and facilitate interaction with other organelles.

1.1.2 Asymmetry in microtubule dynamics and cell polarisation:

The polarity of the cell defines an oriented axis for processes such as secretion, cell migration, differentiation and cell division. Cell polarity is majorly established and maintained by polarised trafficking of proteins. Proteins synthesised in the ER get transported to the golgi apparatus where they are sorted and transported to their destination on microtubules tracks. This section will discuss how the cell regulates polarised trafficking by modulating the underlying microtubule network and its interaction with golgi.

1.1.2.1 Golgi structure and positioning -

Golgi apparatus is the hub for sorting and transporting proteins to the plasma membrane. In most vertebrates, the golgi is positioned adjacent to the centrosome and nucleus. The pericentriolar position allows for directional transport of proteins to one side of the cell. This process is crucial for cell polarisation during cell migration. When the cell decides to move in response to a directional cue, the golgi relocates to the side of the nucleus facing the destined leading edge of the cell. This ensures proper delivery of proteins such as integrins to the leading edge of the cell to facilitate directional motility.

The functional significance of golgi-centrosome proximity is not fully understood. Golgi-centrosome interactions are severed by conditions which alter golgi structure. These conditions include drug-induced golgi fragmentation by use of either nocodazole (Minin, 1997) or illimaquinone (Takizawa et al., 1993) or knocking down golgi structural proteins such as Golgin-84, Golgin-160 or GMAP210 (Diao et al., 2003; Satoh et al., 2003; Yadav et al., 2012). All of these conditions lead to impaired trafficking and cell migration.

Only a few conditions have been shown to alter golgi localisation without disrupting golgi organisation. These involve two proteins - GM130 (cis-golgi protein) and AKAP450 (a scaffolding protein localised to golgi and centrosome), that have been shown to play a role in maintaining the pericentriolar localisation of golgi. Expressing the N-terminal fragment of the AKAP450, a scaffolding protein localised to golgi and centrosome, induced separation of golgi from the centrosome. This was due to the disruption of

AKAP450 -dynactin interaction. It was observed that this inhibited the cell polarisation and thus, directional cell migration(Hurtado et al., 2011).

Another study involved CRISPR-Cas9 knockout of GM130, which displaced the golgi away from the centrosome(Tormanen et al., 2019). Contrarily, in this case, it was observed that protein transport and cell migration remain unaffected. Hence the question of whether the golgi-centrosome connection is required for cell polarisation remains unanswered.

1.1.2.2 Microtubule and polarised trafficking-

The tubulin heterodimers polymerise in a polarised manner generating a growing plus end and a minus-end stably anchored to the MTOC. This intrinsic polarity of the microtubule network has been utilised by motor proteins to transport cargoes in a particular direction and location of the cell.

There are two major families of microtubule-associated motor proteins, namely kinesin and dynein. The kinesin family proteins are configured to travel towards the plus end of the microtubule and contains about 45 members(Miki et al., 2005). These members share the same motor domain but differ at the cargo binding domain(Pfister et al., 2006). In contrast, only one primary dynein form transports cargo towards the minus end of the microtubule, assisted by dynactin for cargo binding(Schroer, 2004).

In addition to the polarity, microtubule network is also asymmetric in terms of orientation, density, dynamics determined by enrichment of several PTMs and MAPs. At the cell periphery, microtubule plus end stabilisation and destabilisation by +TIPs have been shown to dictate cell polarity(van Haren et al., 2018). In the cell cortex, several factors have been implicated in modulating microtubule stability in specific regions of the cell, such as the

leading edge of the cell. Some of these factors have been shown to interact and regulate focal adhesions directly (Noordstra and Akhmanova, 2017). Adaptor proteins KANK1 has been shown to interact with talin and recruit microtubule stabilising factors such as CLASPs (Bouchet et al., 2016; Lansbergen et al., 2006). Stable microtubules tend to accumulate post-translational modifications which further enhance their stability (Magiera et al., 2018). Acetylation is one such PTM which accumulates on stable microtubules and increases its flexibility (Portran et al., 2017; Xu et al., 2017). Long-lived microtubules are preferred by Kinesin-1, which is a major transporter of exocytic vesicles (Cai et al., 2009; Guardia et al., 2016; Tas et al., 2017). Hence, preferential microtubule stabilisation creates long-lived highways for directional transport.

1.1.2.3 Golgi derived microtubule and cell polarity-

The site of microtubule nucleation modulates the geometry of the microtubule network, which in turn affects cell polarity. Unlike centrosomes, which generate a radial microtubule array, Golgi generates an asymmetric microtubule network. This has been attributed to unequal distribution of nucleating factors on the Golgi membrane and hence, increase in microtubule stability on one side of the nucleus.

Microtubules originating from golgi help in maintaining golgi structure.

CLASP dependent golgi associated microtubules aid golgi reassembly after fragmentation during mitosis and migration (Miller et al., 2009). During reassembly golgi, associated microtubules pull the ministacks together which are later transported to the pericentriolar position on the centrosomal array.

Removal of CLASP results in failed golgi clustering and accumulation of

golgi fragments near the centrosome. Although GDMTs are required for golgi reassembly, it is not required for maintenance of golgi structure(Vinogradova et al., 2012).

Recent studies have established the role of golgi derived microtubules (GDMT) in cell polarisation. It has been observed that removal of centrosome has little to no effect on endothelial cell polarisation and migration whereas loss of golgi associated microtubules lead to impaired cell polarisation and sprouting angiogenesis(Martin et al., 2018; Wu et al., 2016). A recent study showed that GDMTs is required for persistent cell migration by acting as tracks for fast cargo transport(Hao et al., 2020). This study also showed that golgi associated microtubules are more stable and have fewer lattice repairs sites compared to the centrosomal microtubules.

1.2 DNA Damage Response:

Faithful propagation of genetic material is the prime objective of all life forms. However, DNA is exposed to several endogenous and environmental insults that result in damaging the DNA. This damage if not repaired leads to a mutation which leads to disease. Nature has evolved a well-coordinated mechanism called DNA damage response to combat this threat. DNA damage response (DDR) involves detecting the damage, signalling its presence and recruiting proteins to repair the damaged DNA (Jackson and Bartek, 2009).

DDR is mainly orchestrated by a group of PI3K-like proteins that include ATM, ATR and DNA-PK. Upon DNA damage, these proteins are activated which mediate cell cycle arrest, activate DNA repair and transcriptionally regulate proteins involved in DDR(Bartek and Lukas, 2007; Patil et al., 2013). DDR is

initiated by sensor proteins which detect the aberrant DNA and phosphorylate the transducers (ATM, ATR and DNA-PK) which lead to activation of proteins such as CHK1 and CHK2, which results in cell cycle arrest, apoptosis, transcription halt and DNA repair (Marechal and Zou, 2013).

1.2.1 DNA repair pathways:

To maintain genome integrity, DNA must be protected from both environmental factors and those generated spontaneously during DNA metabolism. Spontaneous DNA damages can occur due to misincorporation of nucleotides during replication and interconversion of bases due to deamination. Additionally, oxidation of bases by ROS (Reactive oxygen species) generated during healthy cellular metabolism can also cause single-stranded breaks (SSB). Environmental DNA damage by physical and chemical genotoxic agents. Ionising radiation (Kim et al.) and Ultraviolet rays (Sauvanet et al.) can cause pyrimidine dimers, oxidise DNA bases and cause both SSB and double-stranded breaks (DSB). Chemical agents such as those used in chemotherapy alkylate the DNA bases (agents like MMS) or covalently crosslink them (agents like Mitomycin C). Cigarette smoke contains nitrosamines when metabolised forms methyl-nitrosamine derivative, which causes alkylation of DNA which leads to DNA damage.

There are six central DNA repair pathways to counter DNA damage-Base excision repair(BER), Mismatch repair(MMR), Nucleotide excision repair(Webb et al.), Translesion DNA synthesis, Nonhomologous end joining(NHEJ) and Homologous recombination(Burns et al.). While some of these pathways involve a direct protein-mediated reversal of the DNA lesion, most include a series of catalytic events. MMR repairs mismatched DNA, and

BER repairs chemical alterations in DNA base. Pyrimidine dimers and DNA strand crosslinks are tackled by NER, which excises an oligonucleotide of about 30 bp containing the damaged nucleotide. The ATR pathway handles SSBs. However, if these single-stranded DNA breaks are not repaired are converted to DSBs. DSBs are then repaired by either NHEJ or HR pathway which are governed by DNA-PK and ATM respectively.

1.2.2 Microtubule and genome maintenance:

In the recent years, the role of microtubules in genome maintenance has come into light. In 2000, Tito Fojo's group one of first links between microtubules and DDR. They observed that p53, a critical DDR protein, associates with microtubules for its nuclear translocation upon DNA damage(Giannakakou et al., 2000). Further studies from the same group showed that treatment with microtubule poisons such as Taxol and vincristine interrupts the transport of DNA repair proteins to the nucleus(Poruchynsky et al., 2015). Microtubules are physically linked to the nucleus through the LINC (Linker of Nucleoskeleton, and Cytoskeleton) complex and modulate nuclear mechanics. Microtubules interact with SUN1/2 complex of the LINC complex and increase the mobility of the damaged DNA inside the nucleus which aids DNA repair(Lottersberger et al., 2015). Another group studying DNA damage induced chromatin mobility observed that active microtubules dynamics is essential for the process(Lawrimore et al., 2017). The discovery of DNA damage inducible intranuclear microtubule filament (DIMs) added a new angle by which microtubules can influence DNA repair. Karim Mekhail's lab in 2018, showed that DIMs are formed in a Kar3 (kinesin motor) dependent manner and increase DNA mobility(Oshidari et al., 2018).

1.2.3 Effect of DNA damage on Golgi morphology:

Nuclear effects of DNA damage are well studied, which include cell cycle arrest, transcriptional activation and DNA repair. Field and group, for the first time in 2014, showed evidence of possible effects of DNA damage on cytoplasmic organelles such as Golgi(Farber-Katz et al., 2014). This study showed that exposure to agents which caused double-stranded breaks such as ionising radiation, camptothecin or doxorubicin lead to a drastic change in the Golgi morphology from the usual perinuclear ribbon to punctate fragments dispersed throughout the cytoplasm. Previous studies show that GOLPH3 (Golgi Phosphoprotein3), a phosphatidylinositol-4-phosphate binding protein localised to trans-Golgi, binds to unconventional myosin MYO18A and F-actin(Dippold et al., 2009). This interaction was shown to apply a tensile force on golgi to maintain its ribbon structure. The 2014 study mapped the signalling pathway by which DNA damage-induced Golgi dispersal(**Figure I-4**). They found that DNA-PK phosphorylates GOLPH3 at the T143 TQ site, which enhances its interaction with MYO18A-F-actin complex, resulting in increased vesiculation, fragmentation and dispersal of Golgi. This dispersal of Golgi results in impaired trafficking from Golgi to the plasma membrane. In addition to being directly phosphorylated by DNA-PK, authors also show that it binds to Ku80. Although the exact mechanism as to how a nuclear localised DNA-PK transduces the signal to a cytoplasmic effector, such as GOLPH3, remains unclear.

Furthermore, activation of this DNA-PK/GOLPH3/MYO18A pathway is essential for the survival of the cell post DNA damage. Depletion of GOLPH3 or MYO18A using shRNA mediated knockdown results in apoptosis of the cell in response to DNA damage. It is suggested that there exist critical cargo whose trafficking from Golgi to the plasma membrane is vital for the cell survival post DNA damage. However, the cargo(Farber-Katz et al.) and the pathway remains to be identified.

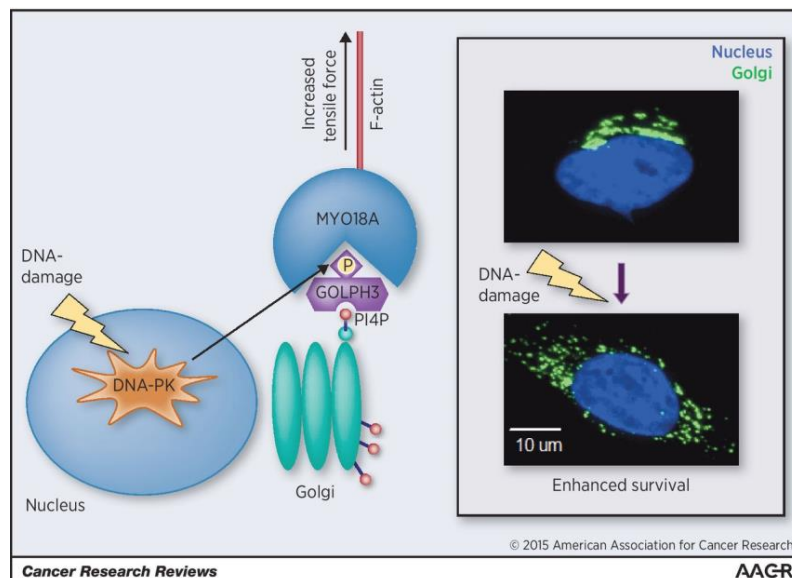


Figure I-4- Schematic is representing the mechanism of Golgi dispersal upon DNA damage. DNA damage activates DNA-PK, which phosphorylates GOLPH3. Phosphorylation of GOLPH3 strengthens its interaction with MYO18A-F-Actin, which exerts a tensile force on the Golgi leading to Golgi dispersal.

Studies from our lab further explored this effect of DNA damage by showing that DNA alkylating agent MNU resulted in activation of DNA-PK and Golgi dispersal leading to the transformation of breast epithelial cells (Anandi et al.,

2017). In addition to Golgi dispersal, a dramatic reorganisation of cytoskeleton resulting in a parallel array of microtubules and loss of actin stress fibres was observed. This project focuses on answering the questions – How and why does DNA damage lead to reorganisation of the cytoskeleton? Is there a functional relationship between Golgi dispersal and the reorganisation of microtubules? Furthermore, to characterise other phenotypes of the cell, which might be a secondary action of the cytoskeletal rearrangement. Through this project, we will be able to provide additional insight into the cytoplasmic effects of DNA damage.

CHAPTER II

Materials and Methods

2.1 Cell line and culturing methods

MCF10A was a kind gift from Prof. Raymond C. Stevens (The Scripps Research Institute, La Jolla, CA). The cells were cultured in DMEM containing high glucose and without sodium pyruvate (Invitrogen) supplemented with growth constituents comprising of - 5% horse serum (Invitrogen), 100 units/ml penicillin/streptomycin (Invitrogen), 10 mg/mL insulin (Sigma-Aldrich), 0.5 mg/mL hydrocortisone (Sigma-Aldrich), 100 ng/mL cholera toxin (Sigma-Aldrich) and 20 ng/mL EGF (Sigma-Aldrich). This media will be referred to as growth media in the further sections. During sub-culturing the cells were resuspended in DMEM containing high glucose and without sodium pyruvate (Invitrogen) supplemented with 20% horse serum and 100 units/ml penicillin/streptomycin (Invitrogen).

HEK293 was grown in DMEM containing high glucose, and sodium pyruvate (Lonza) supplemented with 10% fetal bovine serum (FBS) (Invitrogen) and 100 units/ml penicillin/streptomycin (Lonza) (referred to as complete DMEM in further text). Cells were cultured in tissue culture-treated 100mm or 60mm dishes (Eppendorf) at a 37°C humidified incubator with 5% CO₂ (Eppendorf).

2.2 Immunofluorescence

Cells were seeded at a density of 0.4×10^5 onto coverslips (Bluestar) in a 24-well dish (Eppendorf). After appropriate drug treatment, the cells were fixed with 4% paraformaldehyde. The samples were washed with PBST (PBS + 0.5% Triton-X100) and blocked with 10% FBS. Samples were then incubated in primary antibodies, diluted in 10% FBS, overnight at 4°C. Following incubation in primary antibody, cells were washed with PBST and incubated with secondary antibody (1:500) for one hour at room temperature. After a few

washes with PBST, the samples were incubated in Hoechst 33258 to stain the nucleus. Coverslips were mounted using glycerol mounting media (with 90% glycerol, 20mM Tris, pH 8.0 and 0.5% propyl gallate). All images were obtained using Leica TCS SP8 X Confocal Microscope (Leica Microsystems). Post imaging, the maximum intensity project of the stacks was used for analysis and has been represented in the figures.

2.3 Microtubule regrowth assay

The cells were grown and treated with 2.5mg/ml Nocodazole (Sigma) for 3h at 37°C to depolymerise the microtubules (Zhu and Kaverina, 2011). Following incubation, the cells were washed twice with ice-cold DPBS (Lonza) and supplemented with warm growth media. Alternatively, the cells were incubated on ice for 30mins to depolymerise microtubules. To ensure proper depolymerisation, the coverslips were transferred to a dish containing ice cold DPBS places in an ice bath for cold shock. Following both treatments, the cells were supplemented with pre-warmed media and the microtubules were allowed to repolymerise at 37°C, fixed and stained for microtubule and Golgi. The images were analysed by manually counting the number of microtubule asters in each image.

2.4 EB3 dynamics

MCF10A cells were seeded in Lab-Tek 8-well chamber cover glass (Thermo Scientific) at a density of 0.6×10^5 , treated with NEU (2mM). After 24h of treatment, the samples were transfected with the EB3-GFP construct. Transfections were performed using Lipofectamine 2000 in Opti-MEM (Invitrogen). The cells were then incubated for 4h in the transfected medium, following which the media was changed to MCF10A growth media. The cells

were imaged 24hrs after transfection in a live cell imaging chamber on Leica TCS SP8 X Confocal Microscope (Leica Microsystems). Before imaging, the cells were shifted to an L-15 medium (Lonza), and Hoechst 33342 was added to visualise the nucleus. Images were recorded at a frame rate of 1.5s per frame. The EB3 comets were manually tracked using the MTrackJ plugin (developed by E. Meijering, Biomedical Imaging Group, Erasmus Medical Center, Rotterdam) on Fiji/ImageJ (NIH)(Meijering et al., 2012).

For visualising Golgi associated microtubules, the cells were co-transfected with EB3-GFP and GalT-RFP construct. 24h after transfection, the cells were stained with Hoechst 33342 and shifted to an L-15 medium (Lonza). The cells were imaged on Leica TCS SP8 X Confocal Microscope (Leica Microsystems) at the frame rate of 5s per frame and stack size of 600nm.

2.5 Quantitative analysis

Microtubule alignment- maximum intensity z-project images of cells without and without DNA damage stained with α -tubulin, Phalloidin and Hoechst 33258 were used for this analysis. Individual cells were cropped by drawing the cell boundary using the Phalloidin channel. The cells were pasted onto a black background. The cells were rotated such that longer axis of the nucleus and thus the cell aligns to the x-axis. This would ensure that a cell which had parallel fibres, the peak would appear at 0° in the graph, for the convenience of representation. The images were analysed using the directionality tool on ImageJ.

Morphometry- the cell boundaries were drawn using the freehand drawing tool on ImageJ and shape descriptors such as area, circularity, aspect ratio was measured.

Nocodazole resistant microtubules- the microtubule fibres remaining after nocodazole treatment were detected using the Ridge detection tool on ImageJ. The maximum intensity projected images were processed using the Ridge detection tool and the count obtained were plotted

2.6 Wound healing assay

MCF10A cells were seeded at the density of 0.5×10^6 onto a 35mm dish and incubated at 37°C . Following day, the cells were treated with MNU (1mM) for 24h. The cells with and without MNU treatment were trypsinised and seeded into the Ibidi Culture Inserts at a density of 0.5×10^5 cells per well. 16h post seeding, the cells were treated with growth media without EGF for 6h followed by a treatment with 10mg/mL Mitomycin C (Sigma) for 2h. The inserts were removed and the cells were gently washed with DPBS, supplemented with growth media and the wound was imaged on Nikon Eclipse TS100 microscope using 4x and 10x objectives. The wound was subsequently imaged every 6h. The 4x images were used for analysis and the 10x was used for representation. The area of the wound was quantified using ImageJ and the percentage wound closure was calculated using the formula-

$$\% \text{ WoundClosure} = \frac{(\text{Initial wound area} - \text{Final wound area})}{(\text{Initial wound area})} \times 100$$

2.7 RUSH assay

To prepare the coverslips for low adherent HEK293 cells, they were coated with Matrigel (Corning, Sigma Aldrich) diluted with DPBS (Lonza) at a 1:50 dilution incubated for 4h at 37°C. Subsequently, the cells were seeded at a density of 0.6×10^5 and treated with NEU (2mM). After 24h of treatment, the cells were transfected with RUSH construct using bPEI25 (Sigma) using the protocol described in CYM Hsu and H Uludag, 2012(Hsu and Uludag, 2012). The RUSH constructs were a kind gift from Frank Perez (Institut Curie, Paris). Two RUSH constructs were used in this study – Str-KDEL-ManII-SBP-EGFP and Str-KDEL-SBP-EGFP-GPI. Incomplete DMEM was used as the transfection medium instead of Opti-MEM to avoid the presence of biotin. The cells were then incubated for 4h in the transfected medium, following which the media was changed to complete DMEM. 16h post-transfection, the cells were treated with 40mM of Biotin (Sigma) and incubated at 37°C. The cells were fixed at 0, 10, 20, 30, 40, 60 and 90mins.

For the GPI construct, immunostaining was performed under non-permeabilising conditions to detect the cell surface localised GPI. The samples were transferred to a dish with ice cold DPBS placed in an ice bath to stop the trafficking. Following two washes with cold PBS, the cells were incubated in anti-GFP antibody for 1h at 4°C. The cells were then washed with cold PBS and fixed with 2% PFA for 15mins on ice. After fixation the samples can be processed at room temperature. Next, the samples were given two washes with PBS and then incubated with Alexa Fluor 568 conjugated goat anti mouse secondary antibodies for 1h at room temperature.

After washes the cells were stained with Hoechst 33342 (1:10,000) for 5mins at room temperature and mounted with glycerol mounting media.

To quantify the change in trafficking of GPI to the plasma membrane, the surface GFP/total GFP was calculated. The intensity of GFP was calculated using ImageJ. The cell boundaries were manually marked and the mean grey value and integrated density was measured. The CTCF was calculated using the formula-

$$CTCF = \text{Integrated density} \\ - (\text{Area of selected cell} \\ \times \text{Mean fluorescence of Background readings})$$

2.8 Reagents table

Reagent	Source	Dilution/Concentration
Antibodies and dyes		
α -tubulin	Sigma	1:500
α -tubulin	Abcam	1:500
GM130-FITC conjugated	BD Biosciences	1:100
GM130	Abcam	1:100
Acetylated α -tubulin (K40)	Sigma; a kind gift by Jomon Joseph (NCCS, Pune)	1:500
phospho DNA-PK (T2609)	Abcam	1:200
Anti-GFP antibody	Abcam	1:1000
Hoechst 33258	Invitrogen	1:10,000

Hoechst 33342	Invitrogen	1:1000
Phalloidin (Alexa Fluor 568 or 633 conjugated)	Invitrogen	1:100
Alexa Fluor 488, 568 or 633 conjugated secondary antibodies	Invitrogen	1:500
Chemicals		
N-nitroso-N-ethylurea (NEU)	Sigma	2mM (in MCF10A) and 0.5mM (in HEK293)
DMNB	Tocris	25mM
Latrunculin A	Sigma	250nM
Biotin	Sigma	40mM
Mitomycin C	Sigma	10mg/ml

CHAPTER III

DNA damage leads to microtubule stabilisation

3.1 Background

Nuclear effects of DNA damage are well studied, which include cell cycle arrest, transcriptional activation and DNA repair. For the first time in 2014, Field and the group showed evidence of possible effects of DNA damage on cytoplasmic organelles such as Golgi (Farber-Katz et al., 2014). This study showed that exposure to agents which caused double-stranded breaks such as ionising radiation, camptothecin or doxorubicin led to a drastic change in the Golgi morphology from the usual perinuclear ribbon to punctate fragments dispersed throughout the cytoplasm. Previous studies show that GOLPH3 (Golgi Phosphoprotein3)c, a phosphatidylinositol-4-phosphate binding protein localised to trans-Golgi, binds to unconventional myosin MYO18A and F-actin (Dippold et al., 2009) This interaction was shown to apply a tensile force on golgi to maintain its ribbon structure. The 2014 study mapped the signalling pathway by which DNA damage-induced Golgi dispersal (**Figure III-1**). They found that DNA-PK phosphorylates GOLPH3 at the T143 TQ site, which enhances its interaction with the MYO18A-F-actin complex, resulting in increased vesiculation, fragmentation and dispersal of Golgi. This dispersal of Golgi results in impaired trafficking from Golgi to the plasma membrane. In addition to being directly phosphorylated by DNA-PK, authors also show that it binds to Ku80. Although the exact mechanism as to how a nuclear localised DNA-PK transduces the signal to a cytoplasmic effector, such as GOLPH3, remains unclear.

Furthermore, activation of this DNA-PK/GOLPH3/MYO18A pathway is essential for the survival of the cell post DNA damage. Depleting GOLPH3 or MYO18A using shRNA mediated knockdown results in cell apoptosis in

response to DNA damage. It is suggested that there exists critical cargo whose trafficking from Golgi to the plasma membrane is vital for the cell survival post DNA damage. However, the cargo (Farber-Katz et al., 2014) and the pathway remain to be identified.

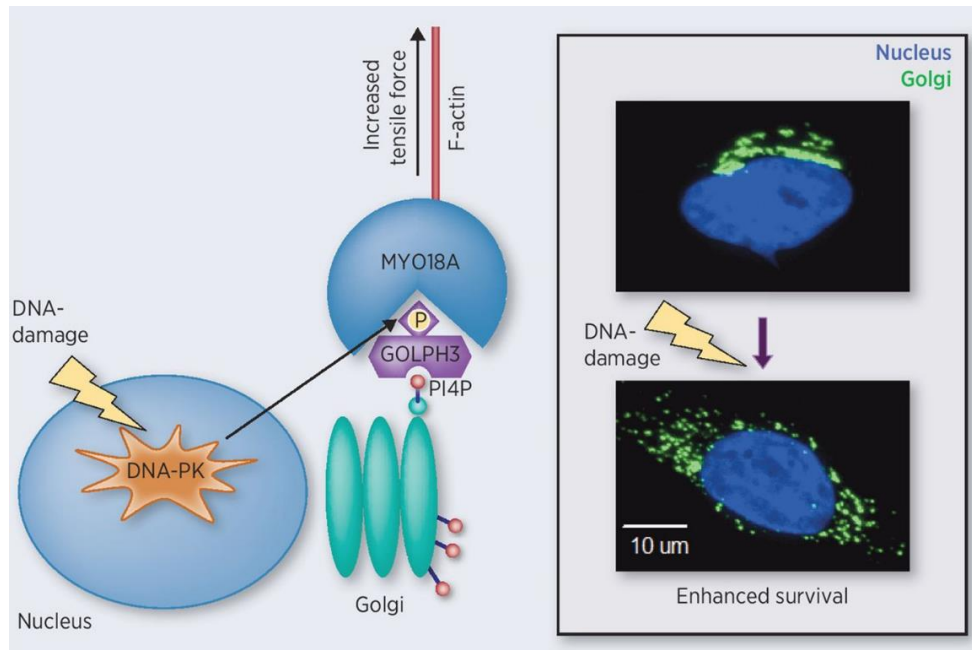


Figure III-1- Schematic represents the Golgi dispersal mechanism upon DNA damage. DNA damage activates DNA-PK, which phosphorylates GOLPH3. Phosphorylation of GOLPH3 strengthens its interaction with MYO18A-F-Actin, which exerts a tensile force on the Golgi, leading to Golgi dispersal ((Buschman et al., 2015).

Studies from our lab further explored this effect of DNA damage by showing that DNA alkylating agent MNU resulted in activation of DNA-PK and Golgi dispersal leading to the transformation of breast epithelial cells (Anandi et al., 2017). In addition to Golgi dispersal, a dramatic reorganisation of cytoskeleton resulting in a parallel array of microtubules and loss of actin stress fibres was

observed. This chapter addresses the observations made concerning changes in microtubule dynamics.

3.2 Results

3.2.1 DNA damage leads to the reorganisation of the microtubule network

MCF10A cells were treated with 1mM MNU (N-Nitroso-N-methyl urea) for 48h and stained for α -tubulin and actin to characterise DNA damage-induced changes in microtubule and actin cytoskeleton. The dose of MNU used was the same as that used in the previous study from the lab, which showed that DNA damage led to the transformation of breast epithelial cells. Upon treatment with MNU (1mM, 48h), it was observed that the microtubule network was rearranged to a more parallel array compared to the radial network in the untreated cells (**Figure III-2a**). A loss of actin stress fibres from the ventral surface of the cells was also observed upon induction of DNA damage (**Figure III 2a**). The arrangement of the microtubule was quantified using the directionality tool in ImageJ. This tool quantifies and plots the proportion of vectors in a cell aligned at a specific angle. The idea was that in a cell with a parallel array, most vectors would have a similar orientation angle and hence would show a prominent peak at a specific angle. On the other hand, in the cells with a radial array, the vectors would be equally distributed amongst all the angles. As expected, it was observed that in cells treated with MNU (1mM, 48h), there was a peak at 0° angle while the vectors were equally distributed in the untreated cells (**Figure III-2b-c**).

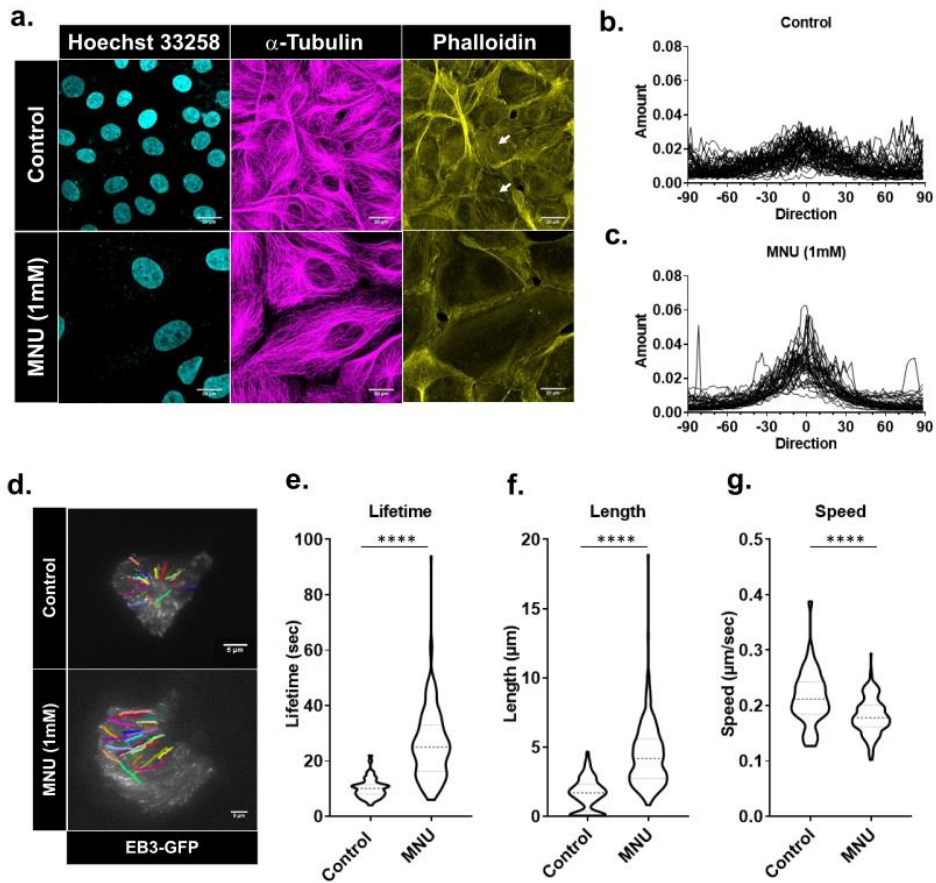


Figure III-2- MNU induced DNA damage leads to reorganisation of the cytoskeleton. (a) Treatment with MNU leads to rearrangement of microtubule cytoskeleton from a mesh-like to a more parallel arrangement and loss of actin stress fibres (N=3, n=145) Scale bar- 20 μ m. (b and c) Quantification of microtubule phenotype (N=3, n=30). The quantification of microtubule dynamics using EB3-GFP constructs shows that MNU slows down microtubule dynamics. d. represents a few microtubule tracks of cells, treated with and without MNU, labelled with EB3-GFP (Scale bar- 5 μ m); e, f and g show the graphs corresponding to microtubule lifetime, length and speed measured by tracking EB3 comets (N=3, n=120, 25 tracks per cell) . Asterisks indicate Mann-Whitney U test significance values; **** p < 0.0001.

To characterise changes in microtubule dynamics, we used a microtubule +TIP marker, EB3 (End Binding protein -3), to visualise the growing end of the microtubules. The cells with and without DNA damage were transfected with the EB3-GFP construct, and a timelapse series was imaged. The resulting images consist of a series of comet-like structures representing the plus-end of the microtubules. The microtubule comets were manually tracked using the MtrackJ plugin to measure the velocity, distance and lifetime of the comets. Polymerising microtubules detected by EB3-GFP in cells treated with DNA damaging agents were slower than control cells and displayed longer tracks (**Figure III 2d**). It was also observed that these microtubules exhibited a longer lifetime, longer length and reduced speed (**Figure III 2e-g**).

To confirm that the observed phenotype was an effect of DNA damage, we used two other DNA damaging agents- NEU (N-Nitroso-N-ethyl urea) and UV radiation. The sublethal dose of NEU and UV was standardised previously in the lab (Bodakuntla et al., 2014; J ANN, 2018), respectively. MCF10A cells were treated with NEU (2mM, 48h) and UV (10J/m², 48h) and stained for α -tubulin and actin. Similar to MNU, we observed a change in organisation and dynamics of microtubules upon NEU (Figure III-3) and UV treatment (Figure III-4)

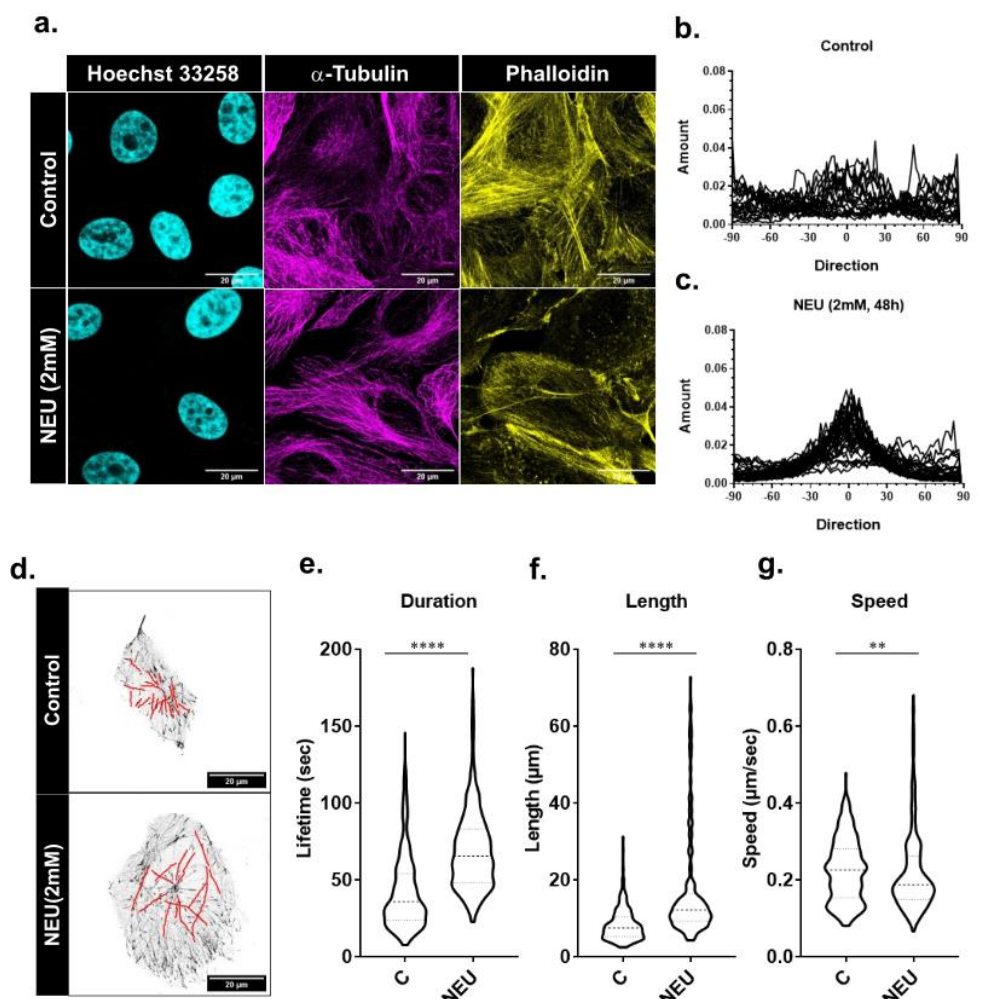


Figure III-3- NEU induced DNA damage leads to reorganisation of the cytoskeleton. (a) Treatment with NEU leads to rearrangement of microtubule cytoskeleton from a mesh-like to a more parallel arrangement and loss of actin stress fibres (N=3, n=140) Scale bar- 20 μ m. (b and c) Quantification of microtubule phenotype (N=3, n=30). Quantifying microtubule dynamics using EB3-GFP constructs shows that NEU slows down microtubule dynamics. d. represents a few microtubule tracks of cells, treated with and without NEU, labelled with EB3-GFP (Scale bar- 5 μ m); e, f and g show the graphs corresponding to microtubule lifetime, length and speed measured by tracking

EB3 comets (N=3, n=120, 25 tracks per cell). Asterisks indicate Mann-Whitney U test significance values; **** $p < 0.0001$, ** $p < 0.01$.

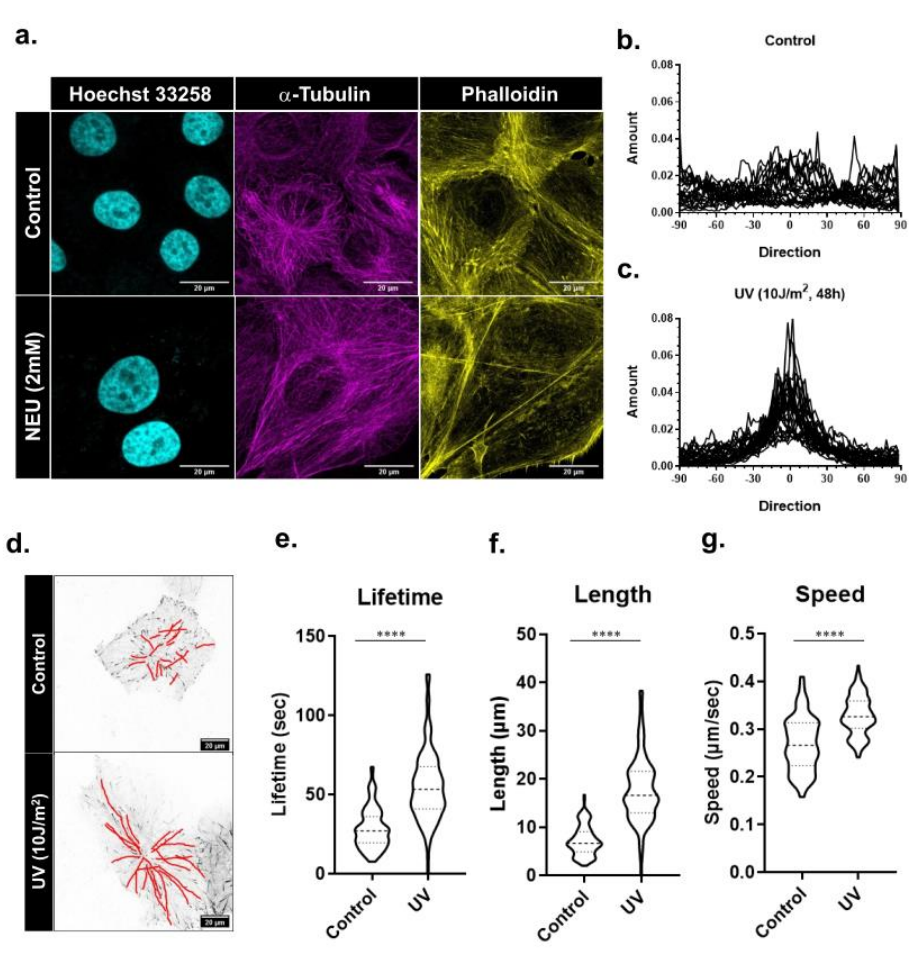


Figure III-4- UV induced DNA damage leads to reorganisation of the cytoskeleton. (a) Treatment with UV leads to rearrangement of microtubule cytoskeleton from a mesh-like to a more parallel arrangement and loss of actin stress fibres (N=3, n=130) Scale bar- 20 μ m. (b and c) Quantification of microtubule phenotype (N=3, n=30). Quantifying microtubule dynamics using EB3-GFP constructs shows that UV slows down microtubule dynamics. d. represents a few microtubule tracks of cells, treated with and without UV, labelled with EB3-GFP (Scale bar- 5 μ m) ; e, f and g show the graphs

corresponding to microtubule lifetime, length and speed measured by tracking EB3 comets (N=3, n=120, 25 tracks per cell). Asterisks indicate Mann-Whitney U test significance values; **** p < 0.0001.

Interestingly, a change in cell shape and size was observed upon DNA damage. An increase in the area occupied by the cell, a decrease in circularity and an increase in aspect ratio were observed (**Figure III-5**). Circularity and aspect ratio indicates elongation of the cell post DNA damage. Although an increase in nuclear size was observed in the images, upon quantification, we observed a decrease in the nucleo-cytoplasmic ratio (**Figure III-5**). The change in cell shape might be due to the reorganisation of the underlying cytoskeleton.

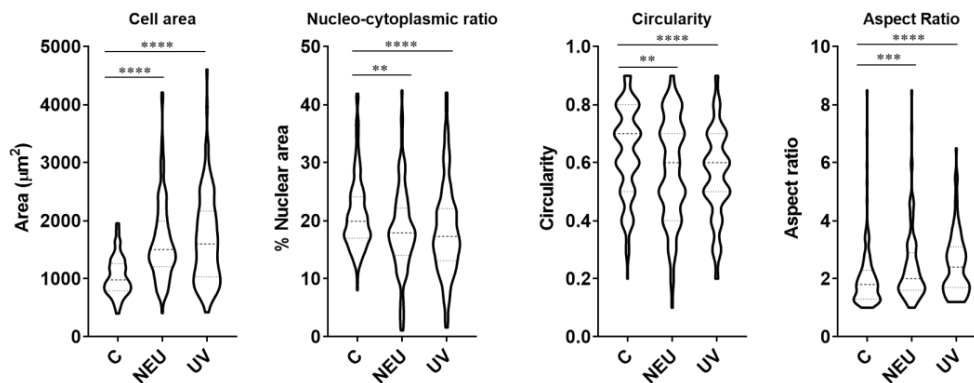


Figure III-5- DNA damage leads to an increase in area and elongation of the cell. Quantification of cell area (d.), circularity (e) and aspect ratio (f.) (N=3, n=160). Asterisks indicate Mann-Whitney U test significance values; **** p < 0.0001; *** p < 0.001; ** p < 0.01

As a complimentary method to quantifying EB3 dynamics, we examined changes in nocodazole sensitivity of cells with and without DNA damage. Nocodazole is a microtubule depolymerising agent and can be used to assess the mechanical stability of microtubules (Xu et al., 2017). After treatment with nocodazole (2.5 μ g/ml, 20mins), complete depolymerisation of microtubules was observed in untreated cells. In contrast, MNU-treated cells had a subset of microtubules which failed to depolymerise upon nocodazole treatment (**Figure III-6a-c**). Similarly, nocodazole-resistant microtubules were observed in cells treated with NEU and UV (**Figure III-6d-e**). This confirms that DNA damage leads to the stabilisation of microtubules. Please note that we had to stop using MNU for further experiments since it could not be procured in India.

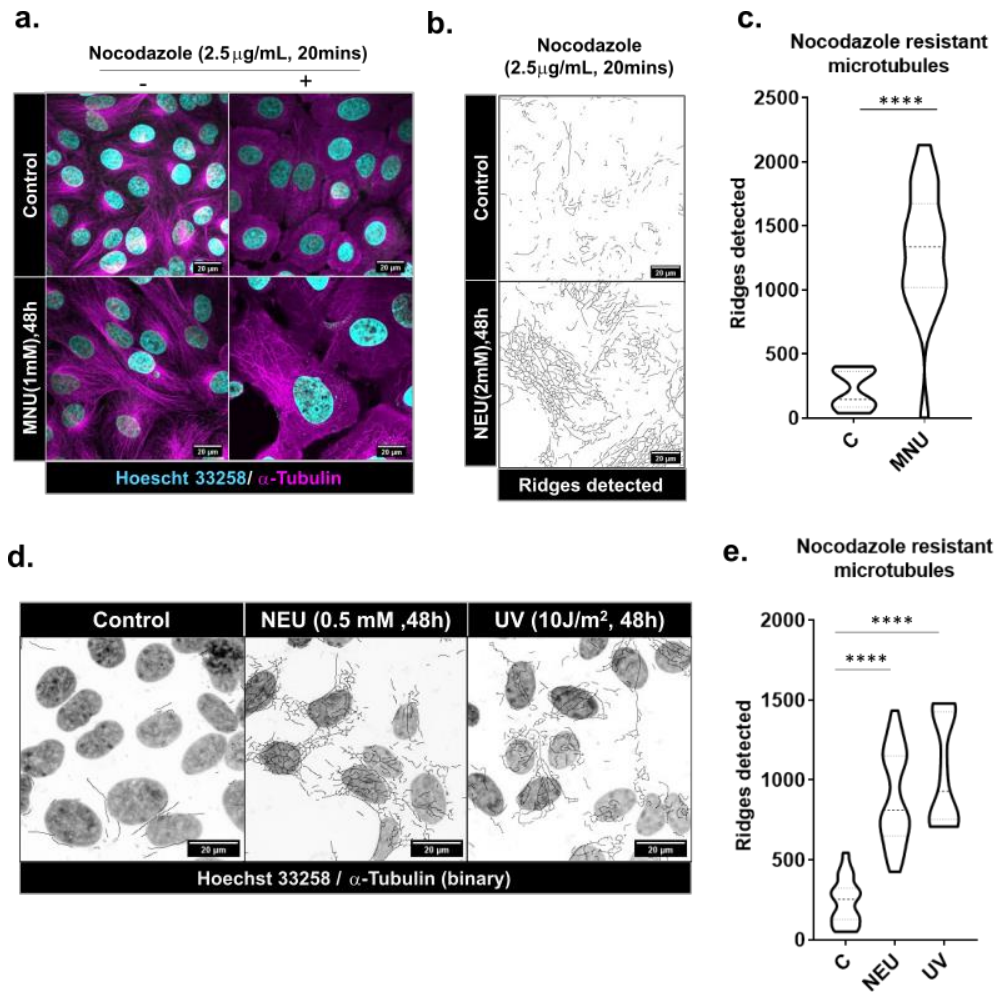


Figure III-6- Treatment with nocodazole reveals a subset of microtubules (a.) in MNU-treated cells, which are resistant to depolymerisation (N=3, n=140). Shown in b. are binary images of the subset of microtubules, quantified in c. using a ridge detection tool. Similarly, (d.) shows binary images of nocodazole-resistant microtubules in NEU and UV-treated cells (N=3, n=130), quantified in (e.). Asterisks indicate Mann-Whitney U test significance values;

**** p < 0.0001. Scale bar- 20 μm

3.2.2 DNA damage leads to an increase in tubulin acetylation

Tubulin post-translational modifications (PTMs) along with Microtubule-associated proteins (MAPs) regulate the function and dynamics of the microtubule. Upon detection of a change in dynamics of microtubules, the next step would be looking at changes in PTMs of microtubules for which changes in tubulin acetylation, deetyrosination and poly-glutamylated were tested.

We checked for changes in tubulin PTMs following DNA damage by immunostaining to address this. Simultaneously, the PTMs were probed after nocodazole treatment to evaluate if the nocodazole-resistant subset of microtubules was enriched in the specific PTM. Tubulin polyglutamylation was probed using two different antibodies to detect general glutamylation (GT335) and long chain polyglutamylation (PolyE). We detected the presence of polyglutamylation (GT335) but no change in NEU-treated cells compared to the control (**Figure III-7**). Interestingly, they were enriched on nocodazole-resistant microtubules in NEU-treated cells. Similarly, no change in long chain tubulin polyglutamylation was observed after NEU treatment, but an overall increase in polyglutamylation was observed after nocodazole treatment (**Figure III-8**). The deetyrosinated α -tubulin antibody was not IF compatible.

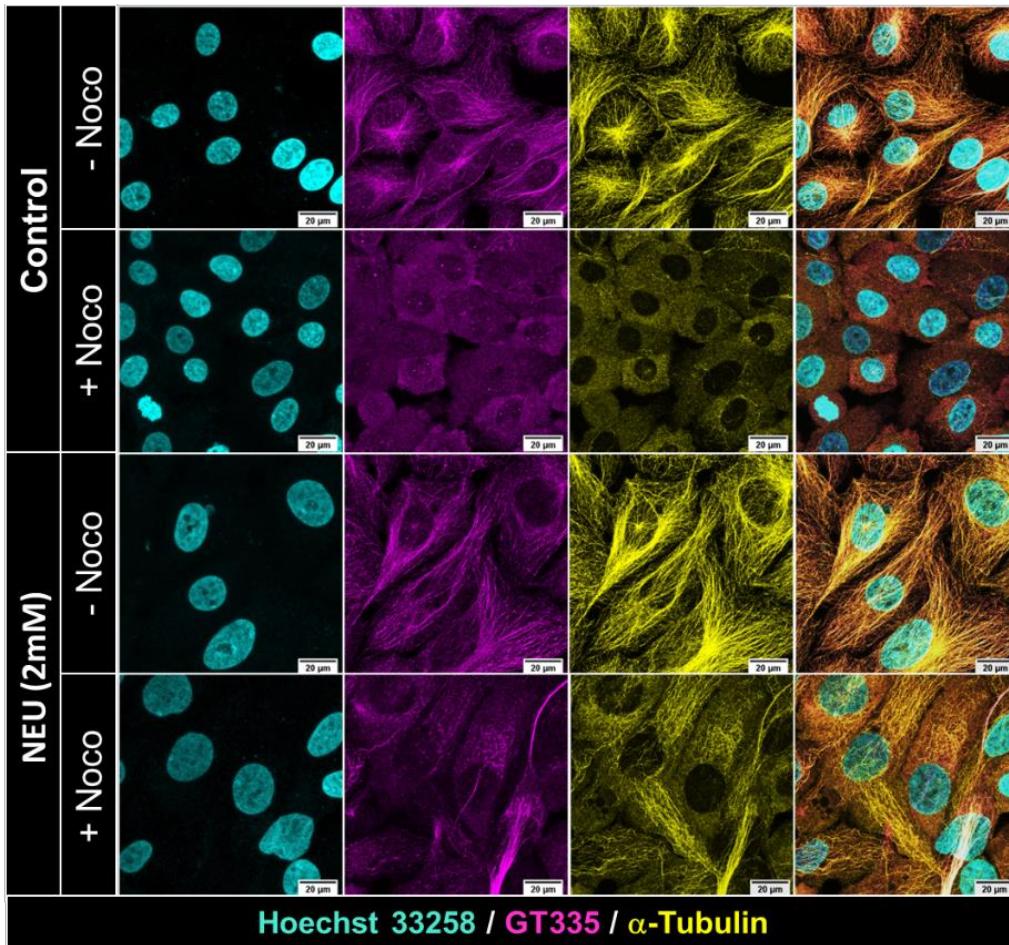


Figure III-7- MCF10A cells treated with and without NEU have poly glutamylation (GT335) shows an enrichment on nocodazole stable microtubules (N=3, n=150). GT335 is labelled in magenta, α -tubulin in yellow and nucleus in cyan. Scale bar- 20 μ m

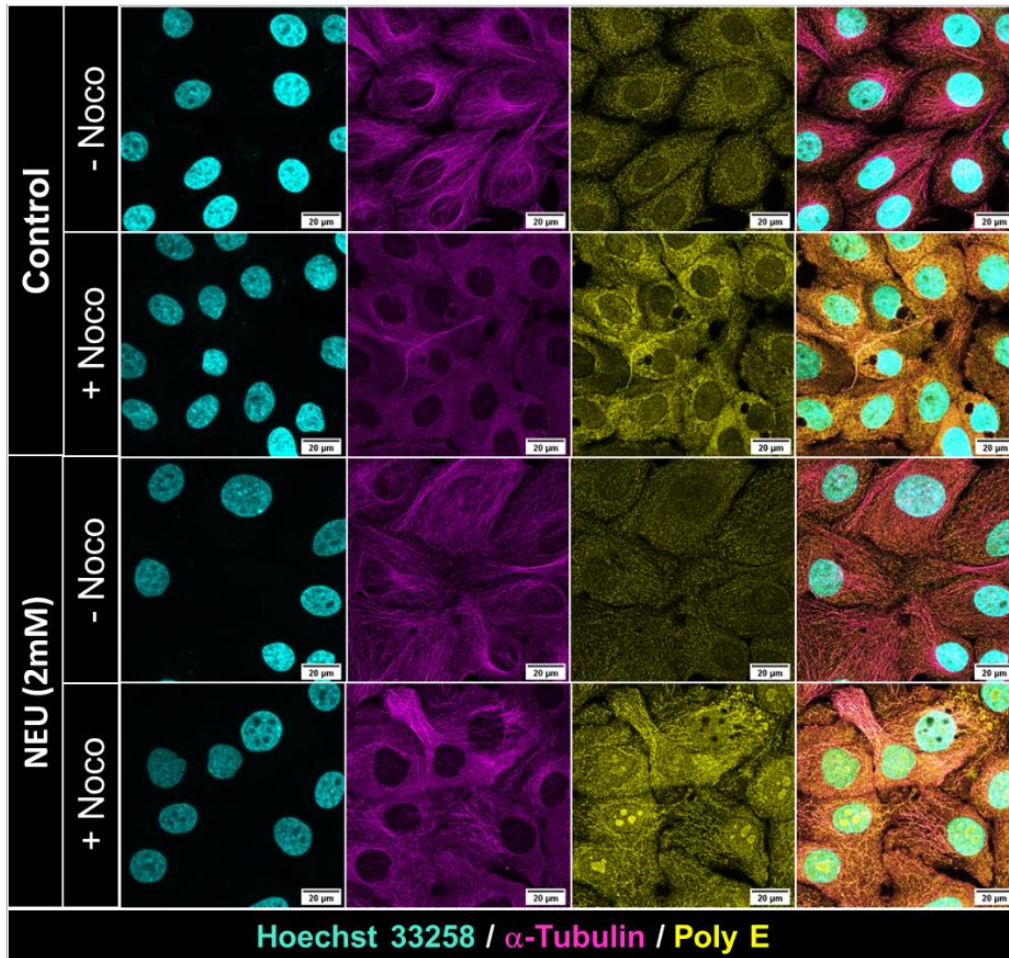
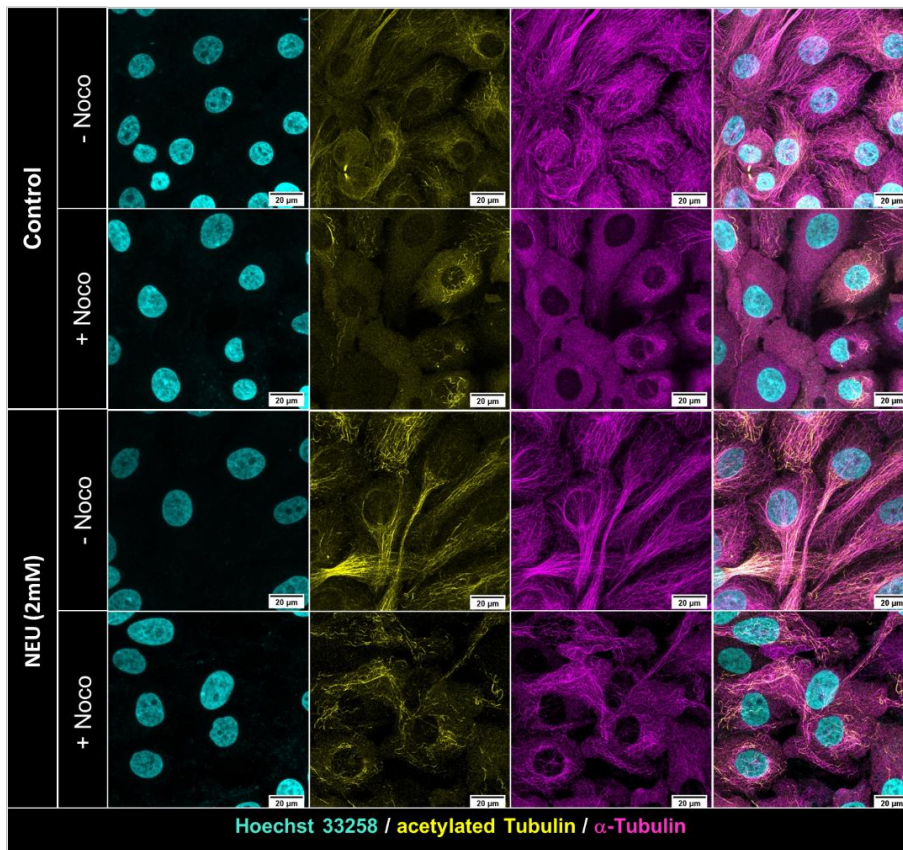


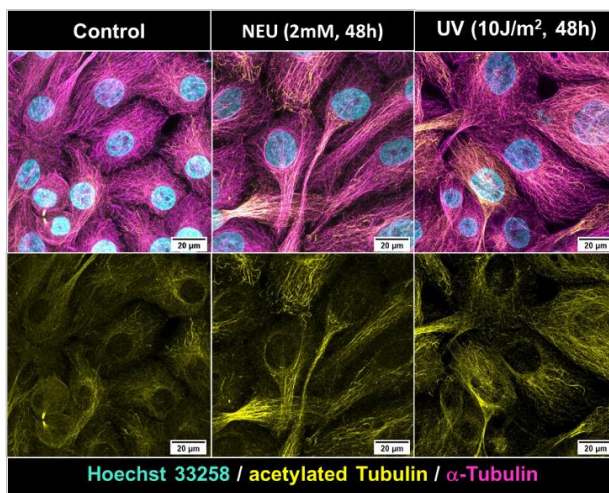
Figure III-8- MCF10A cells treated with and without NEU have very little poly glutamylation (PolyE) but show an enrichment after nocodazole stable microtubules (N=2, n=90). PolyE is labelled in yellow, α -tubulin in magenta and nucleus in cyan. Scale bar- 20 μ m

There was an increase in acetylation α -tubulin post DNA damage (**Figure III-9a**). It was also observed that the acetylation was localised to the nocodazole-resistant microtubules. An increase in tubulin acetylation was also seen after UV (10J/m², 48h) treatment (**Figure III-9b-c**).

a.



b.



c.

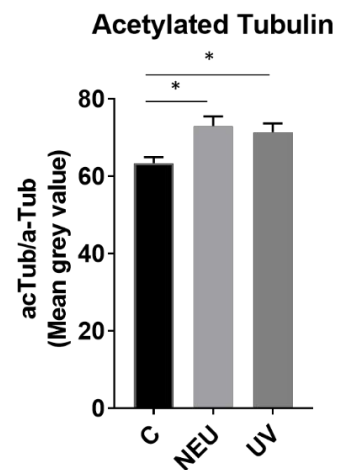


Figure III-9- DNA damage leads to increase α -tubulin acetylation at K40.

Shown in a. are cells with and without DNA damage, stained for α -tubulin K40 acetylation and α -tubulin after treatment with nocodazole (2.5 μ g/mL, 20mins)

(N=3, n=125). The nocodazole-resistant microtubules were enriched with

acetylation. (b.) An increase in K40 acetylation can be observed upon treatment with NEU (2mM, 48h) and UV (10J/m², 48h), which is quantified in c. Asterisks indicate Mann-Whitney U test significance values; * p < 0.05.

Scale bar- 20µm

3.3 Summary and discussion

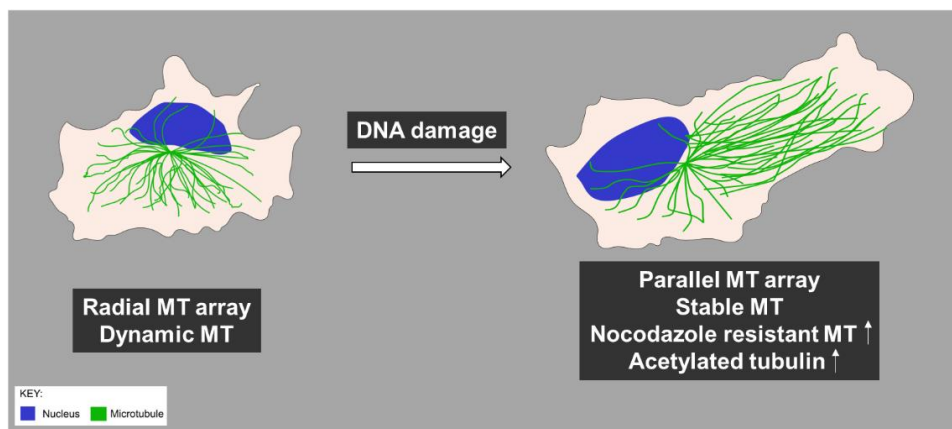


Figure III-10- Schematic summarising the results of this chapter. DNA damage leads to microtubule stabilisation. EB3 assay shows that microtubules in cells treated with a DNA damaging agent have lower speed, higher displacement and longer lifetime. A subset of microtubules remain intact upon nocodazole treatment post DNA damage. Increase in tubulin acetylation was observed upon DNA damage

In this chapter, we characterised the microtubule organisation dynamics. The microtubule phenotype was evaluated following three types of DNA damaging agents – MNU (N-Nitroso-N-methyl urea), NEU (N-Nitroso-N-ethyl urea) and UV. It was observed that following DNA damage, the microtubules were

rearranged to a parallel array compared to the radial array in untreated cells. A parallel array could signify a more polarised microtubule network. A significant increase in cell size was observed post DNA damage, and the cell adopted a more elongated morphology. These changes in cell shape can be attributed to the changes in the underlying microtubule network (Logan et al., 2018). It has been observed that an asymmetric microtubule network aids in cell elongation, which eludes to the involvement of a non-centrosomal microtubule array (Meiring et al., 2020). An increase in non-centrosomal microtubules has also been associated with increased cell size (Gavilan et al., 2018). A non-centrosomal array also supports the observation of a parallel array since a radial centrosomal array cannot form a parallel arrangement.

Upon assessing the change in dynamics using the EB3-GFP construct, it was observed that post DNA damage, the microtubules exhibited slower polymerisation rates. It was also noted that there was an increase in microtubules resistant to nocodazole treatment in cells with DNA damage. Nocodazole-resistant microtubules have often been characterised to be hyper-stable (Portran et al., 2017; Xu et al., 2017). This is in accordance with our data from the EB3 assay, where we see slower dynamics upon DNA damage. Hyper stable microtubules are enriched with acetylated or deetyrosinated tubulin or both (Portran et al., 2017; Wloga et al., 2017). Hence, we went on to check changes in levels of tubulin PTMs post DNA damage. An increase in tubulin acetylation was observed upon NEU (2mM, 48h) and UV (10J/m², 48h) treatment.

CHAPTER IV

**DNA damage leads to microtubule
stabilisation through activation of
DNA-PK and Golgi dispersal**

1.3 Background

Previous studies from our lab and Farber-Katz, et al. have established the link between DNA damage and Golgi apparatus (Anandi et al., 2017; Farber-Katz et al., 2014). Golgi and microtubules are closely associated and functionally interdependent (Sanders and Kaverina, 2015). Golgi is a dynamic structure dependent on the influx of cargo from the endoplasmic reticulum and outflux from Golgi to the destined cellular compartment (Gurel et al., 2014). The transport to and from Golgi depends on the microtubule network (Gurel et al., 2014; Vinogradova et al., 2012). The initial discovery of Golgi and microtubule interactions came from studies which looked at Golgi after disrupting the microtubule network. Microtubule poisons such as nocodazole and taxol have been shown to disperse the Golgi apparatus (Thyberg and Moskalewski, 1993; Wehland et al., 1983).

On the other hand, Golgi plays a significant role in tuning the microtubule architecture by acting as a microtubule nucleation centre (Zhu and Kaverina, 2013). The subset of microtubules originating from Golgi is polarised to the cell's leading edge and known to be dynamically stable (Chabin-Brion et al., 2001). The dynamics of the microtubule network are regulated by three interdependent factors- the site of nucleation, tubulin post-translational modifications and microtubule-associated proteins (Janke and Magiera, 2020). Results in the previous chapter have shown that DNA damage leads to microtubule stabilisation which was marked by an increase in tubulin acetylation and nocodazole-resistant microtubules. In addition, the parallel arrangement of microtubules and changes in cell architecture post DNA damage indicate the involvement of non-centrosomal microtubules.

1.4 Results

1.4.1 DNA damage-induced microtubule stabilisation is preceded by activation of DNA-PK and dispersal of Golgi

To decipher the mechanism which leads to DNA damage-induced microtubule stabilisation, we wanted to understand if the pathway described by Farber-Katz et al. 2014 was active in our scenario. MCF10A cells were treated with NEU (2mM) and UV (10J/m²) and were stained for phosphorylated DNA-PK (T2609) and Golgi. The staining was performed 48h post-treatment as changes in microtubule dynamics were observed at that time. Significant activation of DNA-PK and dispersal of Golgi were observed (**Figure IV-1a-d**). Activation of DNA-PK was quantified by counting the number of foci and plotted as average foci per nucleus (**Figure IV-1e,g**). Golgi dispersal was quantified by measuring the area occupied by Golgi fragments and plotted (**Figure IV-1f,h**).

To gain further insight into the mechanism, we wanted to place DNA-PK activation and Golgi dispersal chronologically to microtubule stabilisation post DNA damage. MCF10A cells were fixed at different timepoints post-NEU (2mM) treatment and probed for phosphorylated DNA-PK(T2609), Golgi and stable microtubules. Tubulin acetylation and nocodazole-resistant microtubules were used to mark stable microtubules. DNA-PK was activated from 10mins onwards post-NEU treatment (**Figure IV-2a-b**), followed by Golgi dispersal, which starts 4h post-NEU treatment (**Figure IV-2c-d**). Tubulin acetylation starts to increase 18h post-treatment, concomitant with the appearance of the nocodazole-resistant population of microtubules (**Figure**

IV-3). DNA-PK activation and Golgi dispersal might be involved in microtubule stabilisation post DNA damage.

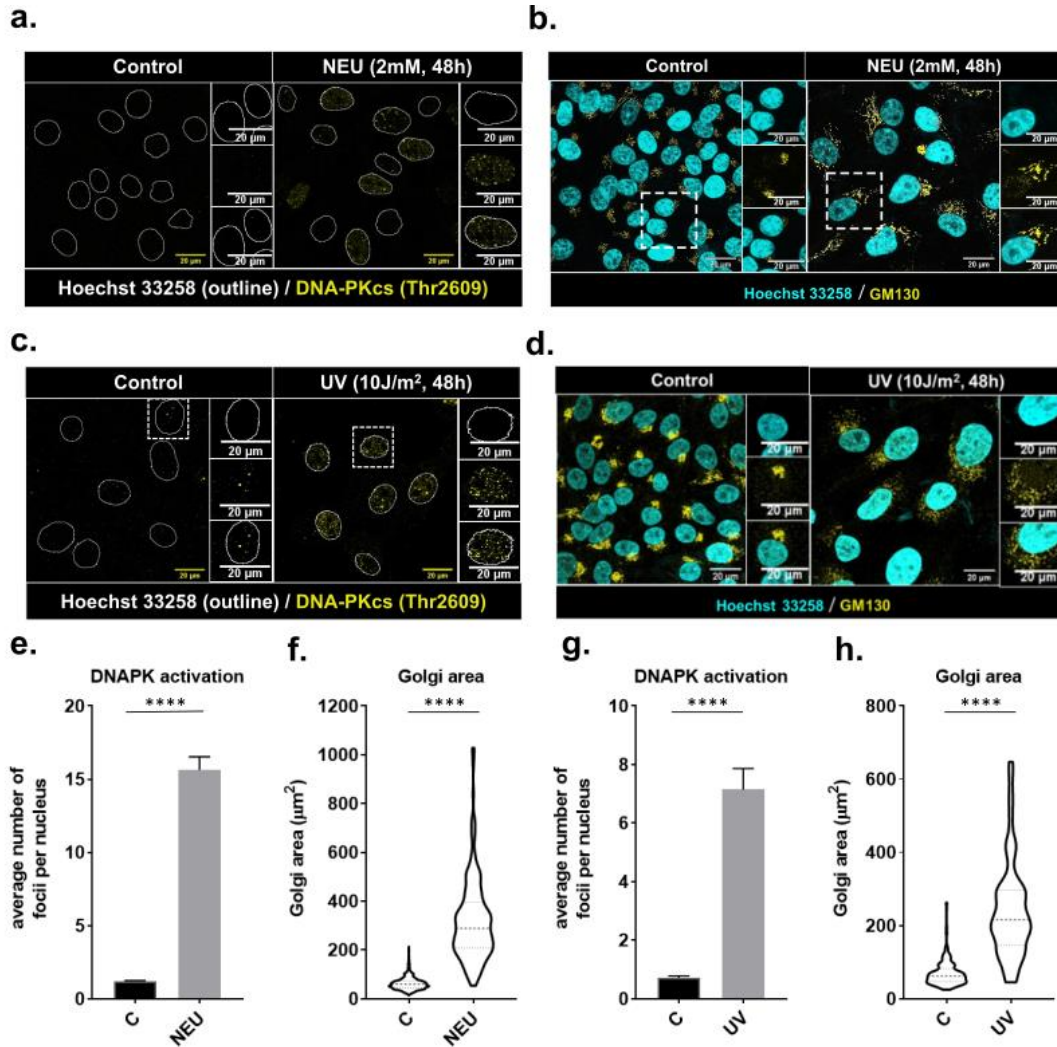


Figure IV-1: MCF10A cells treated with NEU (2mM) and UV (10J/m²) show activation of DNA-PK and Golgi dispersal (N=3, n=200). a. and c. represent cells stained for pDNA-PK (yellow) and nucleus (blue), post-NEU and UV treatments, respectively. e. and g. show plots for quantification of same. b. and d. represent cells stained for Golgi (yellow) and nucleus (cyan), post-NEU and UV treatments, respectively. f. and h. show plots for quantification of

same. Asterisks indicate Mann-Whitney U test significance values; **** p < 0.0001. Scale bar- 20µm

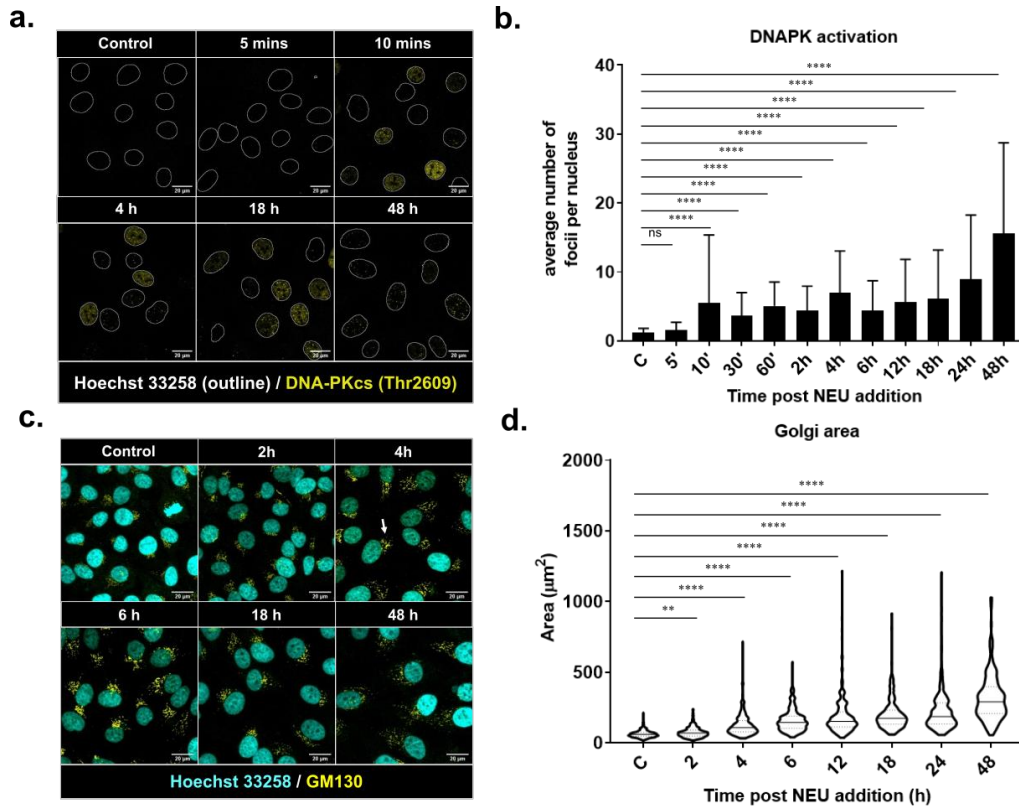


Figure IV-2: Activation of DNAPK and Golgi dispersal precedes microtubule stabilisation. Post-NEU treatment DNAPK gets phosphorylated at T2609 at 10mins and remains active till 48hrs. Shown in a. are representative images of a few selected time points after treatment with NEU(2mM). b. depicts quantification of the number of pDNAPK foci per nucleus (N=3, n=420). Asterisks indicate Kruskal-Wallis test significance values; **** p < 0.0001, ns – Non-significant. Golgi starts to disperse 4h post DNA damage, as shown in c. and d (N=3, n=220). Asterisks indicate Kruskal-Wallis test significance values; **** p < 0.0001, **p< 0.01. Scale bar- 20µm

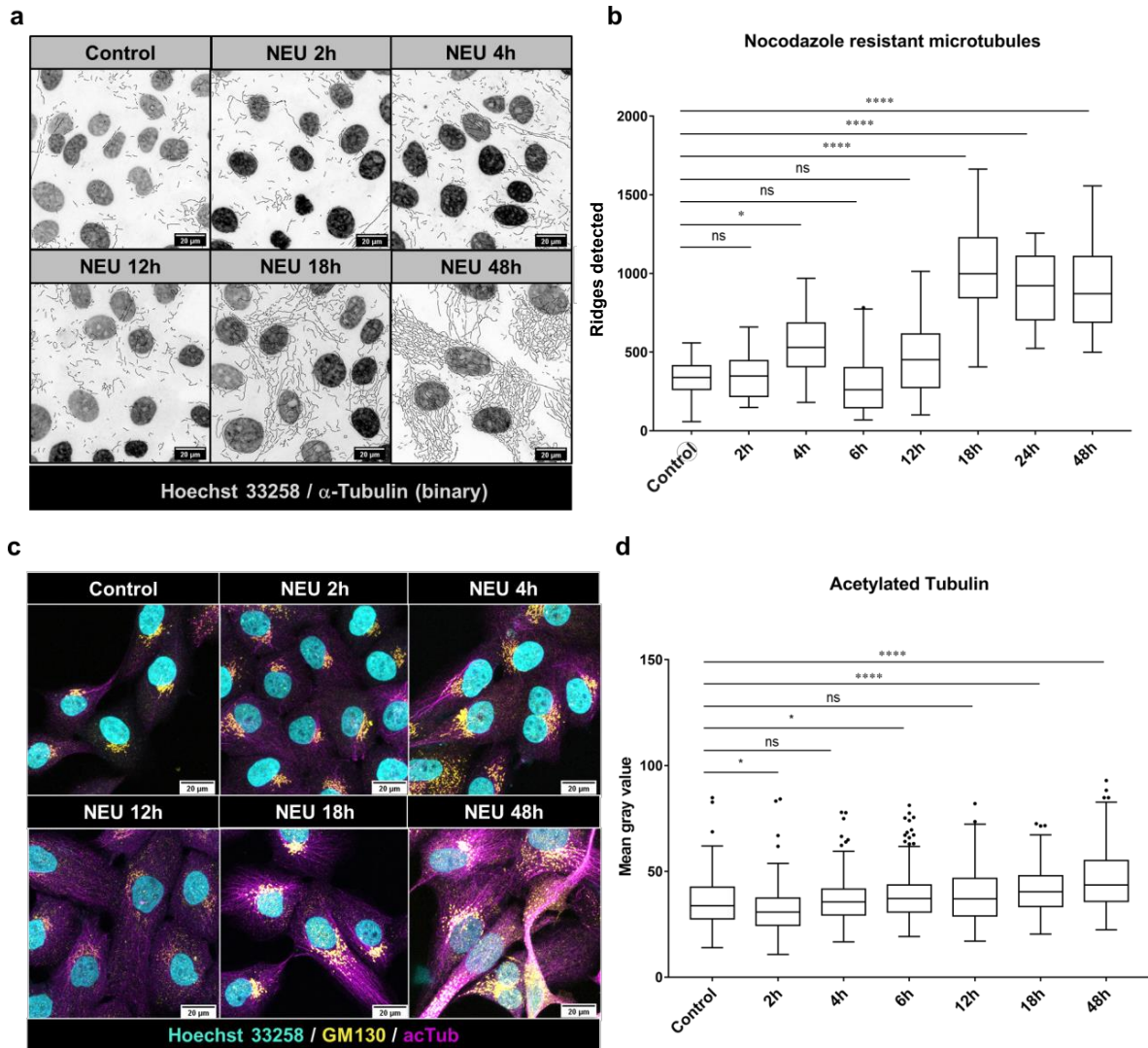


Figure IV-3-Appearance of nocodazole-resistant microtubules starts at 18h after NEU treatment. Shown in a. are binary images of tubulin and nucleus (in grey) of select timepoints post-NEU treatment. b. shows the quantification of the same using a ridge detection tool (N=3, n=240). Asterisks indicate Kruskal-Wallis test significance values; **** $p < 0.0001$, * $p < 0.05$ and ns – Non-significant. c. An increase in tubulin acetylation was observed after Golgi dispersal at 18h (N=3, n=290). d. is the quantification of the same. Asterisks indicate Kruskal-Wallis test significance values; **** $p < 0.0001$, * $p < 0.05$ and ns – Non-significant. Scale bar- 20 μ m

1.4.2 DNA damage leads to microtubule stabilisation in HEK293 cells

Additionally, to validate these results in another cell line, we used the HEK293 cell line. A sub-lethal dose of NEU required to cause the DNA-PK activation at 48h was determined. HEK293 cells were treated with 0.5mM, 1mM and 2mM of NEU, fixed 48h post-treatment and stained for pDNA-PK(T2609). A significant amount of activation was observed at 0.5mM NEU (**Figure IV-4**). Although 1mM and 2mM NEU showed DNA-PK activation, a reduction in cell number was observed upon the treatment which could be attributed to cell death.

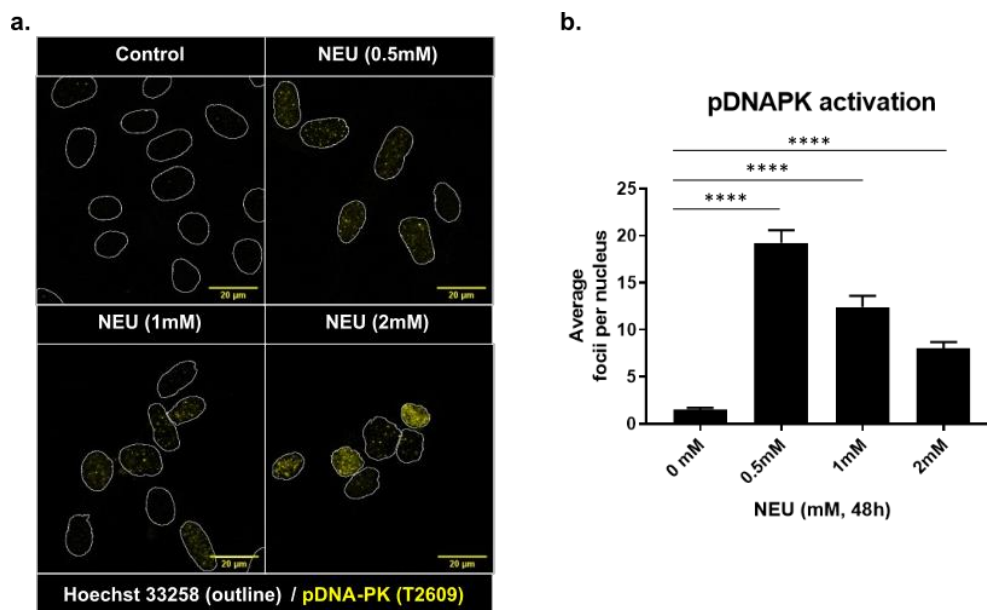


Figure IV-4: HEK293 cells treated with different doses of NEU and stained with pDNA-PK(T2609). a. Activation of DNA-PK can be observed by the presence of foci (green) in the nucleus stained with Hoechst 33258 (blue). b. depicts quantification of the number of pDNAPK foci per nucleus (N=3, n=200). Asterisks indicate Mann-Whitney U test significance values; **** $p < 0.0001$. Scale bar- 20 μ m

We used a NEU dose of 0.5mM and a UV dose of 10J/m² for further experiments. Like MCF10A, HEK293 cells showed Golgi dispersal(**Figure IV-5a-b**), an increase in acetylated tubulin (**Figure IV-5 e-f**) and nocodazole-resistant microtubules (**Figure IV-5c-d**) post DNA damage.

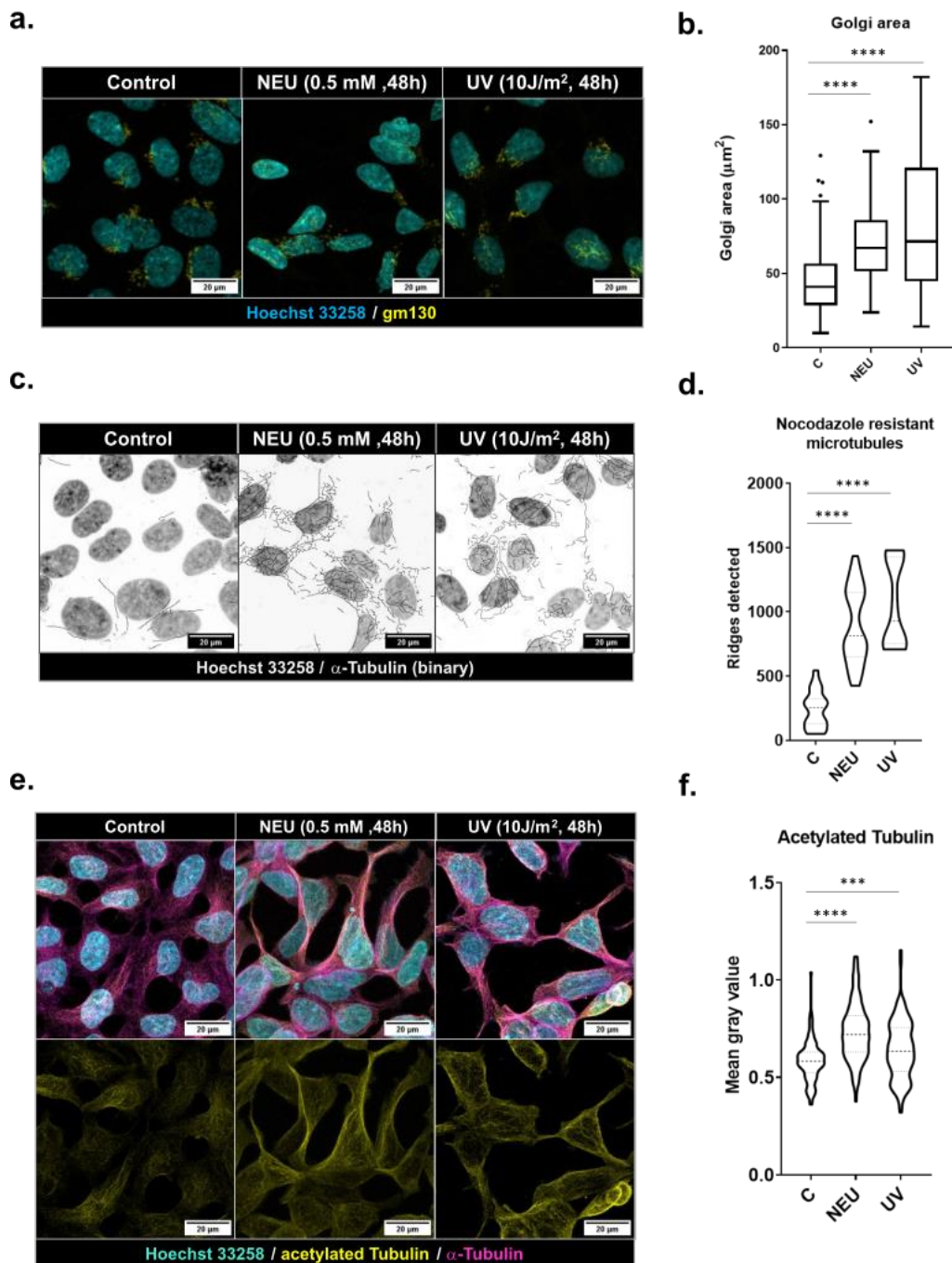


Figure IV-5: DNA damage leads to microtubule Golgi dispersal and microtubule stabilisation in HEK293 cells. a. shows cells stained with Golgi (yellow) and nucleus (cyan) post-treatment with NEU (0.5mM, 48h) and UV (10J/m², 48h). b. shows the quantification of dispersal of Golgi (N=3, n=250). Treatment with nocodazole reveals a subset of microtubules in cells with DNA

damage, which resist depolymerization (N=3, n=150). Shown in c. are binary images of the subset of microtubules and the nucleus, quantified in (d.) using ImageJ ridge detection tool. e. HEK293 cells treated with NEU (0.5mM, 48h) and UV (10J/m²) stained for α -tubulin(magenta), acetylated-Tubulin(yellow), and Hoechst 33258(cyan) show an increase in tubulin acetylation post DNA damage (N=3, n=135). f. plot represents quantification of acetylated tubulin. Asterisks indicate Mann-Whitney U test significance values; **** p < 0.0001;

*** p < 0.001. Scale bar- 20 μ m

1.4.3 Activation of DNA-PK and Golgi dispersal is required for microtubule stabilisation post DNA damage

To confirm that DNA-PK is involved in change in microtubule dynamics post DNA damage, we checked for microtubule stabilisation in the presence of a DNA-PK inhibitor (DMNB) in cells with and without DNA damage. Previous data from the lab showed that inhibition of DNA-PK with DMNB following MNU treatment showed a reversal of the Golgi dispersal and a partial reversal of the transformation phenotype (Anandi et al., 2017). Treatment with DMNB post-NEU treatment led to compaction of the Golgi apparatus (**Figure IV-6a-c**). This proves that the dispersal of Golgi post-NEU is through the DNA-PK-GOLPH3-MYO18A pathway proposed by Farber-Katz(Farber-Katz et al., 2014). Further, a reduction in tubulin acetylation and nocodazole-resistant microtubules was observed upon DMNB treatment (**Figure IV-6d-g**). This confirms the involvement of DNA-PK in microtubule stabilisation post DNA damage.

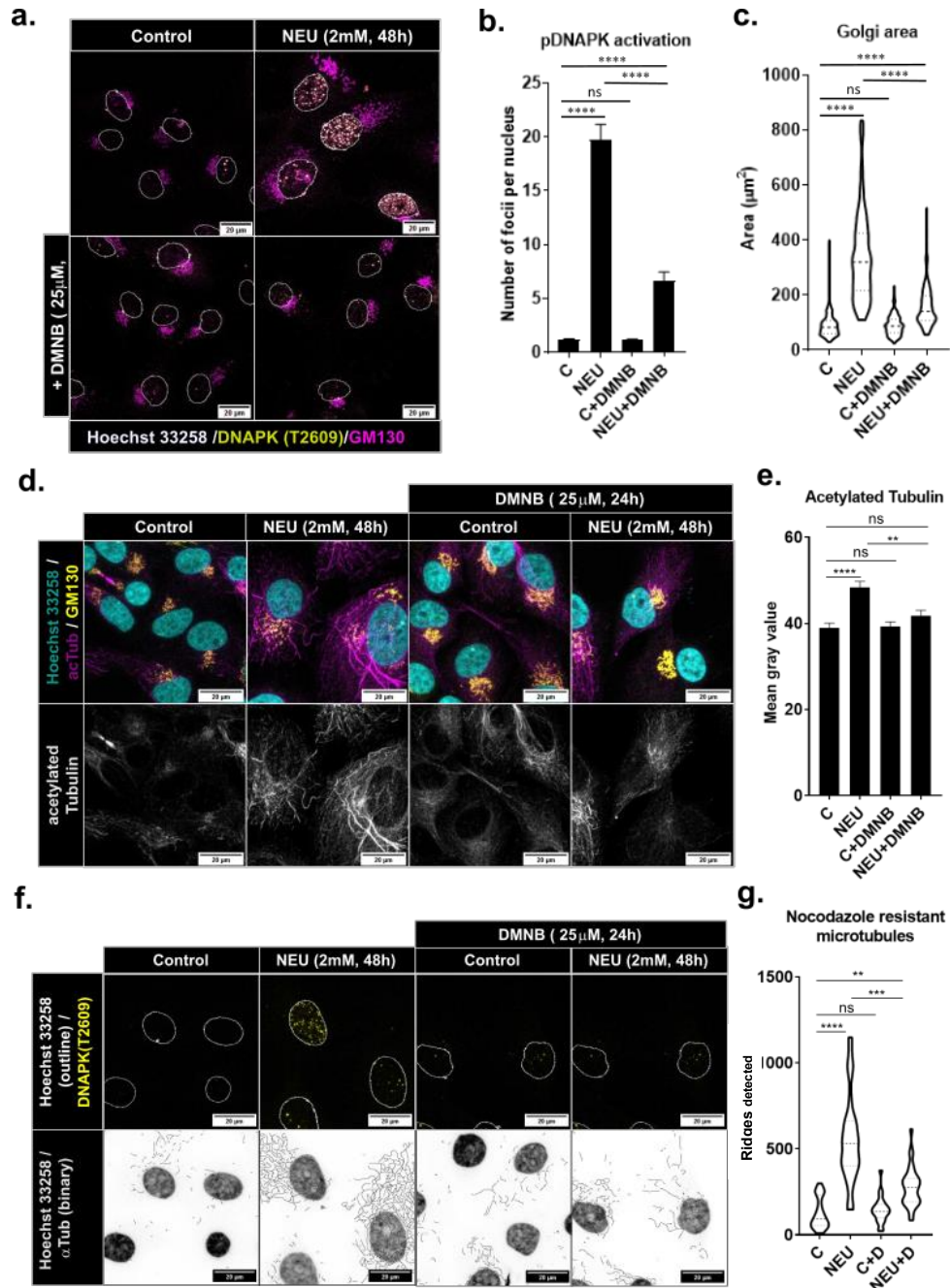


Figure IV-6- DNA damage-induced microtubule stabilisation is through activation of DNA-PK. (a) inhibition of DNAPK and reversal of golgi upon treatment with 25mM DMNB for 24h, quantified in c and d (N=3, n=100). After

NEU treatment, treatment with DMNB also reduces acetylated tubulin (N=3, n=140) (b) and nocodazole-resistant microtubules (N=3, n=140) (f), which are quantified in e and g, respectively. Asterisks indicate Kruskal-Wallis test significance values; **** $p < 0.0001$, ** $p < 0.01$ and ns – Non-significant. Scale bar- 20 μ m

To investigate if microtubule dynamics post DNA damage changes through Golgi structure disruption, we checked for microtubule stabilisation after treatment with Latrunculin A (LatA). Field and group, in their 2014 study, showed that F-actin is required for DNA damage-induced Golgi dispersal (Farber-Katz, 2014). Using LatA to depolymerise actin post DNA damage led to a reversal of the Golgi phenotype (Farber-Katz, 2014). Here we used LatA to disrupt the DNA-PK-GOLPH3-MYO18A pathway and induce Golgi compaction (**Figure IV-7a-b**). Treatment with LatA (250nM) for 6h reduced acetylated tubulin and nocodazole-resistant microtubules (**Figure IV-7c-f**). This indicates that microtubule stabilisation post DNA damage is through an alteration in Golgi structure.

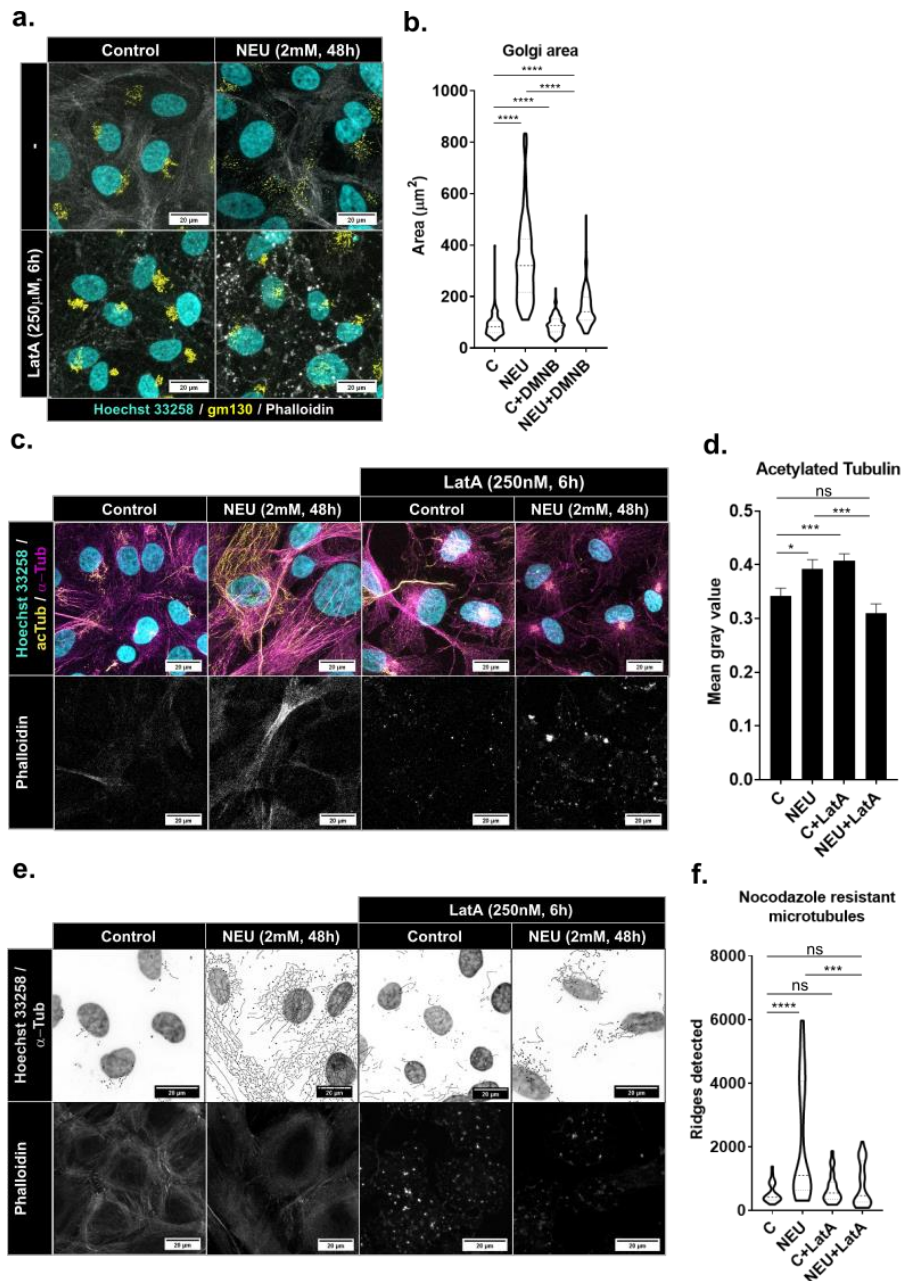


Figure IV-7- DNA damage-induced microtubule stabilisation is through golgi dispersal. (a) Depolymerisation of F-actin by LatA (250nM, 6h) leads to compaction of the dispersed golgi fragment (N=3, n=90), quantified in (b). (c) Treatment with LatA after NEU treatment leads to a reduction of acetylated tubulin (N=3, n=110) and (e) nocodazole-resistant microtubules (N=3, n=110), which are quantified in d and f, respectively. Asterisks indicate Kruskal-Wallis

test significance values; **** $p < 0.0001$, *** $p < 0.001$, ** $p < 0.01$ and ns – Non-significant. Scale bar- 20 μ m

1.4.4 DNA damage leads to an increase in Golgi-derived microtubules

As previously explained, the microtubule and Golgi association is well studied in the literature. This led us to explore if the mutual interaction between Golgi and microtubule plays a role in DNA damage-induced microtubule stabilisation. The results from the previous section indicate that Golgi dispersal precedes microtubule stabilisation and is required for microtubule stabilisation, suggesting that Golgi's reorganisation might lead to microtubule stabilisation. Further, it was observed that acetylated microtubules were closely associated with the dispersed Golgi elements (**Figure IV-8**), which indicates that they might be Golgi nucleated.

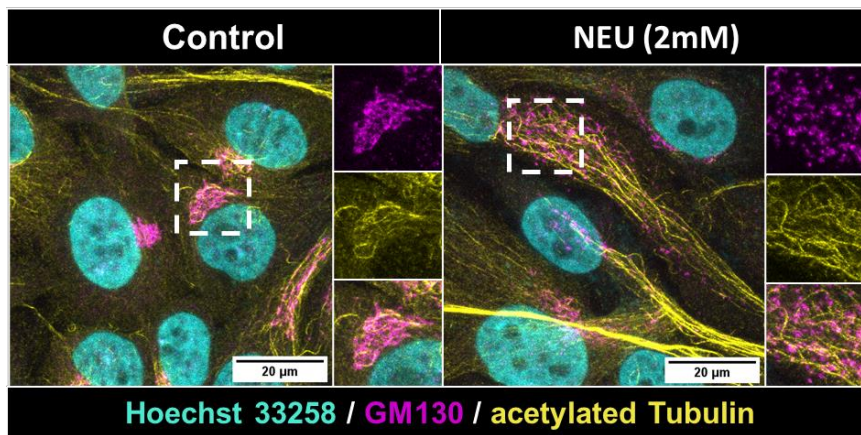


Figure IV-8- Acetylated microtubules are associated with Golgi elements (N=2, n=75). The image shows cells with and without NEU (2mM) treatment

stained for acetylated tubulin (green), Golgi (red) and nucleus (blue). Scale bar- 20 μ m

To evaluate an increase in Golgi-associated microtubule, we sought to quantify the newly originating microtubule at a steady state by using EB3-GFP to label the microtubule plus-end and GalT-RFP to label Golgi. Due to the dense microtubule network in the MCF10A cell, which is predominantly centrosomal in origin, we could not differentiate microtubules originating from the Golgi apparatus (**Figure IV-9**).

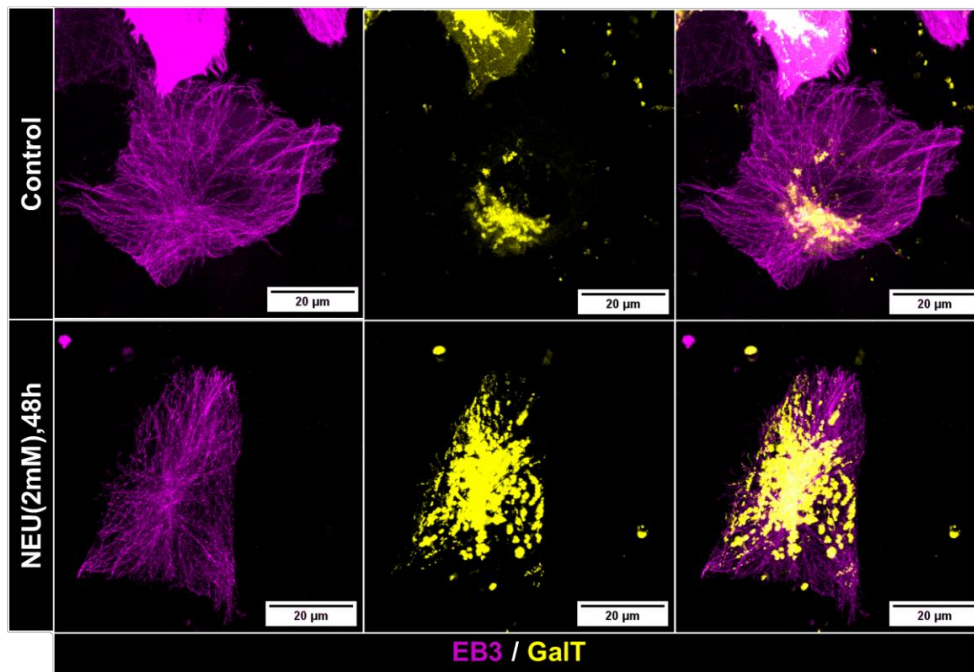


Figure IV-9- Maximum intensity project images of cells expressing EB3-GFP (green) and GalT (red). (N=1, n=10). Scale bar- 20 μ m

To circumvent this issue, we used a microtubule regrowth assay(Grimaldi et al., 2013). The assay involves depolymerising the microtubule network using either nocodazole or cold shock and letting the microtubules recover after removing the depolymerising agent. As the microtubules re-polymerise, the

site of its nucleation can be determined. Due to the presence of nocodazole-resistant microtubules, the nocodazole dose required to depolymerise microtubules completely in NEU-treated cells was standardised. The cells were treated with three different concentrations of nocodazole (2.5 $\mu\text{g}/\text{ml}$, 5 $\mu\text{g}/\text{ml}$ and 10 $\mu\text{g}/\text{ml}$) and incubated for 20mins, 60mins, 2h and 3h (**Figure IV-10**). A nocodazole concentration of 2.5 $\mu\text{g}/\text{ml}$ for 3h was finalised to be used for the assay.

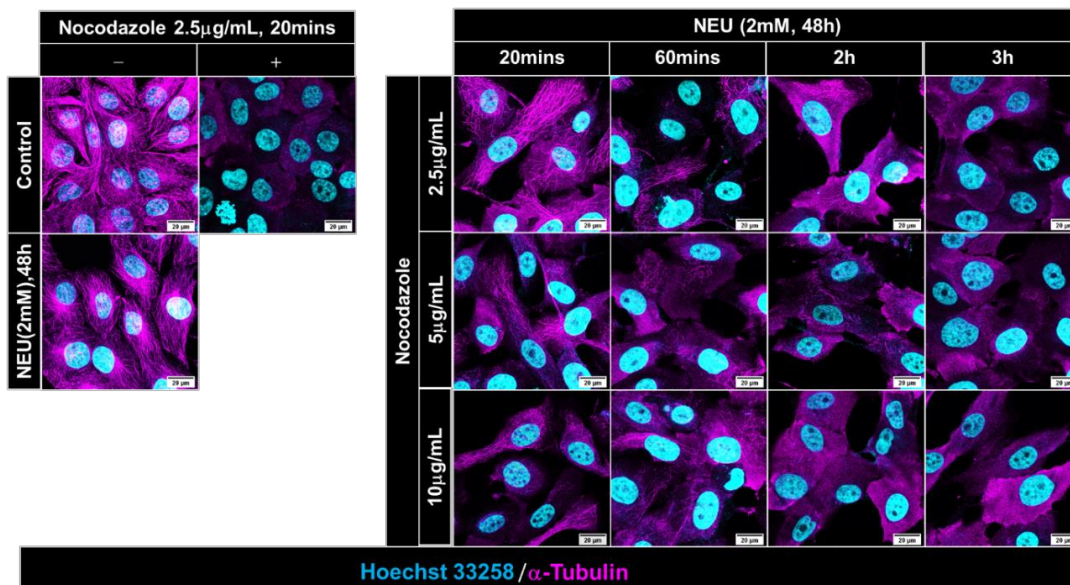


Figure IV-10- Standardisation of nocodazole dose. Images show MCF10A cells with and without NEU treatment incubated with three concentrations of nocodazole (2.5 $\mu\text{g}/\text{ml}$, 5 $\mu\text{g}/\text{ml}$ and 10 $\mu\text{g}/\text{ml}$) and incubated for 20mins, 60mins, 2h and 3h, stained for α -tubulin (magenta) and nucleus (cyan) (N=3, n=210). Scale bar- 20 μm

The cells were treated with 2.5 $\mu\text{g}/\text{ml}$ nocodazole and incubated for 3h. The nocodazole was removed, the cells were supplemented with fresh media, and

the microtubules were allowed to recover at 37°C. Cells were fixed at timepoints during the recovery and stained for tubulin and Golgi to assess the microtubules originating from Golgi. An increase in microtubule nucleation at Golgi was observed 10mins post washout (**Figure IV-11**). However, the microtubules failed to recover completely post washout (**Figure IV-12**). We suspect that the nocodazole dose used was toxic for the cells as the microtubules recovered completely in cells treated with 2.5 µg/ml nocodazole and incubated for 20mins (**Figure IV-13**). Ice was used as an alternative microtubule depolymerisation agent.

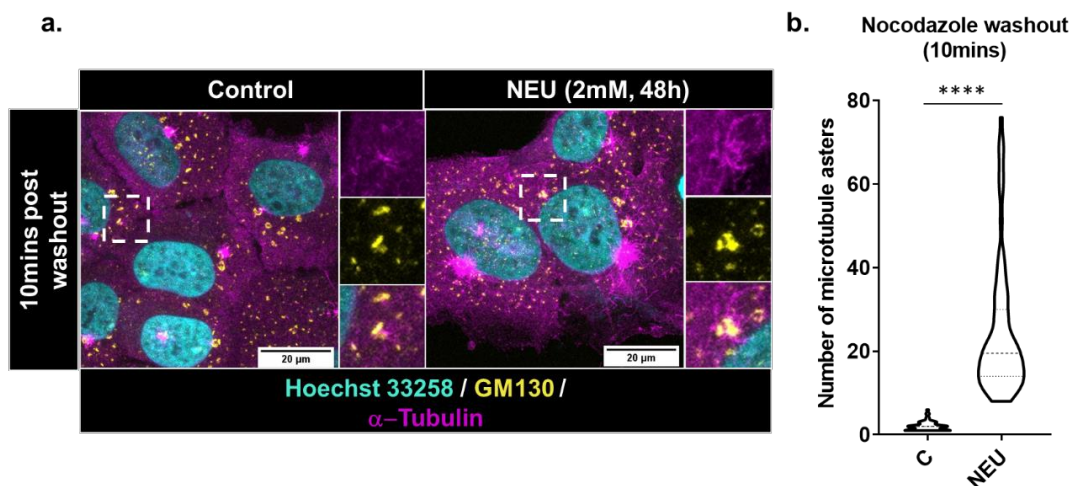


Figure IV-11- NEU induced DNA damage leads to an increase in Golgi-derived microtubules. Nocodazole washout assay was performed to determine changes in the nucleation of microtubules at Golgi. Cells were treated with 2.5µg/mL for 3h, then washed with cold PBS and supplemented with fresh media. Microtubules were allowed to recover at 37°C and fixed and stained for microtubules and Golgi. a. An increase in microtubule (magenta)

nucleation at Golgi (yellow) was observed 10mins post nocodazole washout, which was quantified (b.) by manually counting the number of nucleation sites (N=3, n=70). Asterisks indicate Mann-Whitney U test significance values; ****

p < 0.0001. Scale bar-20 μ m

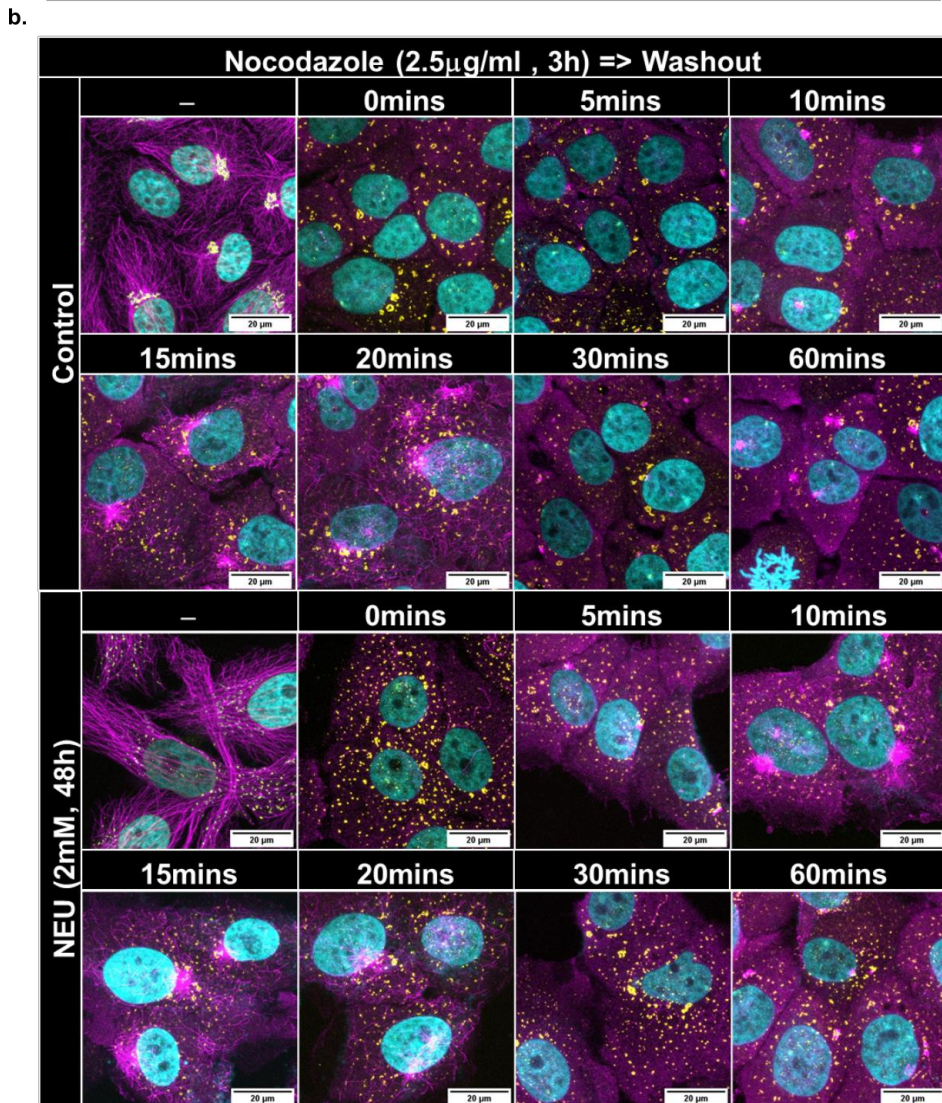
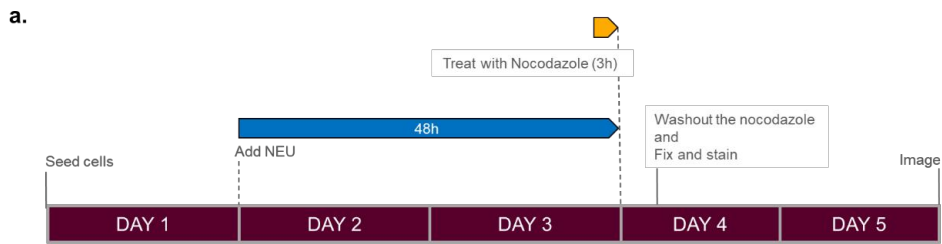


Figure IV-12- Nocodazole washout assay. a. Schematic shows the experimental timeline. The cells were treated with nocodazole for 3h and washout out. The cells were fixed at the indicated time points after washout. As seen in b., the microtubules (magenta) start to repolymerise but stop

recovering at 20mins. Depolymerized microtubules were observed at 30 and 60min timepoints. (N=4, n=150). Scale bar-20 μ m

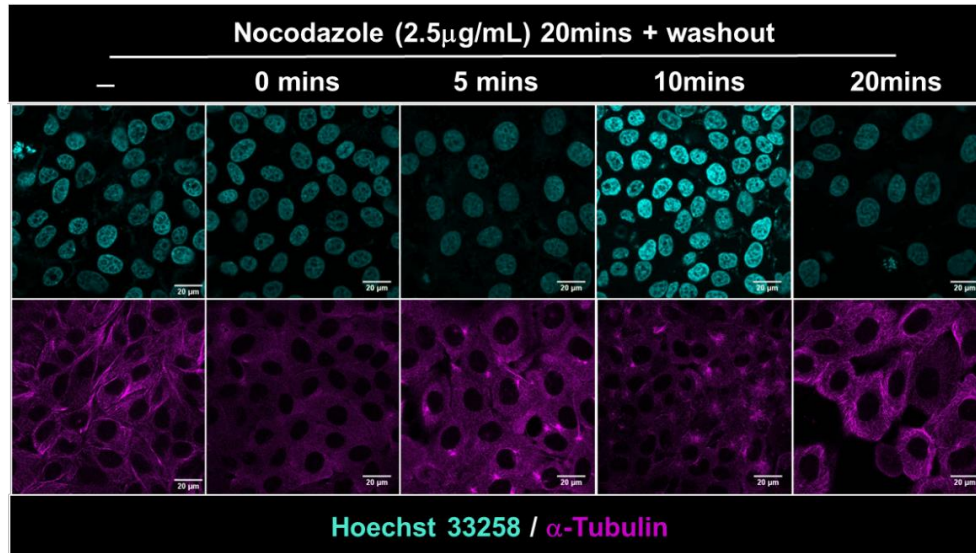


Figure IV-13- MCF10A cells treated with nocodazole (2.5 μ g/ml, 20mins) followed by nocodazole removal. The cells were then supplemented with fresh media, and the microtubules were allowed to recover at 37°C. Cells were fixed at time points during the recovery and stained for tubulin (green) and nucleus (blue). (N=2, n=200). Scale bar-20 μ m

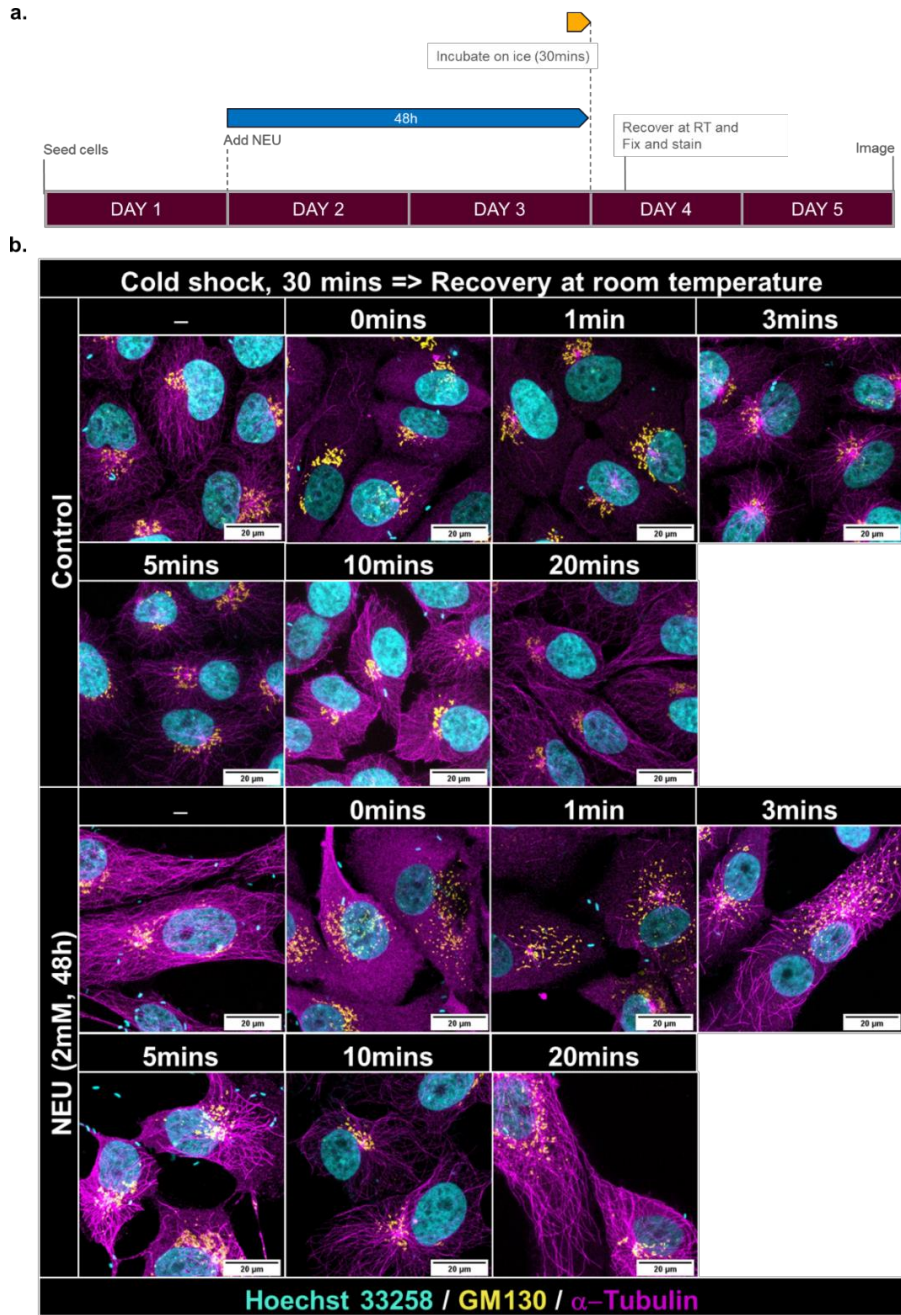


Figure IV-14- Recovery after cold shock. **a.** Schematic shows the experimental timeline. The cells were incubated on ice for 30mins and then shifted to room temperature. The cells were fixed at the indicated time points. **b.** It can be observed that the microtubules recover, and the microtubule (magenta) array is complete by 20mins. It is to be noted that the Golgi

(yellow) does not reassemble in NEU-treated cells, while it reassembles in untreated cells. (N=3, n=110). Scale bar-20 μ m

In case of recovery after cold shock, the microtubules array was restored, but there was no microtubule nucleation at Golgi (**Figure IV-14**). The absence of baseline Golgi-derived microtubules was a concern. Interestingly, NEU-treated cells failed to reassemble their Golgi despite the complete recovery of the microtubule array. Literature suggests that this indicates reduced dynein activity (Miller et al., 2009).

1.5 Summary and discussion

In this chapter, we sought to elucidate how DNA damage led to microtubule stabilisation. We observe that the NEU and UV-induced DNA damage led to Golgi dispersal through the DNA-PK-GOLPH3-MYO18A pathway (Farber-Katz et al., 2014). A reduction of acetylated tubulin and nocodazole-resistant microtubules was observed upon treatment with DMNB post induction of DNA damage. This led us to infer that DNA damage-induced microtubule stabilisation through activation of DNA-PK.

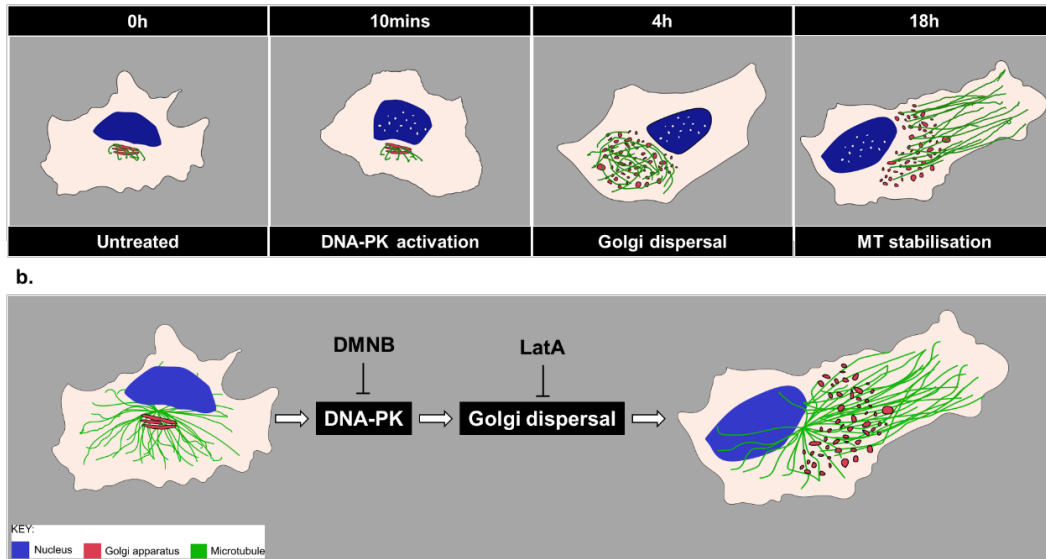


Figure IV-15- DNA-PK activation and Golgi dispersal precede microtubule stabilisation. a. following induction of DNA damage, DNA-PK activation occurs around 10mins, followed by Golgi dispersal, which occurs around 4h. Microtubule stabilisation occurs from 18h onwards. b. inhibition of activation of DNA-PK (using DMNB) and Golgi dispersal (using LatA) led to a reversal of DNA damage-induced microtubule stabilisation.

DNA-PK is known to localise to the centrosome and regulate microtubule dynamics during mitosis. DNA-PK activates Chk2-BRCA1 signalling to ensure proper spindle assembly (Shang et al., 2014). In the interphase of the cell cycle, DNA-PK has been shown to increase microtubule polymerisation from the centrosome in an Akt-dependent manner (Ma et al., 2021). These studies suggest that DNA-PK can potentially regulate microtubule dynamics directly. Alternatively, DNA-PK might be regulating microtubule dynamics by altering Golgi structure. Golgi acts as the second primary microtubule organising centre in the cell. Microtubules nucleated at the Golgi are known to be stable and enriched in tubulin, which is acetylated and detyrosinated(Chabin-Brion et

al., 2001; Skoufias et al., 1990; Thyberg and Moskalewski, 1993). We hypothesised that the stable subset of microtubules we observe post DNA damage are nucleated at the Golgi apparatus.

We used LatA, in the presence of DNA damage, to revert the Golgi to its compact peri-nuclear morphology and looked for markers of microtubule stabilisation. Treatment with LatA led to a reduction of acetylated tubulin and nocodazole-resistant microtubule. This led us to conclude that DNA damage leads to microtubule stabilisation by altering the Golgi structure. A microtubule regrowth assay was performed to confirm the increase in GDMTs, which showed an increase in microtubules arising from Golgi.

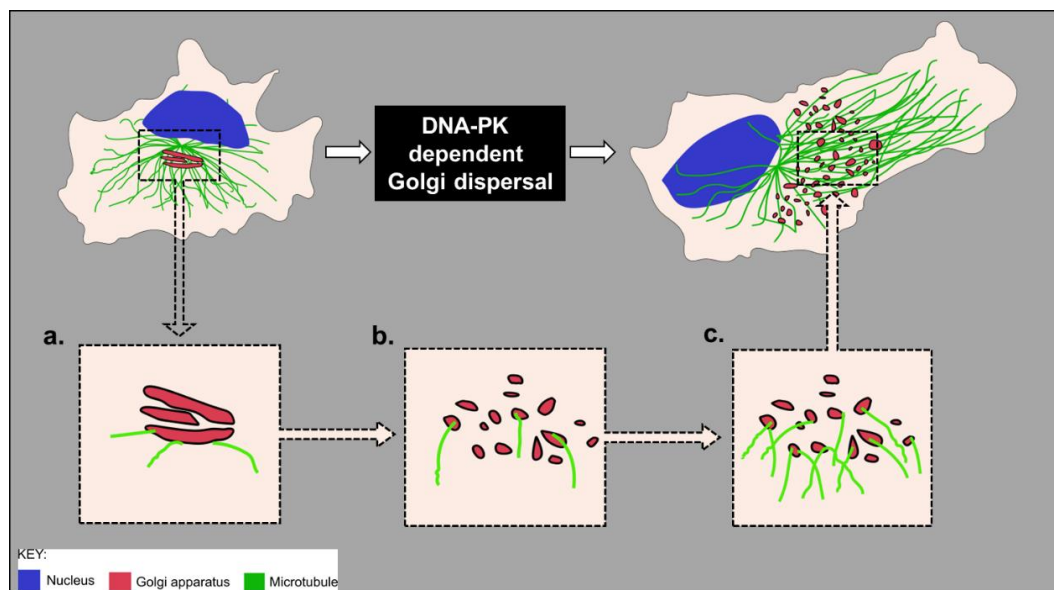


Figure IV-16- DNA damage leads to an increase in Golgi-derived microtubules. Upon treatment with a DNA damaging agent, the intact Golgi (a.) disperses (b.) in a DNA-PK-dependent manner which leads to an increase in Golgi-derived microtubules (c.) which constitute the stable subset of microtubules which are parallel.

When the ice recovery assay was performed, we observed that the Golgi apparatus failed to reassemble in cells treated with NEU despite the complete recovery of the microtubule network. This is a preliminary indication of a defect in dynein function. Further studies need to be performed to explore the possible alteration in dynein function upon DNA damage. It is also interesting to note the difference in the observations made post microtubule regrowth assay when two depolymerising agents are used.

CHAPTER V

DNA damage leads to impaired intracellular trafficking

1.6 Background

Microtubules play an essential role in critical cellular processes. They form the tracks for intracellular transport, enable polarised trafficking for cellular migration and aid in proper chromosome segregation during cell division.

The localisation and function of organelles involved in intracellular transport depend on the microtubule network(Vale, 1987). The centrosome, the primary MTOC in the cells, is often juxtaposed with the endoplasmic reticulum and Golgi apparatus, central organelles responsible for protein synthesis and transport(Rios, 2014). Altering microtubule dynamics is known to change Golgi structure and influence post Golgi transport(Skoufias et al., 1990; Thyberg and Moskalewski, 1993).

Microtubules play a crucial role in migration by regulating front-rear cell polarity and focal adhesion turnover(Vinogradova et al., 2009). Focal adhesions (FAs) are a complex of proteins which connect the actin stress fibres with the extracellular matrix through integrins. FAs turnover enables the cells to crawl during migration. Actin and FA association is well studied, whereas the association of microtubules with FAs has recently come into focus. The microtubule network has been shown to associate and regulate FA turnover physically(Etienne-Manneville, 2013; Seetharaman and Etienne-Manneville, 2019). Microtubules tethered to the FA transport aid in the transport and exocytosis of integrins, facilitating FA turnover. Interestingly, it has been found that acetylated microtubules are involved in regulating FAs(Bance et al., 2019).

In this chapter, we wanted to investigate if any of these key processes are affected by DNA damage-induced microtubule stabilisation.

1.7 Results

1.7.1 DNA damage does not lead alter collective cell migration

Previous studies from the lab, have shown that MNU induced DNA damage led to transformation of breast epithelial cells through activation of DNA-PK (Anandi et al., 2017). Cells transformed due to MNU treatment, showed an increase in migratory capacity. Although, these studies had been done using 16-day acinar cultures, we see a change in microtubule dynamics as early as 48h. We wanted to assess if these changes in microtubule dynamics could lead to changes in migration. Changes in migratory capacity of the cell at the collective cell level were assessed by performing wound healing assay. We did not observe any change in collective cell migration upon treatment with MNU (1mM, 48h) (**Figure V-1**)

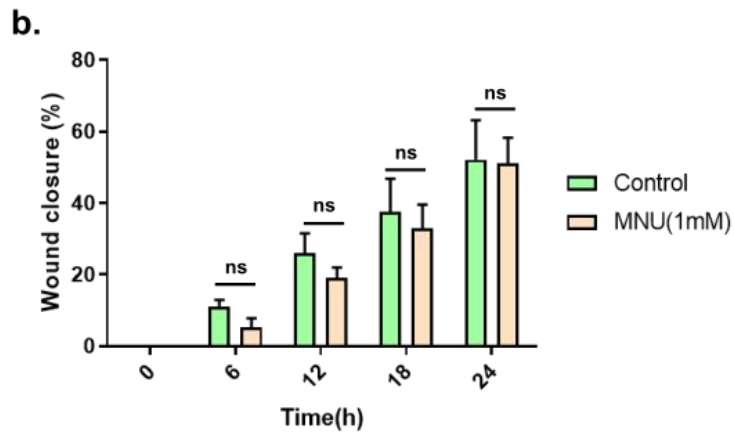
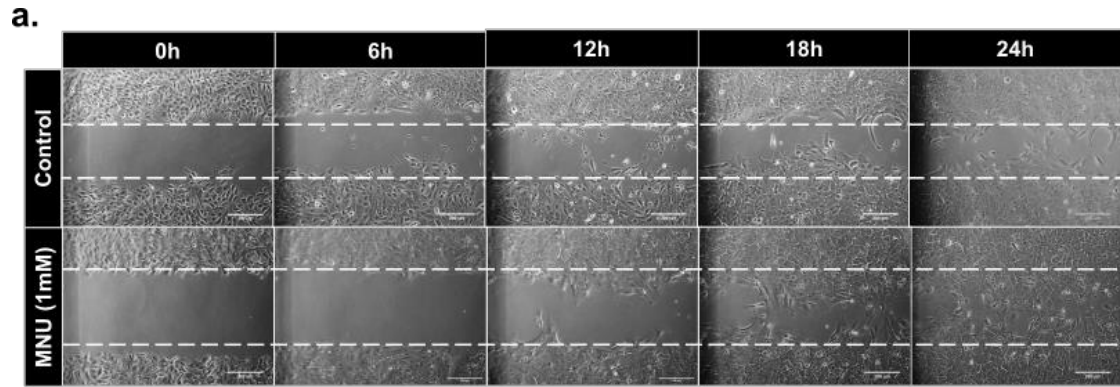


Figure V-1- DNA damage does not lead to change in collective cell migration.
 a. representative images of wound in a confluent monolayer of the cells with and without MNU treatment. Percentage wound closure has been quantified in b. Asterisks indicate Mann-Whitney U test significance values; ns- non-significant. (N=3, n=9). Scale bar-100 μ m

1.7.2 DNA damage led to mislocalisation of cell-cell junction and polarity proteins through impaired intracellular trafficking.

Studies from lab and others show that, DNA damage induced Golgi dispersal led to altered intracellular trafficking. We wanted to validate this in our system

using the RUSH (**R**etention **U**sing a **S**elective **H**ook) construct (Boncompain et al., 2012; Boncompain and Perez, 2014). Two types of reporters were used in this study – 1) ManII (α -Mannosidase II) tagged with EGFP and 2) GPI (Glycosylphosphatidylinositol) anchored EGFP. ManII is a Golgi resident protein is destined to be transported to Golgi and was used to assess ER to Golgi trafficking. GPI anchored proteins are plasma membrane associated and thus were used to study defects in Golgi to plasma membrane trafficking.

When HEK293 cells were transfected with ManII construct, the GFP signal was mainly localised to the ER. When the media was supplemented with biotin, to release the cargo, the cargo was transported to the Golgi. It was observed that the ManII reached the Golgi by 20mins while a delay was observed in NEU treated cells (**Figure V-2a**). The phenotype was quantified by plotting the percentage of cells having the signal at ER, Golgi and both at each of the time points after biotin addition (**Figure V-2b**). A delay in ManII to accumulate at Golgi implied defect in ER to Golgi transport. This observation is concomitant with the failed Golgi reassembly during recovery from cold shock.

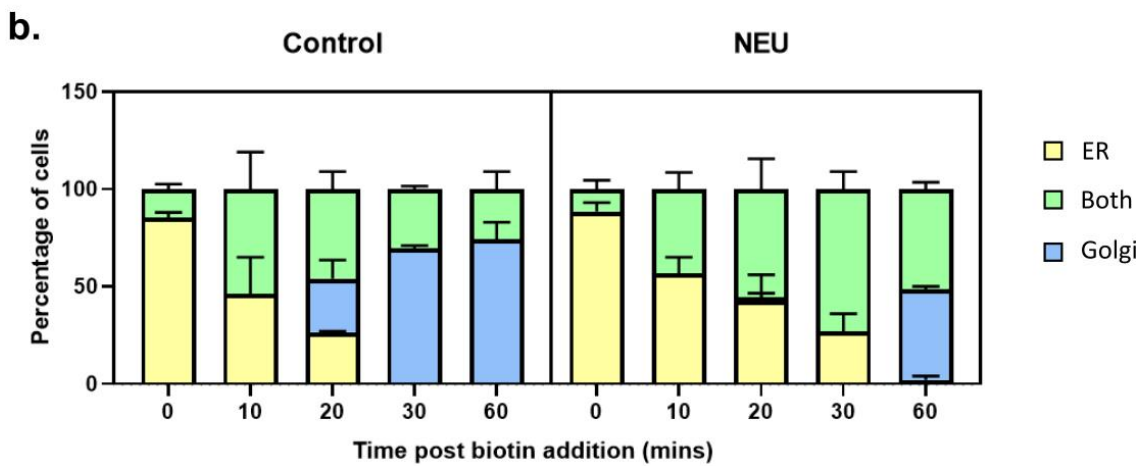
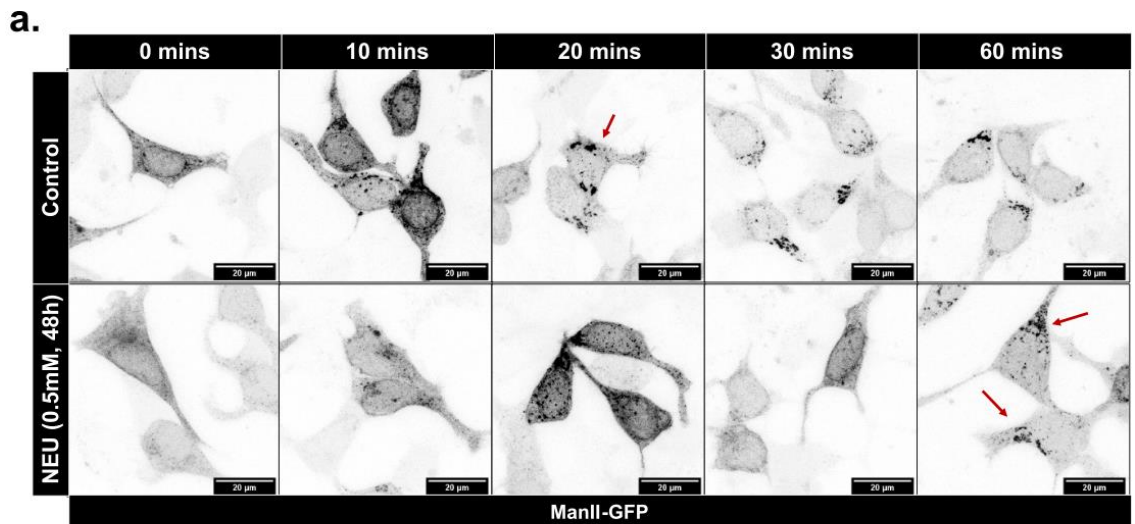


Figure V-2- DNA damage led to altered ER-Golgi trafficking. (a) delayed trafficking of ManII-GFP to golgi apparatus was observed upon induction DNA damage which has been quantified in (c). Graph represents percentage of cells showing GFP signal in ER(yellow), Golgi (blue) or both (green) at the indicated timepoints post biotin addition. (N=3, n=60). Scale bar-20 μ m

Similarly, a delayed transport of GPI anchored GFP to the plasma membrane was also observed (**Figure V-3a**), which has been quantified by measuring a

ratio of surface GFP/total GFP (**Figure V-3b**). This could be a cumulative effect of delayed ER to Golgi and post-Golgi transport.

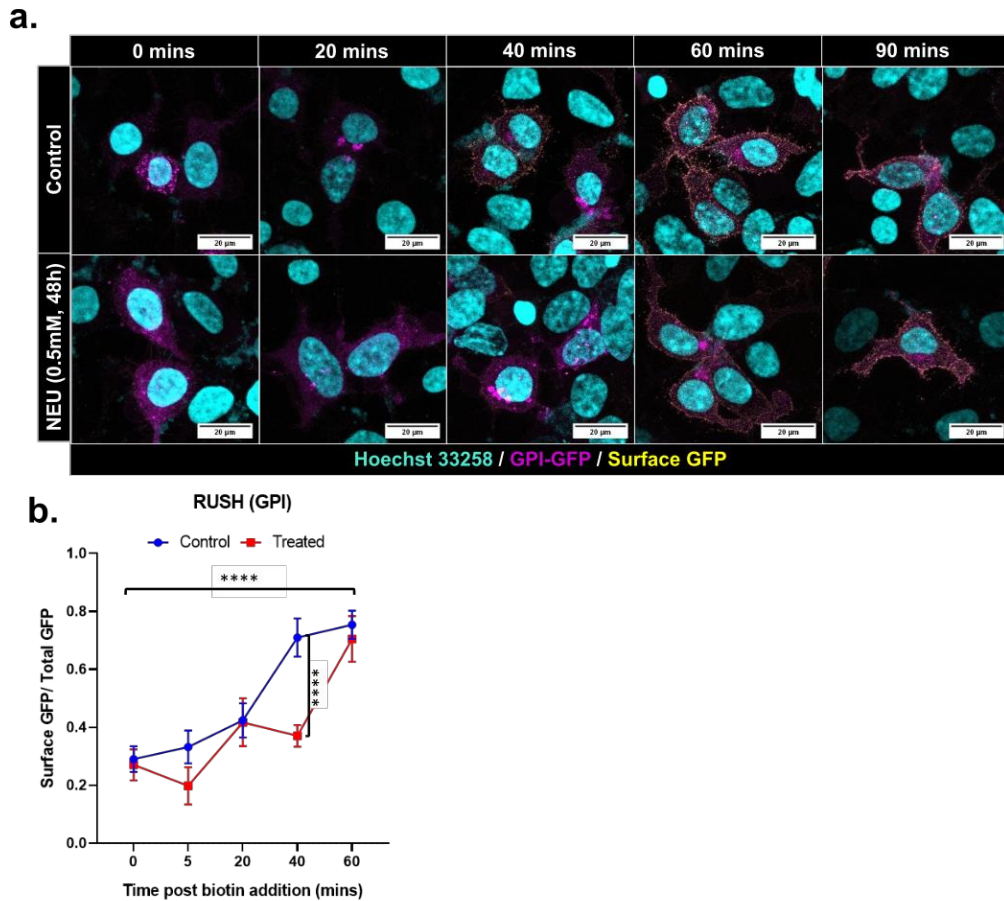


Figure V-3- DNA damage led to altered ER-Golgi trafficking. An impaired trafficking of GPI anchored EGFP was also observed (a) which has been quantified in (b). Each point in the graph represents mean \pm sem with the asterisks indicating two-way ANOVA test significance value of $p < 0.0001$.

(N=3, n=70). Scale bar-20 μ m

As previously discussed, studies from the lab have shown the role of DNA-PK in MNU induced transformation (Anandi et al., 2017). In that study, it has been shown that MNU treatment leads to aberrant Golgi phenotype accompanied by impaired trafficking. A notable loss of cell polarity was also observed, which was considered a part of malignant transformation (Anandi et al., 2017). Hence, we hypothesised that activation of DNA-PK, through changes in cytoskeleton and Golgi, was leading to impaired trafficking of polarity proteins.

Immunostaining cells with E-cadherin (**Figure V-4a**), β -catenin (**Figure V-4b**) and α 3-integrin (**Figure V-4c**), revealed mislocalisation of these proteins in the cytoplasm. Diffused staining at the junctions as well as punctate structures throughout the cytoplasm was seen in NEU treated cells as compared to a clean junctional localisation in untreated cells (**Figure V-4d-f**). This suggests impaired intracellular trafficking leading to mislocalisation of proteins destined to the plasma membrane.

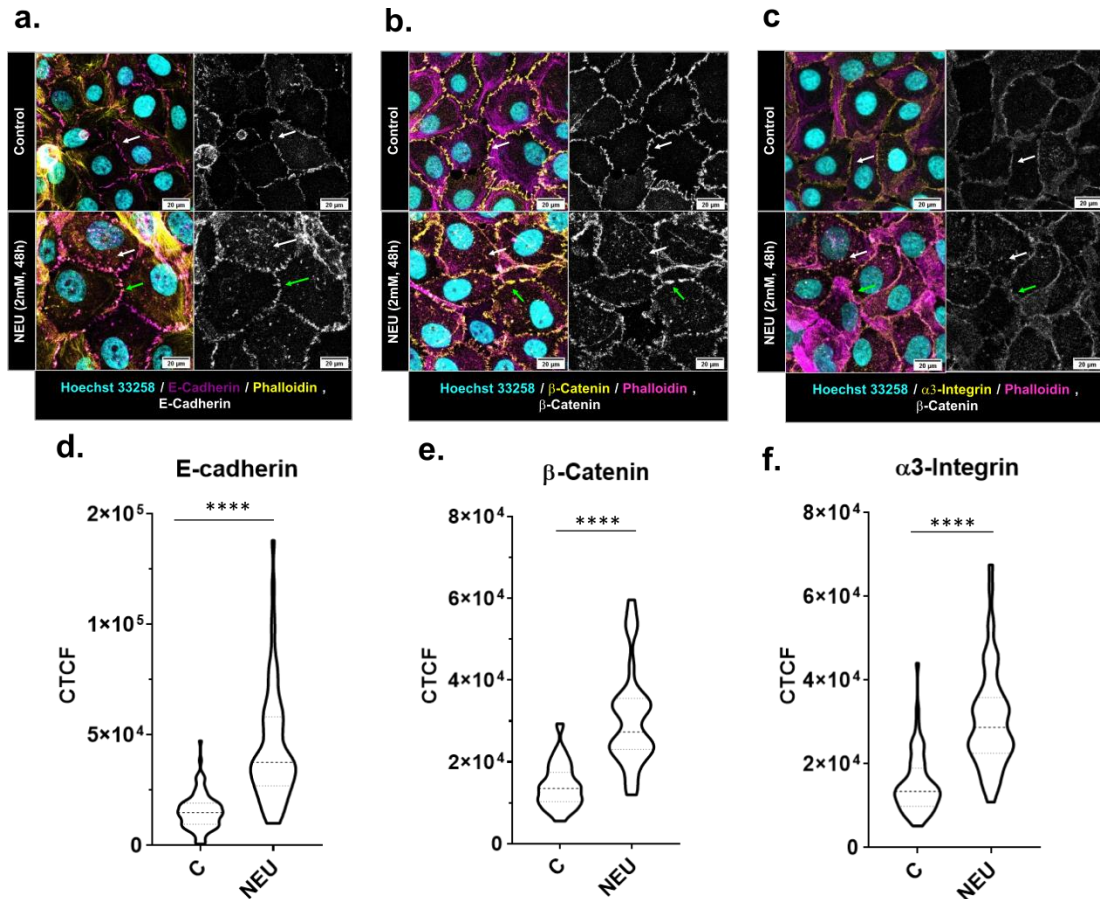


Figure V-4- Mis-localization of E-cadherin, β-Catenin and α3-Integrin post DNA damage. Immunostaining NEU treated cells for a. E-cadherin (N=3, n=64), b. β-Catenin (N=3, n=40), and c. α3-Integrin (N=3, n=56) showed an altered localisation of the cell-cell junction proteins. A pronounced distribution of the proteins in the cytoplasm (white arrow) and a diffused staining (green arrow) at the junctions was observed. The cytoplasmic proteins have been quantified by measuring CTCF (Corrected Total Cell Fluorescence) and plotted in (d-f). Asterisks indicate Mann-Whitney U test significance values;

**** $p < 0.0001$. Scale bar-20 μ m

1.7.3 DNA damage leads to a permanent change in microtubule dynamics

Long-time-course experiment was performed in which the cells were cultured after DNA damage to assess if the change in microtubule dynamics was a temporary effect of DNA damage. The cells were extracted every 3 days and immuno-stained for pDNA-PK(T2609), Golgi, acetylated microtubules and nocodazole resistant microtubules. It was observed the DNA-PK was active till day 9 (**Figure V-5**) along with a dispersed Golgi apparatus (**Figure V-6**). Interestingly, microtubules remained stabilised till day 9 long after the initial dose of NEU has been washed away (**Figure V-7;Figure V-8**). We could not examine microtubule stabilisation in cells further than 10days as MCF10A cannot be kept in continuous culture for more than 10days.

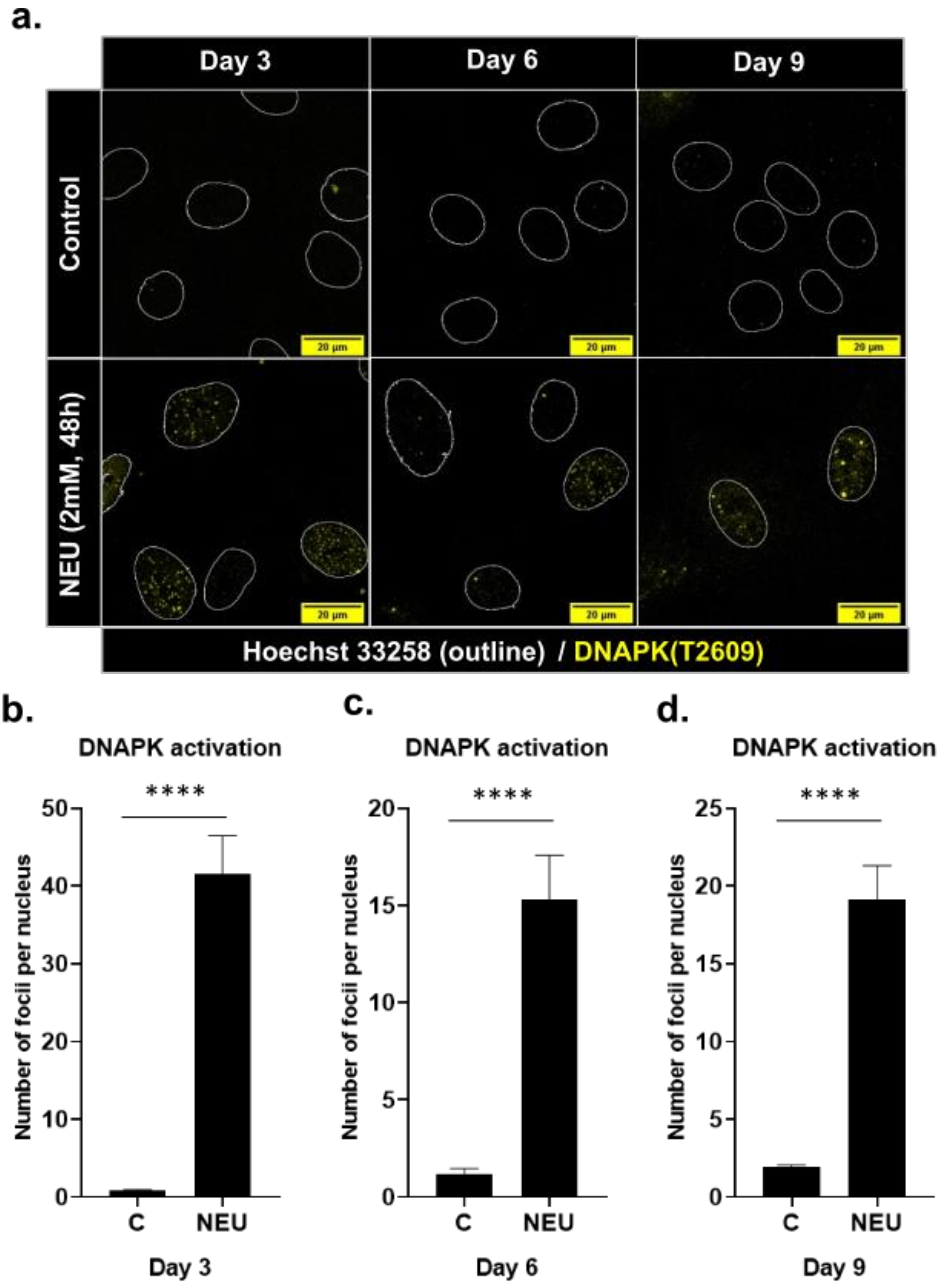


Figure V-5- Long-time course experiment shows activation of DNA-PK till day 9. Images showing pDNA-PK(T2609) foci (yellow) against nucleus (blue). The foci have been quantified per day (b-d). Asterisks indicate Mann-Whitney U test significance values; **** $p < 0.0001$ (N=2, n=80). Scale bar-20 μ m

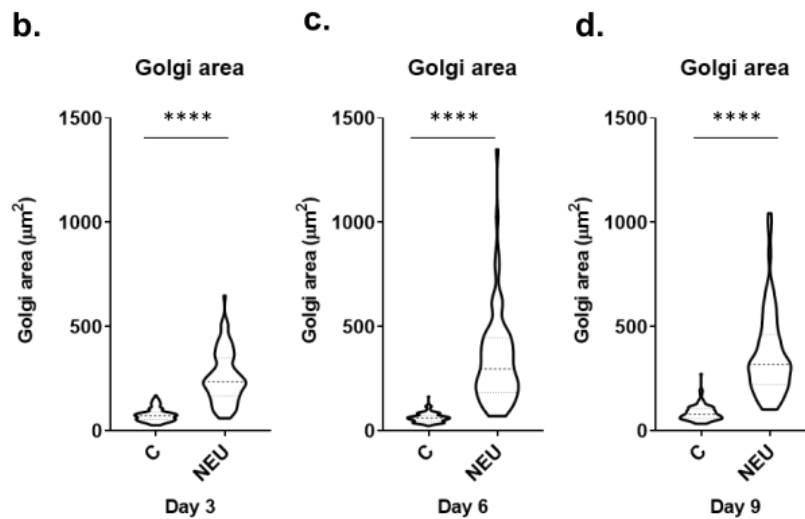
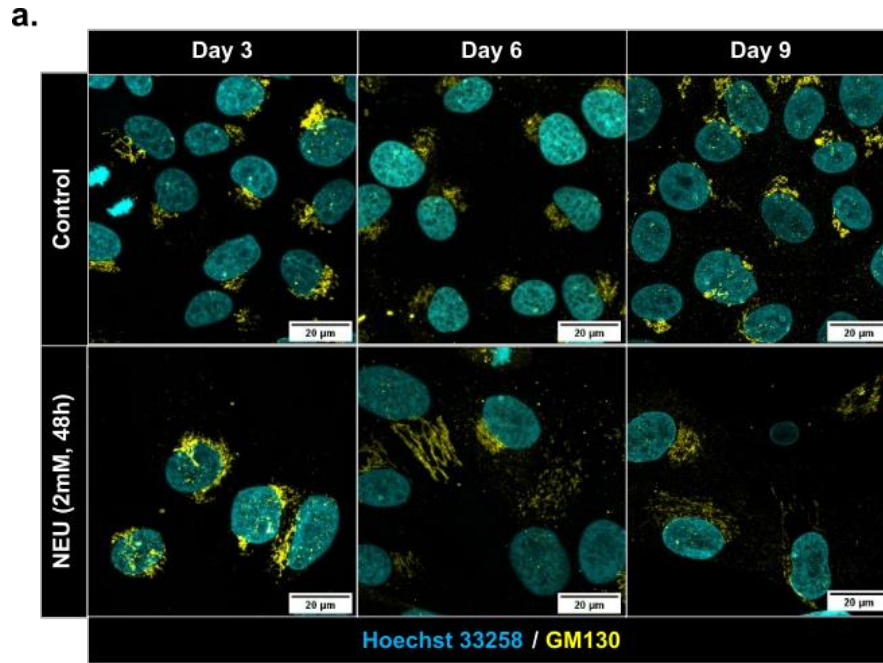


Figure V-6- Long-time course experiment shows activation of Golgi dispersal till day 9. Images showing Golgi (yellow) against nucleus (cyan). The Golgi area has been quantified per day (b-d). Asterisks indicate Mann-Whitney U test significance values; **** $p < 0.0001$ ($N=2$, $n=80$). Scale bar- $20\mu\text{m}$

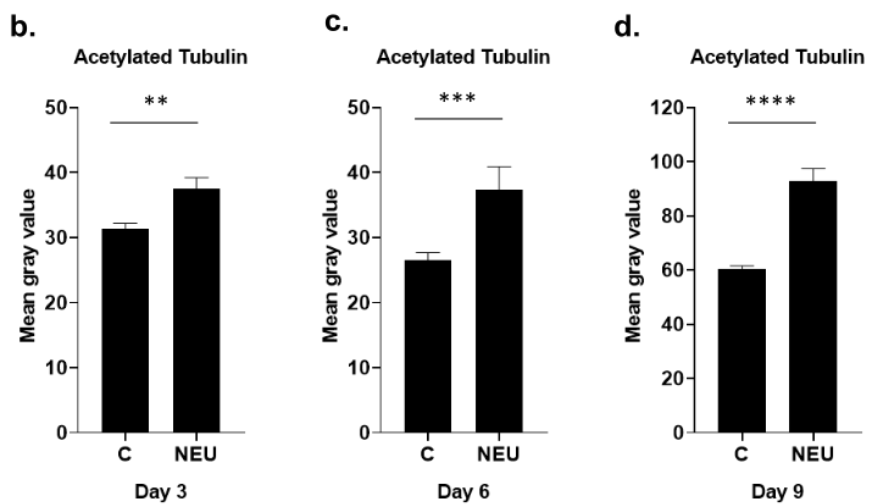
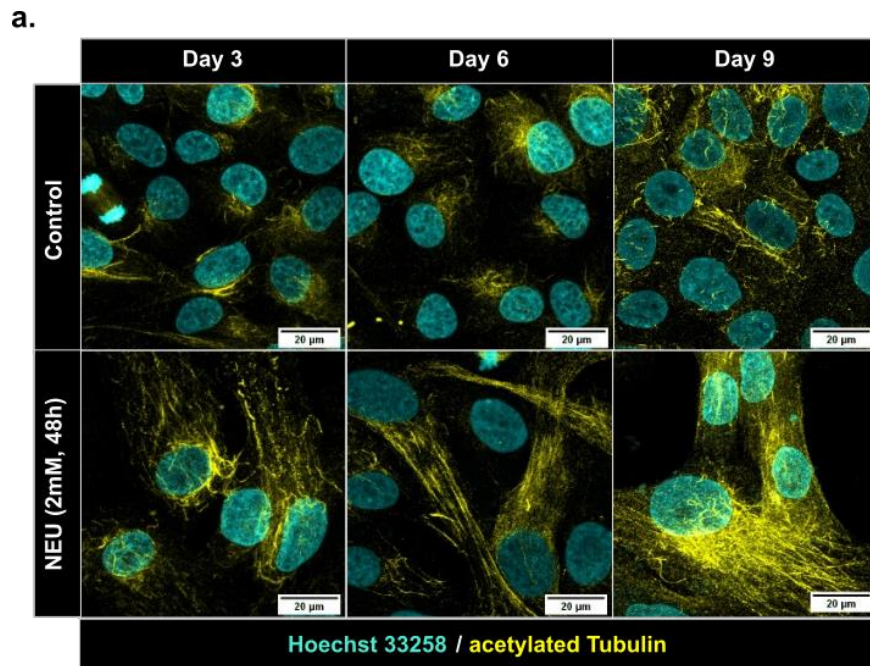


Figure V-7- Long-time course experiment shows increase tubulin acetylation till day 9. Images showing acetylated tubulin (yellow) against nucleus (cyan).

Tubulin acetylation has been quantified per day (b-d). Asterisks indicate Mann-Whitney U test significance values; **** $p < 0.0001$; *** $p < 0.001$; ** $p <$

0.01 (N=2, n=75). Scale bar-20 μ m

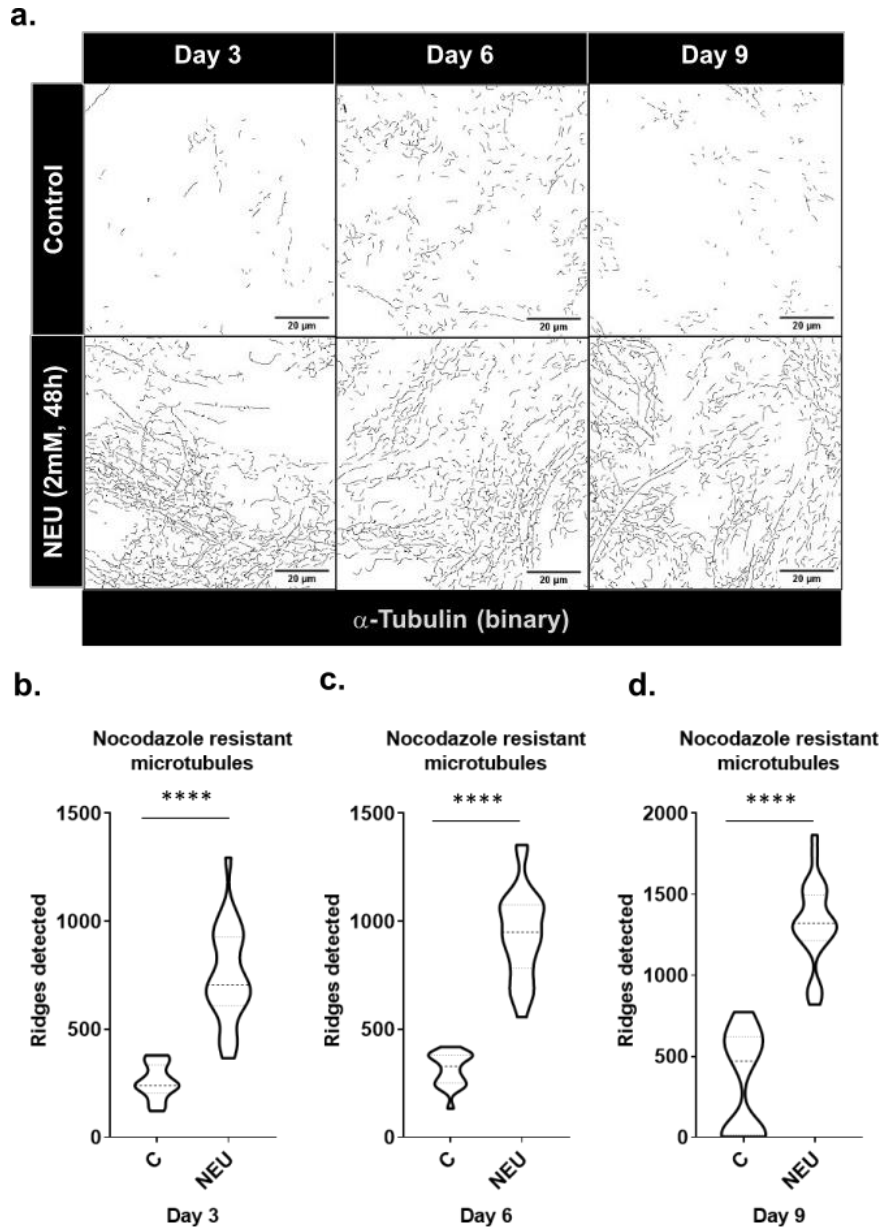


Figure V-8- Long-time course experiment shows presence of nocodazole resistant microtubules till day 9. (a) Images showing binary images of nocodazole resistant microtubules. The nocodazole resistant microtubules have been quantified per day (b-d). Asterisks indicate Mann-Whitney U test significance values; **** $p < 0.0001$ (N=2, n=70). Scale bar-20 μ m

1.8 Summary and discussion

In this chapter, we sought to examine the possible effect of DNA damage induced microtubule stabilisation. We assessed for changes in cell migration and intracellular trafficking. Wound healing assay was performed to examine changes in cell migration. Previous studies with MNU from lab report no change in collective cell migration but an increase in single cell migration was observed. Further experiments checking single cell migration need to be performed to ascertain that there no change in migratory capacity of the cell after DNA damage.

Although we did not observe any change in cell migration, we observed a significant delay in intracellular trafficking. A prominent mislocalisation of cell-cell junction proteins such E-cadherin and b-catenin was observed post DNA damage. This further, ties in with studies from lab which have shown loss of polarity upon treatment with NEU and MNU-induced transformation (Anandi et al., 2017; Bodakuntla et al., 2014).

We also observed that DNA damage induced a lasting change in microtubule dynamics. From these observations, we hypothesise that DNA damage-induced microtubule stabilisation might be an early sign of transformation.

CHAPTER VI

Discussion and Future perspectives

1.9 Conclusion

Based on this study's results and supporting data from previous studies, we report a model of change in microtubule dynamics as a response to DNA damage. DNA damage leads to activation of DNA-PK, which leads to Golgi dispersal in the GOLPH3-MYO18A-F-actin pathway (Farber-Katz et al., 2014). Active DNA-PK phosphorylates GOLPH3, which strengthens its association with the MYO18A-F-Actin complex, which leads to Golgi dispersal. Golgi dispersal leads to an increase in microtubules nucleated at Golgi through an unknown mechanism. These Golgi-derived microtubules are stable, marked by an enrichment of acetylated tubulin and resistance to nocodazole. An increase in Golgi-derived microtubules changes the balance of centrosomal to non-centrosomal microtubules in the cells, which results in altered intracellular transport. It was observed that change in intracellular trafficking led to mislocalisation of cell-cell junction and polarity proteins such as E-cadherin, β -catenin and α 3-integrin.

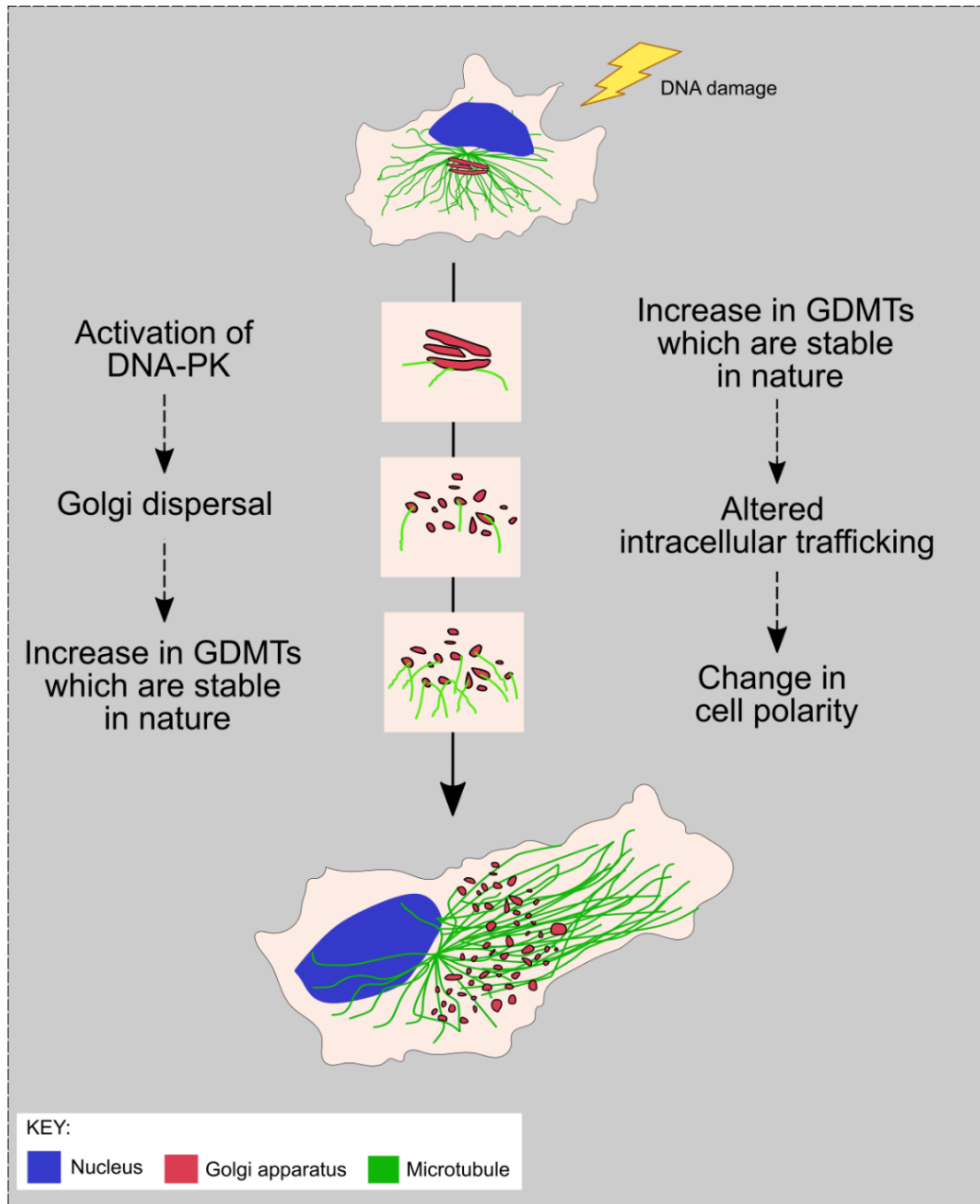


Figure VI-1- DNA damage leads to Golgi dispersal through the DNA-PK-GOLPH3-MYO18A axis. Golgi dispersal leads to an increase in GDMTs. Due to the difference in dynamics of GDMTs, the trafficking of proteins to the membrane gets altered, leading to the mislocalisation of polarity proteins. We hypothesise that this is the mechanism through which DNA damage might lead to transformation.

This study falls at the juncture of DNA damage response and regulation of the cytoskeleton. Therefore, this study unlocks several questions, expanding our understanding of cellular response to genotoxic stress and improving our regulation of Golgi- microtubule association. Two future directions are discussed below.

1.10 Microtubule stabilisation as a cell stress response

Microtubules play diverse roles in the cell, and microtubule dynamics is essential in regulating these functions. Microtubule dynamics and variations in tubulin isotypes, tubulin PTMs and MAPs are increasingly recognised to maintain cell homeostasis and influence cellular response to stress. Emerging evidence indicates the role of tubulin code in regulating the response to hypoxia, metabolic, mechanical and genotoxic stress(Parker et al., 2014).

A dramatic reorganisation of microtubules was observed when cells were exposed to reduced oxygen levels. An increase in microtubule polymerisation and stabilisation was observed under hypoxic conditions. The changes in microtubule dynamics were associated with inhibition of GSK3b by activation of Akt(Yoon et al., 2005). This led to microtubule stabilisation marked by an increase in de-tyrosinated tubulin. Interestingly, they observed an increase in Rab11-dependent trafficking of $\alpha 6 \beta 4$ -Integrin(Yoon et al., 2005). Other mechanisms involve MAP4 and non-phosphorylated DYNLT1 protecting microtubules against depolymerisation(Fang et al., 2011; Xu et al., 2013).

Microtubules have been shown to sense and respond to metabolic stress and modulate cellular metabolic processes. One of the early studies reported that microtubules are sensitive to ATP levels and depolymerise in response to elevated ATP levels. AMPK, a metabolic sensor, modulates microtubule dynamics by phosphorylating CLIP170(Nakano et al., 2010). CLIP170 phosphorylation leads to an increase in microtubule growth and rescue. Another study showed that AMPK regulates α -tubulin acetyltransferase-1 (a-TAT1) activity leading to tubulin hyperacetylation upon metabolic stress(Mackeh et al., 2014). Cell stress in the form of treatment with NaCl and UV radiation led to phosphorylation of CLIP170 through JNK activation, resulting in microtubule stabilisation(Henrie et al., 2020).

p53, a key regulator of genotoxic stress, depends on the microtubule for its translocation to the nucleus in response to DNA damage(Giannakakou et al., 2000). Later studies from the same group showed that disrupting microtubules interfered with the transport of DDR proteins to the nucleus(Poruchynsky et al., 2015). DNA damage has been reported to cause microtubule acetylation through aTAT1(α -tubulin acetyltransferase) and is essential for checkpoint activation post DNA damage(Ryu and Kim, 2020). Although this was the first study to report microtubule stabilisation upon DNA damage, they did not delve into the mechanism. Another study in 2021 showed that DSBs (double-strand breaks) increase microtubule polymerisation (Ma et al., 2021). They showed that DSBs resulted in an increase in centrosomal microtubules in a DNA-PK-Akt-dependent manner. The change in microtubule dynamics was shown to be transient and required for proper NHEJ(Ma et al., 2021). They do not comment on non-centrosomal microtubules.

Interestingly, the Golgi apparatus is another organelle which responds to a wide range of cell stress (Machamer, 2015). Golgi is known to fragment and disperse when the cell is exposed to pharmacological and oxidative stress (Alvarez-Miranda et al., 2015). Together, it would be interesting to study if Golgi dispersal-dependent microtubule stabilisation is limited to genotoxic stress or might be a general stress response of the cell and how DNA damage-induced Golgi dispersal leads to an increase in GDMTs.

1.11 Microtubules, Golgi-derived microtubules and cancer

Changes in microtubule dynamics and Golgi dispersal have frequently been associated with cancer. Golgi in cancer cells is often fragmented and dispersed throughout the cytoplasm instead of a ribbon-shaped perinuclear localisation in non-cancerous cells (Bui et al., 2021). One significant factor influenced by Golgi structure is protein sorting and glycosylation (Zhang and Wang, 2016). Studies show that Golgi fragmentation led to accelerated trafficking of proteins such as $\alpha 5$ -integrin and VSV-G (Kellokumpu et al., 2002; Xiang et al., 2013). The Golgi structure is known to influence and be influenced by several hallmarks of cancer. Cell migration, EMT, cell survival and proliferation, significant hallmarks of cancer, have all been shown to regulate or regulate the Golgi apparatus (Bisel et al., 2008; Bui et al., 2021).

Microtubule dynamics are directly associated with cell migration and invasion through their essential role in intracellular trafficking and cell mechanics. As discussed earlier, microtubules modulate cell polarity by selectively transporting cargo towards the cell's leading edge, which is crucial for migration (Etienne-Manneville, 2013; Seetharaman and Etienne-Manneville, 2019). Microtubules also influence focal adhesion turnover by regulating

integrin exocytosis in an α -TAT1-dependent manner(Bance et al., 2019; Ezratty et al., 2005). Years before the mechanism by which microtubules regulate focal adhesion dynamics was elucidated, an association between increased tubulin acetylation and cancer progression was made. Upregulation of tubulin acetylation was observed in metastatic breast tumours and cell lines(Boggs et al., 2015). Tubulin acetylation was necessary for the reattachment of circulating tumour cells due to its role in the micro-tentacle formation. Tubulin de-tyrosination was also associated with micro-tentacle formation(Whipple et al., 2007).

Cell migration requires the cell to coordinate the microtubule-Golgi association and dynamics(Rios, 2014). Golgi-derived microtubules are central to generating and maintaining cell asymmetry crucial for cell migration(Vinogradova et al., 2009). GDMTs are stable, enriched in acetylated and de-tyrosinated tubulin, and are both upregulated in cancers(Thyberg and Moskalewski, 1993). An increase in GDMTs leads to cell elongation, often associated with the malignant transformation of epithelial cells(Gavilan et al., 2018). Although the connection is apparent when all the evidence is put together, there is no study directly associating change in the level of GDMTs with cancer progression.

Studies from the lab have shown that DNA damage induced by NEU and MNU led to the transformation of breast epithelial cells(Anandi et al., 2017; Bodakuntla et al., 2014). DNA-PK activation was shown to be central in the transformation of MCF10A cells after MNU treatment(Anandi et al., 2017). Both studies' observations were made on the 16th day of MCF10A acinar culture while changes in microtubule dynamics are observed as early as 18h

post DNA damage. The results from this study might give an insight into the early events of transformation. Further studies must be performed to understand how the increase in GDMTs might contribute to DNA damage-induced transformation. This would further contribute to a more extensive understanding of how GDMTs are associated with cancer progression.

BIBLIOGRAPHY

Anandi, L., Chakravarty, V., Ashiq, K.A., Bodakuntla, S., and Lahiri, M. (2017). DNA-dependent protein kinase plays a central role in transformation of breast epithelial cells following alkylation damage. *J Cell Sci* *130*, 3749-3763.

Bartek, J., and Lukas, J. (2007). DNA damage checkpoints: from initiation to recovery or adaptation. *Curr Opin Cell Biol* *19*, 238-245.

Bieling, P., Kandels-Lewis, S., Telley, I.A., van Dijk, J., Janke, C., and Surrey, T. (2008). CLIP-170 tracks growing microtubule ends by dynamically recognizing composite EB1/tubulin-binding sites. *J Cell Biol* *183*, 1223-1233.

Bodakuntla, S., Libi, A.V., Sural, S., Trivedi, P., and Lahiri, M. (2014). N-nitroso-N-ethylurea activates DNA damage surveillance pathways and induces transformation in mammalian cells. *BMC cancer* *14*, 287.

Boggs, A.E., Vitolo, M.I., Whipple, R.A., Charpentier, M.S., Goloubeva, O.G., Ioffe, O.B., Tuttle, K.C., Slovic, J., Lu, Y., Mills, G.B., *et al.* (2015). alpha-tubulin acetylation elevated in metastatic and basal-like breast cancer cells promotes microtentacle formation, adhesion, and invasive migration. *Cancer Res* *75*, 203-215.

Bouchet, B.P., Gough, R.E., Ammon, Y.C., van de Willige, D., Post, H., Jacquemet, G., Altelaar, A.M., Heck, A.J., Goult, B.T., and Akhmanova, A. (2016). Talin-KANK1 interaction controls the recruitment of cortical microtubule stabilizing complexes to focal adhesions. *eLife* *5*.

Bugnard, E., Zaal, K.J., and Ralston, E. (2005). Reorganization of microtubule nucleation during muscle differentiation. *Cell motility and the cytoskeleton* *60*, 1-13.

Burns, S., Thrasher, A.J., Blundell, M.P., Machesky, L., and Jones, G.E. (2001). Configuration of human dendritic cell cytoskeleton by Rho GTPases, the WAS protein, and differentiation. *Blood* 98, 1142-1149.

Buschman, M.D., Rahajeng, J., and Field, S.J. (2015). GOLPH3 links the Golgi, DNA damage, and cancer. *Cancer Res* 75, 624-627.

Cai, D., McEwen, D.P., Martens, J.R., Meyhofer, E., and Verhey, K.J. (2009). Single molecule imaging reveals differences in microtubule track selection between Kinesin motors. *PLoS biology* 7, e1000216.

Castro-Castro, A., Janke, C., Montagnac, G., Paul-Gilloteaux, P., and Chavrier, P. (2012). ATAT1/MEC-17 acetyltransferase and HDAC6 deacetylase control a balance of acetylation of alpha-tubulin and cortactin and regulate MT1-MMP trafficking and breast tumor cell invasion. *Eur J Cell Biol* 91, 950-960.

Chabin-Brion, K., Marceiller, J., Perez, F., Settegrana, C., Drechou, A., Durand, G., and Pous, C. (2001). The Golgi complex is a microtubule-organizing organelle. *Mol Biol Cell* 12, 2047-2060.

Clarke, P.R., and Zhang, C. (2008). Spatial and temporal coordination of mitosis by Ran GTPase. *Nat Rev Mol Cell Biol* 9, 464-477.

Deakin, N.O., and Turner, C.E. (2014). Paxillin inhibits HDAC6 to regulate microtubule acetylation, Golgi structure, and polarized migration. *J Cell Biol* 206, 395-413.

Diao, A., Rahman, D., Pappin, D.J., Lucocq, J., and Lowe, M. (2003). The coiled-coil membrane protein golgin-84 is a novel rab effector required for Golgi ribbon formation. *J Cell Biol* 160, 201-212.

Dippold, H.C., Ng, M.M., Farber-Katz, S.E., Lee, S.K., Kerr, M.L., Peterman, M.C., Sim, R., Wiharto, P.A., Galbraith, K.A., Madhavarapu, S., *et al.* (2009). GOLPH3 bridges phosphatidylinositol-4-phosphate and actomyosin to stretch and shape the Golgi to promote budding. *Cell* *139*, 337-351.

Erck, C., Peris, L., Andrieux, A., Meissirel, C., Gruber, A.D., Vernet, M., Schweitzer, A., Saoudi, Y., Pointu, H., Bosc, C., *et al.* (2005). A vital role of tubulin-tyrosine-ligase for neuronal organization. *Proc Natl Acad Sci U S A* *102*, 7853-7858.

Farber-Katz, S.E., Dippold, H.C., Buschman, M.D., Peterman, M.C., Xing, M., Noakes, C.J., Tat, J., Ng, M.M., Rahajeng, J., Cowan, D.M., *et al.* (2014). DNA damage triggers Golgi dispersal via DNA-PK and GOLPH3. *Cell* *156*, 413-427.

Gavilan, M.P., Gandolfo, P., Balestra, F.R., Arias, F., Bornens, M., and Rios, R.M. (2018). The dual role of the centrosome in organizing the microtubule network in interphase. *EMBO reports* *19*.

Giannakakou, P., Sackett, D.L., Ward, Y., Webster, K.R., Blagosklonny, M.V., and Fojo, T. (2000). p53 is associated with cellular microtubules and is transported to the nucleus by dynein. *Nat Cell Biol* *2*, 709-717.

Grimaldi, A.D., Fomicheva, M., and Kaverina, I. (2013). Ice recovery assay for detection of Golgi-derived microtubules. *Methods Cell Biol* *118*, 401-415.

Guardia, C.M., Farias, G.G., Jia, R., Pu, J., and Bonifacino, J.S. (2016). BORC Functions Upstream of Kinesins 1 and 3 to Coordinate Regional Movement of Lysosomes along Different Microtubule Tracks. *Cell reports* *17*, 1950-1961.

Gurel, P.S., Hatch, A.L., and Higgs, H.N. (2014). Connecting the cytoskeleton to the endoplasmic reticulum and Golgi. *Current biology* : CB 24, R660-R672.

Hao, H., Niu, J., Xue, B., Su, Q.P., Liu, M., Yang, J., Qin, J., Zhao, S., Wu, C., and Sun, Y. (2020). Golgi-associated microtubules are fast cargo tracks and required for persistent cell migration. *EMBO reports* 21, e48385.

Howes, S.C., Alushin, G.M., Shida, T., Nachury, M.V., and Nogales, E. (2014). Effects of tubulin acetylation and tubulin acetyltransferase binding on microtubule structure. *Mol Biol Cell* 25, 257-266.

Hsu, C.Y., and Uludag, H. (2012). A simple and rapid nonviral approach to efficiently transfect primary tissue-derived cells using polyethylenimine. *Nature protocols* 7, 935-945.

Hurtado, L., Caballero, C., Gavilan, M.P., Cardenas, J., Bornens, M., and Rios, R.M. (2011). Disconnecting the Golgi ribbon from the centrosome prevents directional cell migration and ciliogenesis. *J Cell Biol* 193, 917-933.

J ANN, K.L., MAYURIKA (2018). Role of DNA damaging agents in the transformation of breast epithelial cells. Indian Institute of Science Education and Research.

Jackson, S.P., and Bartek, J. (2009). The DNA-damage response in human biology and disease. *Nature* 461, 1071-1078.

Janke, C., and Bulinski, J.C. (2011). Post-translational regulation of the microtubule cytoskeleton: mechanisms and functions. *Nat Rev Mol Cell Biol* 12, 773-786.

Janke, C., and Magiera, M.M. (2020). The tubulin code and its role in controlling microtubule properties and functions. *Nat Rev Mol Cell Biol* 21, 307-326.

Jiang, K., Hua, S., Mohan, R., Grigoriev, I., Yau, K.W., Liu, Q., Katrukha, E.A., Altelaar, A.F., Heck, A.J., Hoogenraad, C.C., *et al.* (2014). Microtubule minus-end stabilization by polymerization-driven CAMSAP deposition. *Dev Cell* 28, 295-309.

Khawaja, S., Gundersen, G.G., and Bulinski, J.C. (1988). Enhanced stability of microtubules enriched in detyrosinated tubulin is not a direct function of detyrosination level. *J Cell Biol* 106, 141-149.

Kim, D.I., Birendra, K.C., and Roux, K.J. (2015). Making the LINC: SUN and KASH protein interactions. *Biological chemistry* 396, 295-310.

King, S.J., Asokan, S.B., Haynes, E.M., Zimmerman, S.P., Rotty, J.D., Alb, J.G., Jr., Tagliatela, A., Blake, D.R., Lebedeva, I.P., Marston, D., *et al.* (2016). Lamellipodia are crucial for haptotactic sensing and response. *J Cell Sci* 129, 2329-2342.

Kodani, A., and Sutterlin, C. (2009). A new function for an old organelle: microtubule nucleation at the Golgi apparatus. *EMBO J* 28, 995-996.

Kollman, J.M., Merdes, A., Mourey, L., and Agard, D.A. (2011). Microtubule nucleation by gamma-tubulin complexes. *Nat Rev Mol Cell Biol* 12, 709-721.

Kollman, J.M., Polka, J.K., Zelter, A., Davis, T.N., and Agard, D.A. (2010). Microtubule nucleating gamma-TuSC assembles structures with 13-fold microtubule-like symmetry. *Nature* 466, 879-882.

Kreis, T.E. (1987). Microtubules containing detyrosinated tubulin are less dynamic. *EMBO J* 6, 2597-2606.

Lansbergen, G., Grigoriev, I., Mimori-Kiyosue, Y., Ohtsuka, T., Higa, S., Kitajima, I., Demmers, J., Galjart, N., Houtsmuller, A.B., Grosveld, F., *et al.*

(2006). CLASPs attach microtubule plus ends to the cell cortex through a complex with LL5beta. *Dev Cell* 11, 21-32.

Lawrimore, J., Barry, T.M., Barry, R.M., York, A.C., Friedman, B., Cook, D.M., Akialis, K., Tyler, J., Vasquez, P., Yeh, E., *et al.* (2017). Microtubule dynamics drive enhanced chromatin motion and mobilize telomeres in response to DNA damage. *Molecular biology of the cell* 28, 1701-1711.

Li, H., DeRosier, D.J., Nicholson, W.V., Nogales, E., and Downing, K.H. (2002). Microtubule structure at 8 Å resolution. *Structure* 10, 1317-1328.

Logan, C.M., Bowen, C.J., and Menko, A.S. (2018). Functional role for stable microtubules in lens fiber cell elongation. *Exp Cell Res* 362, 477-488.

Lotterberger, F., Karssemeijer, R.A., Dimitrova, N., and de Lange, T. (2015). 53BP1 and the LINC Complex Promote Microtubule-Dependent DSB Mobility and DNA Repair. *Cell* 163, 880-893.

Luders, J., Patel, U.K., and Stearns, T. (2006). GCP-WD is a gamma-tubulin targeting factor required for centrosomal and chromatin-mediated microtubule nucleation. *Nat Cell Biol* 8, 137-147.

Ma, S., Rong, Z., Liu, C., Qin, X., Zhang, X., and Chen, Q. (2021). DNA damage promotes microtubule dynamics through a DNA-PK-AKT axis for enhanced repair. *The Journal of cell biology* 220.

Magiera, M.M., Singh, P., Gadadhar, S., and Janke, C. (2018). Tubulin Posttranslational Modifications and Emerging Links to Human Disease. *Cell* 173, 1323-1327.

Marechal, A., and Zou, L. (2013). DNA damage sensing by the ATM and ATR kinases. *Cold Spring Harb Perspect Biol* 5.

Martin, M., Veloso, A., Wu, J., Katrukha, E.A., and Akhmanova, A. (2018). Control of endothelial cell polarity and sprouting angiogenesis by non-centrosomal microtubules. *eLife* 7.

Masoud, K., Herzog, E., Chaboute, M.E., and Schmit, A.C. (2013). Microtubule nucleation and establishment of the mitotic spindle in vascular plant cells. *The Plant journal : for cell and molecular biology* 75, 245-257.

Meijering, E., Dzyubachyk, O., and Smal, I. (2012). Methods for cell and particle tracking. *Methods in enzymology* 504, 183-200.

Meiring, J.C.M., Shneyer, B.I., and Akhmanova, A. (2020). Generation and regulation of microtubule network asymmetry to drive cell polarity. *Curr Opin Cell Biol* 62, 86-95.

Mialhe, A., Lafanechere, L., Treilleux, I., Peloux, N., Dumontet, C., Bremond, A., Panh, M.H., Payan, R., Wehland, J., Margolis, R.L., *et al.* (2001). Tubulin detyrosination is a frequent occurrence in breast cancers of poor prognosis. *Cancer Res* 61, 5024-5027.

Miki, H., Okada, Y., and Hirokawa, N. (2005). Analysis of the kinesin superfamily: insights into structure and function. *Trends in cell biology* 15, 467-476.

Miller, P.M., Folkmann, A.W., Maia, A.R., Efimova, N., Efimov, A., and Kaverina, I. (2009). Golgi-derived CLASP-dependent microtubules control Golgi organization and polarized trafficking in motile cells. *Nat Cell Biol* 11, 1069-1080.

Minin, A.A. (1997). Dispersal of Golgi apparatus in nocodazole-treated fibroblasts is a kinesin-driven process. *J Cell Sci* 110 (Pt 19), 2495-2505.

Moritz, M., Braunfeld, M.B., Guenebaut, V., Heuser, J., and Agard, D.A. (2000). Structure of the gamma-tubulin ring complex: a template for microtubule nucleation. *Nat Cell Biol* 2, 365-370.

Murphy, S.M., Preble, A.M., Patel, U.K., O'Connell, K.L., Dias, D.P., Moritz, M., Agard, D., Stults, J.T., and Stearns, T. (2001). GCP5 and GCP6: two new members of the human gamma-tubulin complex. *Mol Biol Cell* 12, 3340-3352.

Nogales, E., Wolf, S.G., and Downing, K.H. (1998). Structure of the alpha beta tubulin dimer by electron crystallography. *Nature* 391, 199-203.

Noordstra, I., and Akhmanova, A. (2017). Linking cortical microtubule attachment and exocytosis. *F1000Research* 6, 469.

Oshidari, R., Strecker, J., Chung, D.K.C., Abraham, K.J., Chan, J.N.Y., Damaren, C.J., and Mekhail, K. (2018). Nuclear microtubule filaments mediate non-linear directional motion of chromatin and promote DNA repair. *Nat Commun* 9, 2567.

Patil, M., Pabla, N., and Dong, Z. (2013). Checkpoint kinase 1 in DNA damage response and cell cycle regulation. *Cell Mol Life Sci* 70, 4009-4021.

Paturle-Lafanechere, L., Manier, M., Trigault, N., Pirollet, F., Mazarguil, H., and Job, D. (1994). Accumulation of delta 2-tubulin, a major tubulin variant that cannot be tyrosinated, in neuronal tissues and in stable microtubule assemblies. *J Cell Sci* 107 (Pt 6), 1529-1543.

Peris, L., They, M., Faure, J., Saoudi, Y., Lafanechere, L., Chilton, J.K., Gordon-Weeks, P., Galjart, N., Bornens, M., Wordeman, L., *et al.* (2006). Tubulin tyrosination is a major factor affecting the recruitment of CAP-Gly proteins at microtubule plus ends. *J Cell Biol* 174, 839-849.

Peris, L., Wagenbach, M., Lafanechere, L., Brocard, J., Moore, A.T., Kozielski, F., Job, D., Wordeman, L., and Andrieux, A. (2009). Motor-dependent microtubule disassembly driven by tubulin tyrosination. *J Cell Biol* 185, 1159-1166.

Pfister, K.K., Shah, P.R., Hummerich, H., Russ, A., Cotton, J., Annuar, A.A., King, S.M., and Fisher, E.M. (2006). Genetic analysis of the cytoplasmic dynein subunit families. *PLoS genetics* 2, e1.

Pinyol, R., Scrofani, J., and Vernos, I. (2013). The role of NEDD1 phosphorylation by Aurora A in chromosomal microtubule nucleation and spindle function. *Curr Biol* 23, 143-149.

Portran, D., Schaedel, L., Xu, Z., Thery, M., and Nachury, M.V. (2017). Tubulin acetylation protects long-lived microtubules against mechanical ageing. *Nat Cell Biol* 19, 391-398.

Poruchynsky, M.S., Komlodi-Pasztor, E., Trostel, S., Wilkerson, J., Regairaz, M., Pommier, Y., Zhang, X., Kumar Maity, T., Robey, R., Burotto, M., *et al.* (2015). Microtubule-targeting agents augment the toxicity of DNA-damaging agents by disrupting intracellular trafficking of DNA repair proteins. *Proc Natl Acad Sci U S A* 112, 1571-1576.

Raybin, D., and Flavin, M. (1975). An enzyme tyrosylating alpha-tubulin and its role in microtubule assembly. *Biochem Biophys Res Commun* 65, 1088-1095.

Reed, N.A., Cai, D., Blasius, T.L., Jih, G.T., Meyhofer, E., Gaertig, J., and Verhey, K.J. (2006). Microtubule acetylation promotes kinesin-1 binding and transport. *Curr Biol* 16, 2166-2172.

Rivero, S., Cardenas, J., Bornens, M., and Rios, R.M. (2009). Microtubule nucleation at the cis-side of the Golgi apparatus requires AKAP450 and GM130. *EMBO J* 28, 1016-1028.

Roubin, R., Acquaviva, C., Chevrier, V., Sedjai, F., Zyss, D., Birnbaum, D., and Rosnet, O. (2013). Myomegalin is necessary for the formation of centrosomal and Golgi-derived microtubules. *Biology open* 2, 238-250.

Sanders, A.A., and Kaverina, I. (2015). Nucleation and Dynamics of Golgi-derived Microtubules. *Frontiers in neuroscience* 9, 431.

Satoh, A., Wang, Y., Malsam, J., Beard, M.B., and Warren, G. (2003). Golgin-84 is a rab1 binding partner involved in Golgi structure. *Traffic* 4, 153-161.

Sauvanet, C., Wayt, J., Pelaseyed, T., and Bretscher, A. (2015). Structure, regulation, and functional diversity of microvilli on the apical domain of epithelial cells. *Annu Rev Cell Dev Biol* 31, 593-621.

Schroer, T.A. (2004). Dynactin. *Annu Rev Cell Dev Biol* 20, 759-779.

Scrofani, J., Sardon, T., Meunier, S., and Vernos, I. (2015). Microtubule nucleation in mitosis by a RanGTP-dependent protein complex. *Curr Biol* 25, 131-140.

Shang, Z., Yu, L., Lin, Y.F., Matsunaga, S., Shen, C.Y., and Chen, B.P. (2014). DNA-PKcs activates the Chk2-Brca1 pathway during mitosis to ensure chromosomal stability. *Oncogenesis* 3, e85.

Sirajuddin, M., Rice, L.M., and Vale, R.D. (2014). Regulation of microtubule motors by tubulin isotypes and post-translational modifications. *Nat Cell Biol* 16, 335-344.

Skoufias, D.A., Burgess, T.L., and Wilson, L. (1990). Spatial and temporal colocalization of the Golgi apparatus and microtubules rich in deetyrosinated tubulin. *J Cell Biol* *111*, 1929-1937.

Takizawa, P.A., Yucel, J.K., Veit, B., Faulkner, D.J., Deerinck, T., Soto, G., Ellisman, M., and Malhotra, V. (1993). Complete vesiculation of Golgi membranes and inhibition of protein transport by a novel sea sponge metabolite, ilimaquinone. *Cell* *73*, 1079-1090.

Tas, R.P., Chazeau, A., Cloin, B.M.C., Lambers, M.L.A., Hoogenraad, C.C., and Kapitein, L.C. (2017). Differentiation between Oppositely Oriented Microtubules Controls Polarized Neuronal Transport. *Neuron* *96*, 1264-1271 e1265.

Tassin, A.M., Maro, B., and Bornens, M. (1985). Fate of microtubule-organizing centers during myogenesis in vitro. *J Cell Biol* *100*, 35-46.

Teixido-Travesa, N., Roig, J., and Luders, J. (2012). The where, when and how of microtubule nucleation - one ring to rule them all. *J Cell Sci* *125*, 4445-4456.

Thyberg, J., and Moskalewski, S. (1993). Relationship between the Golgi complex and microtubules enriched in deetyrosinated or acetylated alpha-tubulin: studies on cells recovering from nocodazole and cells in the terminal phase of cytokinesis. *Cell and tissue research* *273*, 457-466.

Thyberg, J., and Moskalewski, S. (1999). Role of microtubules in the organization of the Golgi complex. *Exp Cell Res* *246*, 263-279.

Tormanen, K., Ton, C., Waring, B.M., Wang, K., and Sutterlin, C. (2019). Function of Golgi-centrosome proximity in RPE-1 cells. *PloS one* *14*, e0215215.

van Dijk, J., Rogowski, K., Miro, J., Lacroix, B., Edde, B., and Janke, C. (2007). A targeted multienzyme mechanism for selective microtubule polyglutamylation. *Mol Cell* 26, 437-448.

van Haren, J., Charafeddine, R.A., Ettinger, A., Wang, H., Hahn, K.M., and Wittmann, T. (2018). Local control of intracellular microtubule dynamics by EB1 photodissociation. *Nat Cell Biol* 20, 252-261.

Vinogradova, T., Paul, R., Grimaldi, A.D., Loncarek, J., Miller, P.M., Yampolsky, D., Magidson, V., Khodjakov, A., Mogilner, A., and Kaverina, I. (2012). Concerted effort of centrosomal and Golgi-derived microtubules is required for proper Golgi complex assembly but not for maintenance. *Molecular biology of the cell* 23, 820-833.

Wang, Z., Wu, T., Shi, L., Zhang, L., Zheng, W., Qu, J.Y., Niu, R., and Qi, R.Z. (2010). Conserved motif of CDK5RAP2 mediates its localization to centrosomes and the Golgi complex. *The Journal of biological chemistry* 285, 22658-22665.

Webb, D.J., Donais, K., Whitmore, L.A., Thomas, S.M., Turner, C.E., Parsons, J.T., and Horwitz, A.F. (2004). FAK-Src signalling through paxillin, ERK and MLCK regulates adhesion disassembly. *Nat Cell Biol* 6, 154-161.

Wehland, J., Henkart, M., Klausner, R., and Sandoval, I.V. (1983). Role of microtubules in the distribution of the Golgi apparatus: effect of taxol and microinjected anti- α -tubulin antibodies. *Proc Natl Acad Sci U S A* 80, 4286-4290.

Whipple, R.A., Cheung, A.M., and Martin, S.S. (2007). Detyrosinated microtubule protrusions in suspended mammary epithelial cells promote reattachment. *Exp Cell Res* 313, 1326-1336.

- Wloga, D., Joachimiak, E., and Fabczak, H. (2017). Tubulin Post-Translational Modifications and Microtubule Dynamics. *International journal of molecular sciences* *18*.
- Wu, J., and Akhmanova, A. (2017). Microtubule-Organizing Centers. *Annu Rev Cell Dev Biol* *33*, 51-75.
- Wu, J., de Heus, C., Liu, Q., Bouchet, B.P., Noordstra, I., Jiang, K., Hua, S., Martin, M., Yang, C., Grigoriev, I., *et al.* (2016). Molecular Pathway of Microtubule Organization at the Golgi Apparatus. *Dev Cell* *39*, 44-60.
- Xu, Z., Schaedel, L., Portran, D., Aguilar, A., Gaillard, J., Marinkovich, M.P., Thery, M., and Nachury, M.V. (2017). Microtubules acquire resistance from mechanical breakage through intraluminal acetylation. *Science* *356*, 328-332.
- Yadav, S., Puthenveedu, M.A., and Linstedt, A.D. (2012). Golgin160 recruits the dynein motor to position the Golgi apparatus. *Dev Cell* *23*, 153-165.
- Zhu, X., and Kaverina, I. (2011). Quantification of asymmetric microtubule nucleation at subcellular structures. *Methods in molecular biology* *777*, 235-244.
- Zhu, X., and Kaverina, I. (2013). Golgi as an MTOC: making microtubules for its own good. *Histochemistry and cell biology* *140*, 361-367.

VIII. PUBLICATIONS

DNA damage leads to microtubule stabilisation through an increase in Golgi-derived microtubules

Aishwarya Venkataravi and Mayurika Lahiri*

Department of Biology, Indian Institute of Science Education and Research, Dr. Homi Bhabha Road, Pune, Maharashtra 411008, India

*Author for correspondence (mayurika.lahiri@iiserpune.ac.in)

Orcid ID: M.L.: 0000-0001-9456-4920

Abstract

The site of nucleation strongly determines microtubule organisation and dynamics. The centrosome is a primary site for microtubule nucleation and organisation in most animal cells. In recent years, the Golgi apparatus has emerged as a site of microtubule nucleation and stabilisation. The microtubules originating from Golgi are essential for maintaining Golgi integrity post-Golgi trafficking, establishing cell polarity and enabling cell motility. Although the mechanism of nucleation and functional relevance of the Golgi-nucleated microtubule is well established, its regulation needs to be better studied. In this study, we report that DNA damage leads to aberrant Golgi structure and function accompanied by reorganisation of the microtubule network. Characterisation of microtubule dynamics post DNA damage showed the presence of a stable pool of microtubules resistant to depolymerisation by nocodazole and enriched in acetylated tubulin. Investigation of the functional association between Golgi dispersal and microtubule stability revealed that the Golgi elements were distributed along the acetylated microtubules. Microtubule regrowth assays showed an increase in Golgi-derived microtubule post DNA damage. Interestingly, reversal of Golgi dispersal reduces microtubule stabilisation. Altered intracellular trafficking resulting in mislocalisation of cell-cell junction proteins was observed post DNA damage. We propose that the increase in stable microtubules deregulates intracellular trafficking, resulting in cell polarity changes. This study would thus be the first to demonstrate the link between Golgi dispersal and microtubule reorganisation orchestrating changes in cell polarity.

Keywords

DNA damage, microtubule dynamics, tubulin acetylation, Golgi-derived microtubules, intracellular trafficking, genomic instability

Introduction

Microtubules (MTs) are one of three dynamic polymers that constitute the cell's cytoskeleton. Microtubules are formed by end-to-end polymerisation of α/β - tubulin heterodimers which come together to form a hollow cylindrical structure. They are polarised filaments with the minus (-) end anchored at the nucleating centre and the plus (+) end radiating towards the cell membrane. The centrosome is the primary microtubule organising centre in mammalian cells, followed by the Golgi apparatus. The organisation and dynamics of the MT arrays are determined by their site of nucleation. Golgi-derived microtubules (GDMTs) are dynamically different from centrosomal microtubules. GDMTs are more stable and enriched in tubulin acetylation and detyrosination (Chabin-Brion et al., 2001; Skoufias et al., 1990; Thyberg and Moskalewski, 1993). They contribute to cell asymmetry by facilitating polarised trafficking toward the cell's leading edge during cell migration (Vinogradova et al., 2009).

Microtubules play myriad functions inside the cell, and microtubule dynamics are essential in regulating these functions. A complex signalling mechanism is in place to translate external cues to a cellular response through changes in microtubule dynamics. A growing body of literature emphasises the role of microtubules in the cellular response to stress such as hypoxia, metabolic stress, mechanical stress and genotoxic stress (Parker et al., 2014).

A decrease in microtubule polymerisation is observed in anoxic conditions, while increased polymerisation is observed under hypoxia (Hu et al., 2010). The response to hypoxia has been reported to occur through GSK3 β , resulting in Rab11-dependent trafficking of $\alpha 6\beta 4$ -integrin (Yoon et al., 2005). Under anoxic conditions, MAP4 phosphorylation leads to microtubule stabilisation (Hu et al., 2010). The dynein light chain has been shown to regulate mitochondrial permeability through its interaction with voltage-gated anion channels (Fang et al., 2011). Microtubules are known to respond to metabolic stress and have been implicated in regulating cellular metabolism (Bershadsky and Gelfand, 1981). AMPK, a metabolic stress sensor, phosphorylates CLIP170 and affects microtubule dynamics (Nakano et al., 2010). In neuronal cells, axonal microtubule growth is inhibited upon metabolic stress in an AMPK-dependent manner (Williams et al., 2011). Nutrient starvation has also been

shown to lead to microtubule hyperacetylation and has been associated with starvation-induced autophagy (Geeraert et al., 2010).

DNA damage response (DDR) is a well-orchestrated signalling network which, in response to DNA damage, leads to the detection of DNA lesions, cell cycle arrest, transcriptional activation of DNA repair genes and, ultimately, DNA repair (Jackson and Bartek, 2009). Classical studies contributing to our understanding of DDR majorly involve nuclear processes. The cytoplasmic effect of DDR, especially concerning the cytoskeleton, is recently being explored.

One of the initial studies linking DDR to cytoskeleton showed that p53, an essential DDR protein, is transported to the nucleus via microtubules in response to DNA damage (Giannakakou et al., 2000). Later a study in 2014 reported that upon DNA damage, DNA-PK phosphorylates GOLPH3 leading to Golgi dispersal through actin modulation (Farber-Katz et al., 2014). GOLPH3 is a Golgi membrane protein that interacts with the unconventional MYO18A-F-actin complex to maintain the perinuclear ribbon morphology of the Golgi apparatus (Dippold et al., 2009). Phosphorylation by DNA-PK leads to increased interaction between GOLPH3-MYO18A which adds a tensile force on the Golgi, thereby dispersing it throughout the cytoplasm (Farber-Katz et al., 2014). The following year, Tito Fijo's group showed that microtubule poisons interfere with the transport of DNA repair proteins to the nucleus, delaying DNA repair (Poruchynsky et al., 2015). A more recent study by Mi Ryu reports microtubule stabilisation upon induction of genotoxic stress. An increase in tubulin acetylation by α TAT1 (α -Tubulin acetyltransferase) is essential for activating the S and G2/M checkpoints post-DNA damage (Ryu and Kim, 2020). Although this was the first study to report a direct association of microtubule dynamics with DNA damage, it did not delve into how DNA damage might lead to microtubule stabilisation. A more recent study reported that DNA damage leads to a transient change in microtubule dynamics which is necessary for DNA repair through the non-homologous end joining (NHEJ) pathway. They observed an increase in the polymerisation of centrosomal microtubules through the activation of DNA-PK but did not comment on the stability of the microtubules (Ma et al., 2021).

In this study, we report that DNA damage leads to dramatic reorganisation of the microtubules and their dynamics through increased GDMTs. Treatment with DNA damaging agents led to microtubule stabilisation accompanied by dispersal of Golgi,

as previously reported. Further investigation revealed that the changes in Golgi morphology were essential for microtubule stabilisation. DNA damage-induced Golgi dispersal led to an increase in GDMTs, which are stable. Interestingly, an increase in genomic instability induced stable microtubules and Golgi-derived microtubules were observed in MCF10CA1a cells in comparison to MCF10A. We also report impaired intracellular trafficking leading to a mislocalisation of cell-cell junction proteins, possibly due to altered microtubule dynamics.

Results

DNA damage leads to microtubule stabilisation

Non-tumorigenic MCF10A cells were treated with a sub-lethal dose of 2mM NEU (Bodakuntla et al., 2014) or 10J/m² UV (Fong et al., 2010) to induce DNA damage and were analysed for microtubule stabilisation. Microtubule stabilisation was tested using two complementary methods – one, checking for resistance to depolymerisation induced by nocodazole treatment (Xu et al., 2017), and the other was monitoring the +TIP dynamics using the EB3 construct (Miller et al., 2009). MCF10A cells with and without DNA damage were treated with nocodazole (2.5µg/ml, 20mins) and stained for α -tubulin to assess the extent of microtubule depolymerisation. We observed that cells post DNA damage showed resistance to nocodazole treatment (**Fig 1a-b**). Nocodazole treatment revealed a subset of microtubules which were hyper stable and resistant to depolymerisation, indicating a change in microtubule dynamics.

Further, we used EB3 dynamics as a surrogate for assessing microtubule growth dynamics. Cells with and without DNA damage were transfected with the EB3 construct, and the EB3 comets were imaged. NEU-treated cells appeared to have longer microtubule tracks than untreated cells (**Fig 1c**). Quantifying EB3 dynamics showed a significant increase in MT lifetime and length. At the same time, a decrease in speed was observed in the NEU-treated cells compared to the untreated control, indicating MT stabilisation (**Fig 1d-f**). Tubulin acetylation is a tubulin PTM which is often associated with stable microtubules. Hence, cells were stained with α -tubulin to check if DNA damage led to changes in tubulin acetylation. A significant increase in K40 tubulin acetylation was observed in both NEU and UV-treated MCF10A cells compared to the untreated control cells (**Fig 1 g and h**). We also

observed that post DNA damage, the microtubules were arranged in parallel arrays, compared to the radial arrays observed in the untreated cells (**Supp Fig 1 a-c**). In addition, a dramatic change in the morphology of the cells was observed after treatment with NEU. The cells appeared to be more elongated and larger, where the NEU-treated cells showed significant increases in the cell area, nucleo-cytoplasmic ratio, circularity and aspect ratio (**Supp Fig 1 d-g**), which might be attributed to the changes in the microtubule network. This phenotype was further confirmed in the HEK293 cell line. The NEU dose was first standardised for the HEK293 cells where the cells were treated with 0.5 mM, 1 mM and 2 mM NEU and stained for phosphorylated DNA-PK (T2609) to obtain a sublethal dose of NEU with sufficient DNA damage (**Supp Fig 2 a-b**). NEU dose of 0.5 mM dose was used for further experiments. An increase in nocodazole-resistant microtubules, as well as an increase in tubulin acetylation, were observed when HEK293 cells were treated with 0.5 mM NEU for 48 hrs and 10 J/m² UV for 48 hrs (**Supp Fig 2 c-f**) thus demonstrating that the changes in microtubule dynamics are not cell line specific.

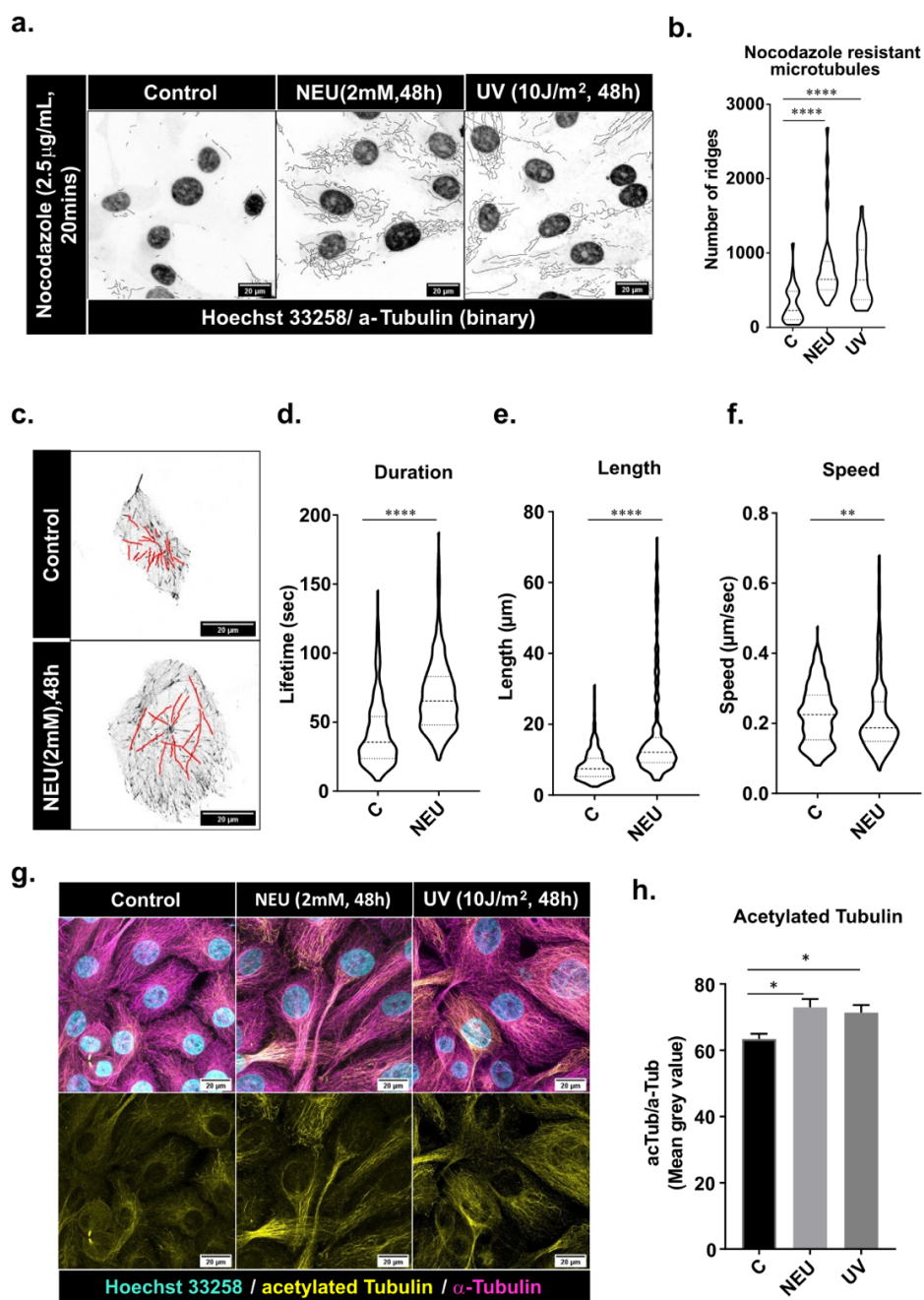


Figure 1: MCF10A cells showed an increase in microtubule stability post-DNA damage. (a) NEU (2 mM, 48 hrs) or UV (10 J/m²) damaged cells, when treated with nocodazole, revealed a subset of microtubules resistant to depolymerisation that were represented as binary images. (b) The nocodazole-resistant MTs were quantified using ImageJ ridge detection tool (N=3, n=140 cells). Asterisks indicate Mann-Whitney U test significance values; **** p < 0.0001. (c) EB3 assay was performed on cells treated with and without 2 mM NEU for 48 hrs, and live-cell imaging was performed. A few EB3 comets are shown. The EB3 comets were

manually tracked and quantified using MtrackJ plugin on ImageJ to show comet (**d**) duration, (**e**) length and (**f**) speed (N=3, n=120 cells, 25 MT tracks per cell). (**g**) MCF10A cells treated with NEU (2mM, 48h) and UV (10J/m²) were stained for α -tubulin (magenta), acetylated tubulin (yellow), and Hoechst 33258 (cyan), showed increased tubulin acetylation post DNA damage. (**h**) Bar graph representing the quantification of acetylated tubulin (N=3, n=125 cells). Statistics analysis was performed for all the experiments using the Mann-Whitney U test with significance values **** p < 0.0001; ** p < 0.01; * p < 0.05.

Activation of DNA-PK precedes Golgi dispersal, followed by the appearance of a stable pool of microtubules.

To decipher how DNA damage might lead to changes in microtubule dynamics, we investigated the activation of DNA-PK and Golgi dispersal following DNA damage. Since Golgi has a close association with microtubules, we proposed that changes in microtubule dynamics might be through Golgi dispersal. Activation of DNA-PK (T2609) and dispersal of Golgi were detected 48 hrs post-NEU and UV treatment (**Supp Fig 3 a-h**), thus implying that Golgi dispersal post-NEU and UV treatment might be through the DNA-PK-GOLPH3 pathway (Farber-Katz et al., 2014). The presence of active DNA-PK foci at 48 hrs demonstrated that DNA damage lesions have not been repaired and that the change in microtubule dynamics may be in response to the DNA damage. To investigate the temporal dynamics of DNA-PK activation, Golgi morphology changes and tubulin acetylation occurring post DNA damage, cells were treated with 2 mM NEU for different time durations and analysed. Phosphorylation of DNA-PK (T2609) was observed as early as 10 mins, while Golgi dispersal was observed from 4 hours post-NEU treatment (**Fig 2 a-b; Supp Fig 4 a-b**). Both these events preceded the presence of nocodazole-resistant microtubules and tubulin acetylation, that were observed 18 hrs post-NEU treatment (**Fig 2 c-f**).

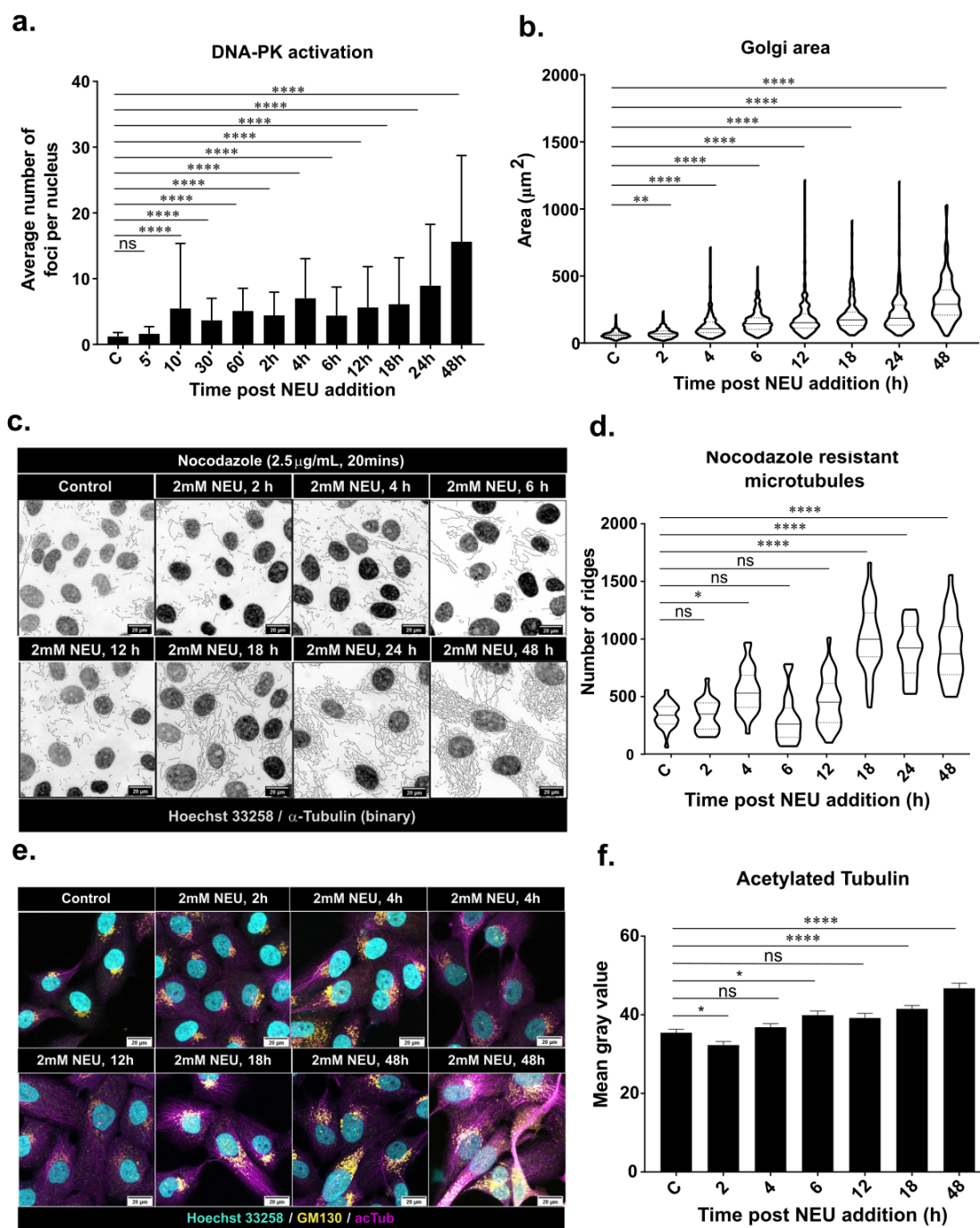


Figure 2: The activation of DNA-PK and Golgi dispersal precedes microtubule stabilisation. MCF10A cells were treated with 2 mM NEU and checked for (a) activation of DNA-PK at threonine 2609 at different time points. A significant increase in pDNA-PK foci was observed from 10 mins post NEU treatment which remained active till 48 hrs (N=3, n=420 cells). (b) Golgi dispersal was observed 4 hrs post DNA damage (N=3, n=220). (c) the appearance of nocodazole-resistant microtubules at 18hrs after NEU treatment was depicted as binary images of tubulin and nucleus (both in grey) that were quantified in (d) using a ridge detection tool (N=3, n>10

fields per timepoint). **(e)**. An increase in tubulin acetylation (magenta) was observed at 18 hrs in cells with dispersed Golgi (yellow). Hoechst 33258 (cyan) was used to stain the nucleus in the cells (N=3, n=290 cells). **(d)** Bar graphs showing the quantification of acetylated tubulin in the cells. Kruskal-Wallis test for significance was performed on all the data **** p < 0.0001, **p< 0.01, *p< 0.05 ns – non-significant.

To test whether activation of DNA-PK is required for microtubule stabilisation, cells were treated with DMNB, a small molecule inhibitor against the catalytic subunit of DNA-PK (Durant and Karran, 2003). A significant reduction in tubulin acetylation (**Fig 3 a-b**) and nocodazole-resistant microtubules (**Fig 3 c-d**) were observed in cells treated with DMNB following 2mM NEU treatment for 48 hrs compared to the untreated control cells. Inhibition of DNA-PK was previously reported to revert DNA damage-induced Golgi dispersal (Anandi et al., 2017; Durant and Karran, 2003; Farber-Katz et al., 2014). DNA damage-induced Golgi dispersal has been shown to involve the actin cytoskeleton, and its depolymerisation to revert the dispersal of Golgi (Dippold et al., 2009; Farber-Katz et al., 2014). To assess whether activation of DNA-PK leads to microtubule reorganisation by altering Golgi distribution, Latrunculin A (LatA, an actin depolymerising agent) was used to condense Golgi in the presence of DNA damage. LatA treatment led to a significant reduction in acetylated tubulin (**Fig 3 e-f**) and nocodazole-resistant microtubules (**Fig 3 g-h**), similar to the inhibition of DNA-PK. Thus, it may be inferred that the stabilisation of microtubule post DNA damage is mediated through the DNA-PK-Golgi axis.

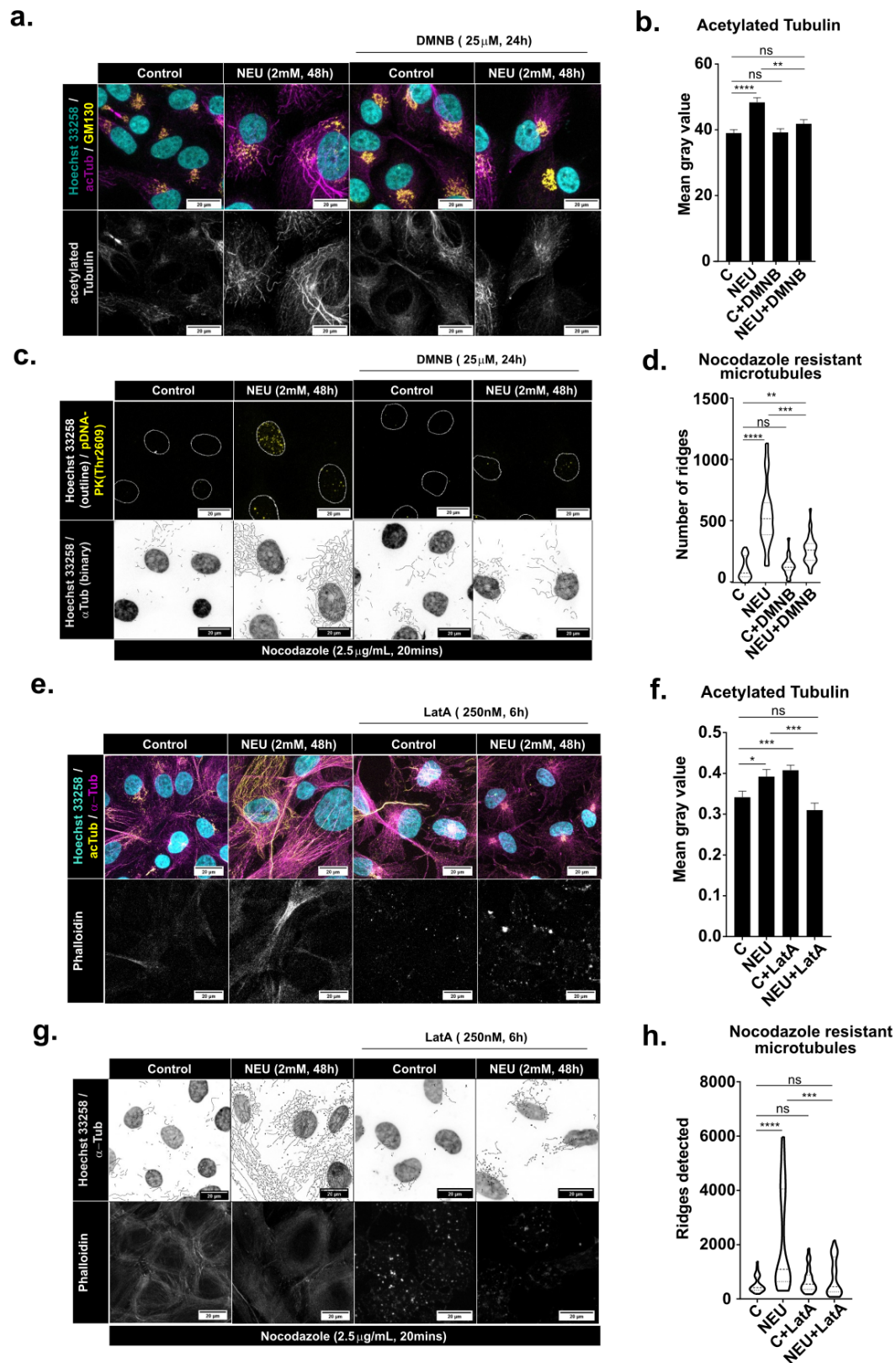


Figure 3: DNA damage-induced microtubule stabilisation is through activation of DNA-PK and Golgi dispersal. Cells were treated with 2 mM NEU for 48 hrs and to one set DMNB (25 μ M, two doses 12 hrs each) was added to inhibit DNA-PK. (a)

The cells were stained for GM130 (yellow) that marked the Golgi, Hoechst 33258 (cyan) for the nucleus and acetylated tubulin (magenta). Inhibition of DNA-PK using DMNB post-NEU treatment showed a reduction in the acetylated tubulin in DMNB and NEU-treated cells compared to cells with only NEU treatment (N=3, n=100 cells). **(b)** The intensity of acetylated tubulin was quantified and represented as bar graphs. **(c)** 2.5 μ g/ml nocodazole was added to 2 mM NEU-treated cells for 48 hrs with or without DMNB and checked for pDNA-PK (Thr 2609) foci (yellow) and α -tubulin (binary image) (N=3, n>10 fields per treatment). **(d)** violin plots representing nocodazole-resistant microtubules that were quantified using a ridge detection tool. **(e)** Latrunculin A (Lat A) was added at 250 nM for 6 hrs to the NEU-treated (2mM, 48 hrs) cells and control cells and stained for Hoechst 33258 (cyan) for the nucleus, acetylated tubulin (yellow) and α -tubulin (magenta). Phalloidin was used as a positive control for Lat A treatment (N=3, n=110 cells). Depolymerisation of F-actin by Lat A led to a reduction in tubulin acetylation that was quantified in **(f)** and represented as bar graphs. **(g)** Lat A (250 nM, 6 hrs) was added to nocodazole (2.5 μ g/ml, 20 mins) treated control and NEU (2 mM, 48 hrs) treated cells and stained for Hoechst 33258 and α -tubulin. Phalloidin was used as a positive control for Lat a treatment (N=3, n>10 fields per treatment). **(h)** Violin plots representing nocodazole-resistant MTs that were quantified using a ridge detection tool. Statistical analysis was performed using Kruskal-Wallis test with significance values; **** p < 0.0001, ***p < 0.001, **p < 0.01 and ns – non-significant.

DNA damage leads to an increase in Golgi-derived microtubules.

Golgi and microtubules are functionally dependent on each other. Microtubules play an essential role in maintaining Golgi structure (Vinogradova et al., 2012). Treating cells with microtubule poisons displays a fragmented and dispersed Golgi (Thyberg and Moskalewski, 1993; Wehland et al., 1983). On the other hand, a significant proportion of microtubules in mammalian cells originate from Golgi, and there is increasing evidence that these microtubules are stable. We hypothesised that the stable pool of microtubules which appear post DNA damage are non-centrosomal microtubules that nucleated at the Golgi apparatus. In the cells treated with NEU, we observed that the stable acetylated microtubules were associated with the dispersed Golgi apparatus, which indicated that they may have nucleated from the Golgi (**Fig. 4a**). To confirm whether there is an increase in GDMTs, microtubule regrowth assay

was performed following treatment of cells with 2.5 $\mu\text{g/ml}$ nocodazole. A time-course was performed to check for complete depolymerisation of the microtubules. A treatment of 2.5 $\mu\text{g/ml}$ nocodazole for 3 hrs resulted in almost complete depolymerisation of microtubules which was used for the washout assay (**Fig. 4b**). Close observation of cells recovering from microtubule depolymerisation showed that a significant number of microtubules were nucleated from the Golgi post-NEU treatment (**Fig.4c-d**).

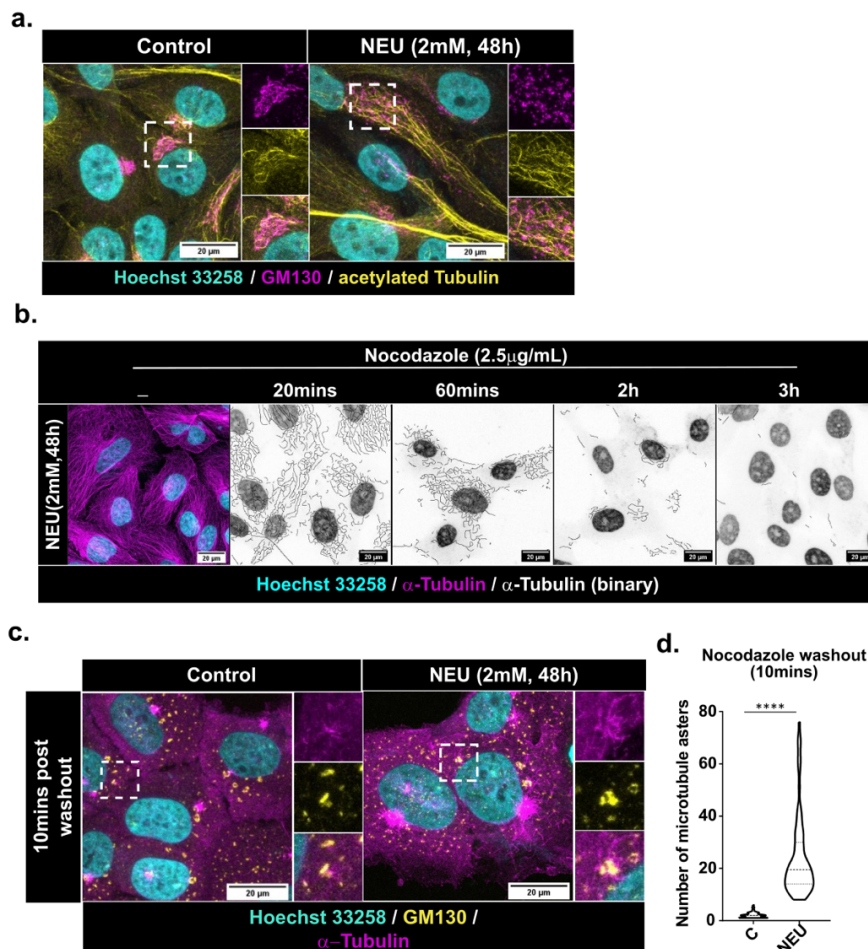


Figure 4: NEU-induced DNA damage leads to an increase in Golgi-derived microtubules. (a) Untreated and 2 mM NEU treated (48 hrs) MCF10A cells were stained for acetylated tubulin (yellow), GM130 (magenta) and Hoechst 33258 (cyan) to check for Golgi elements distributed along the acetylated microtubules (N=2, n=75 cells). (b) Representative images of NEU-treated cells incubated with 2.5 $\mu\text{g/ml}$ nocodazole for 20 mins, 60 mins, 2 hrs and 3 hrs are shown. Nocodazole dose of 2.5 $\mu\text{g/ml}$ for 3 hrs led to complete depolymerisation of microtubules in NEU-treated cells. (c) A Nocodazole washout assay was performed to determine changes in the

nucleation of microtubules from the Golgi. Cells were treated with 2.5µg/mL for 3h, then washed with cold PBS and supplemented with fresh media. Microtubules were allowed to recover at 37°C and fixed and stained for α -tubulin (magenta), GM130 (yellow) and Hoechst 33258 (cyan). An increase in microtubule nucleation at Golgi was observed 10 mins post nocodazole washout, which was quantified in **(d)** by manually counting the number of nucleation sites (N=3, n=70). Asterisks indicate Mann-Whitney U test significance values; **** p < 0.0001.

Golgi-derived microtubules are associated with genome instability.

DNA damage-induced Golgi dispersal has been proposed to be an adaptive mechanism in response to genotoxic insults through altering the trafficking of proteins (Buschman et al., 2015; Farber-Katz et al., 2014). Given the importance of the Golgi-microtubule association in intracellular trafficking, we hypothesised that GDMTs might contribute to the survival of cells with genomic instability. To ascertain the association of an increase in GDMT to genome instability, we compared the levels of GDMTs in a malignant cell line with the non-tumorigenic MCF10A. The MCF10A isogenic cell line series was used to investigate the association for a valid comparison. Anandi et al. have shown that MCF10AT1 and MCF10CA1a have an aberrant Golgi structure due to atypically active DNA-PK, which confirmed that the DNA-PK-Golgi axis is active in the cell line (Anandi et al., 2017). Thus, it was interesting to study if the malignant cell line, MCF10CA1a, had higher levels of stable microtubules and Golgi-derived microtubules compared to MCF10A cells.

It was observed that MCF10CA1a had increased levels of tubulin acetylation (**Supp Fig.5 a and b**). Additionally, increased levels of nocodazole-resistant microtubules were detected at 2.5mg/ml nocodazole incubated for 20 mins (**Supp Fig.5 c and d**). For studying microtubule regrowth in MCF10CA1a cells, the nocodazole dose was standardised, and a dose of 2.5mg/ml for 3h was found appropriate (**Supp Fig.5 e**). MCF10CA1a was observed to have a higher number of microtubules nucleated at the Golgi (**Fig.5 a-b**). Hence, MCF10CA1a, a malignant cell line with inherent DNA damage, has more stabilised microtubules and Golgi-derived microtubules.

To assess if the microtubule dynamics in MCF10CA1a are linked to Golgi dispersal, we checked for stable microtubules following Latrunculin A (Lat A) treatment. Upon Lat A treatment, a reduction in tubulin acetylation and nocodazole-resistant microtubules were observed in the MCF10CA1a cells compared to the MCF10A cells

(Fig.5 c-f). Therefore, we conclude that microtubule stabilisation in MCF10CA1a cells is also through the DNA-PK-Golgi axis.

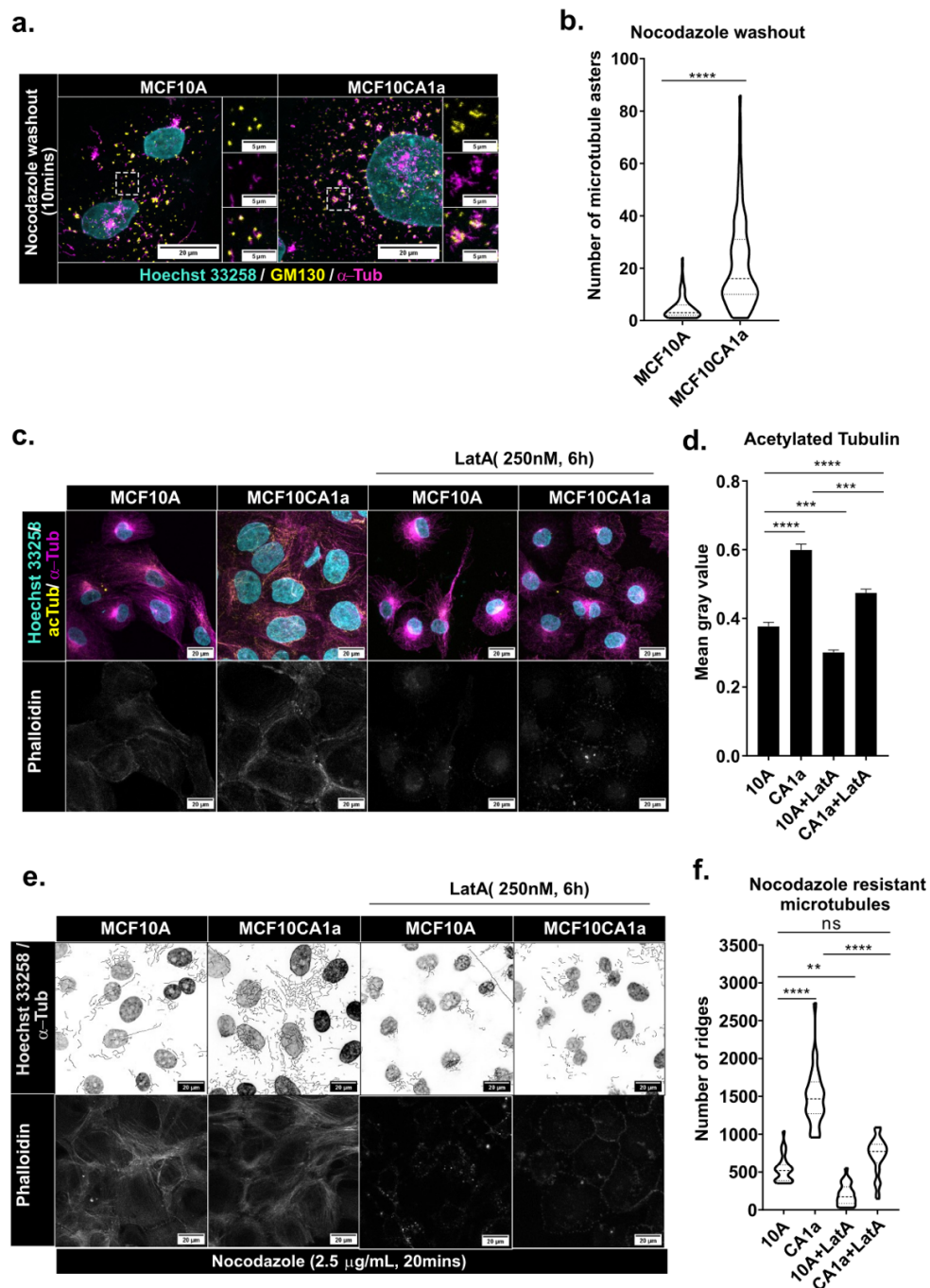


Figure 5: The malignant MCF10CA1a cells have higher levels of Golgi-derived microtubules. MCF10A and MCF10CA1a were stained for microtubules and Golgi post nocodazole washout as previously described. **a.** A higher number of microtubules (magenta) were observed to be nucleated from Golgi (yellow) in

MCF10CA1a in comparison to MCF10A, which was quantified by counting the nucleation sites and plotted in **(b.)**. Asterisks indicate Mann-Whitney U test significance values; **** $p < 0.0001$. Microtubule stabilisation in MCF10CA1a was seen to be dependent on Golgi dispersal. Treatment with Lat A (250nM, 6h) led to a reduction in tubulin acetylation **(c. and d.)** and nocodazole-resistant microtubules **(e. and f.)** in MCF10CA1a cells. Asterisks indicate Kruskal-Wallis test significance values; **** $p < 0.0001$, *** $p < 0.001$, ** $p < 0.01$ and ns – non-significant.

DNA damage results in impaired intracellular trafficking

Golgi and microtubule dynamics are fundamental for transporting cargo from the endoplasmic reticulum (ER) to the destined cellular compartments. Studies have reported that DNA damage-induced Golgi dispersal leads to an impaired intracellular trafficking (Anandi et al., 2017; Farber-Katz et al., 2014). In this study, we wanted to investigate whether NEU treatment leads to impaired intracellular trafficking, thereby affecting cell polarity. RUSH assay with GPI (Glycosylphosphatidylinositol) anchored EGFP as reporters were used for testing for defects in intracellular trafficking post-NEU induced DNA damage (Boncompain et al., 2012). A delayed transport of GPI-EGFP to the plasma membrane was observed, indicating a defect in Golgi trafficking **(Fig. 6a-b)**. A dispersed Golgi could also result in defective transport of the cargo to the Golgi. To test this, we used the RUSH construct with mannosidase-II tagged with EGFP (ManII-EGFP) as a cargo. A delayed accumulation of ManII in Golgi was also observed in NEU-treated cells, indicating a defective ER to Golgi transport **(Supp Fig. 6a-b)**. To examine if the defects in trafficking affected the localisation of cell polarity proteins, immunostaining of cells with E-cadherin, β -catenin, and α 3-integrin showed either mislocalisation of these proteins in the cytoplasm or diffused staining at the junctions **(Fig. 6c-e)** which was quantified **(Fig. 6f-h)** by measuring the CTCF (Corrected Total Cell Fluorescence) of the cytoplasm.

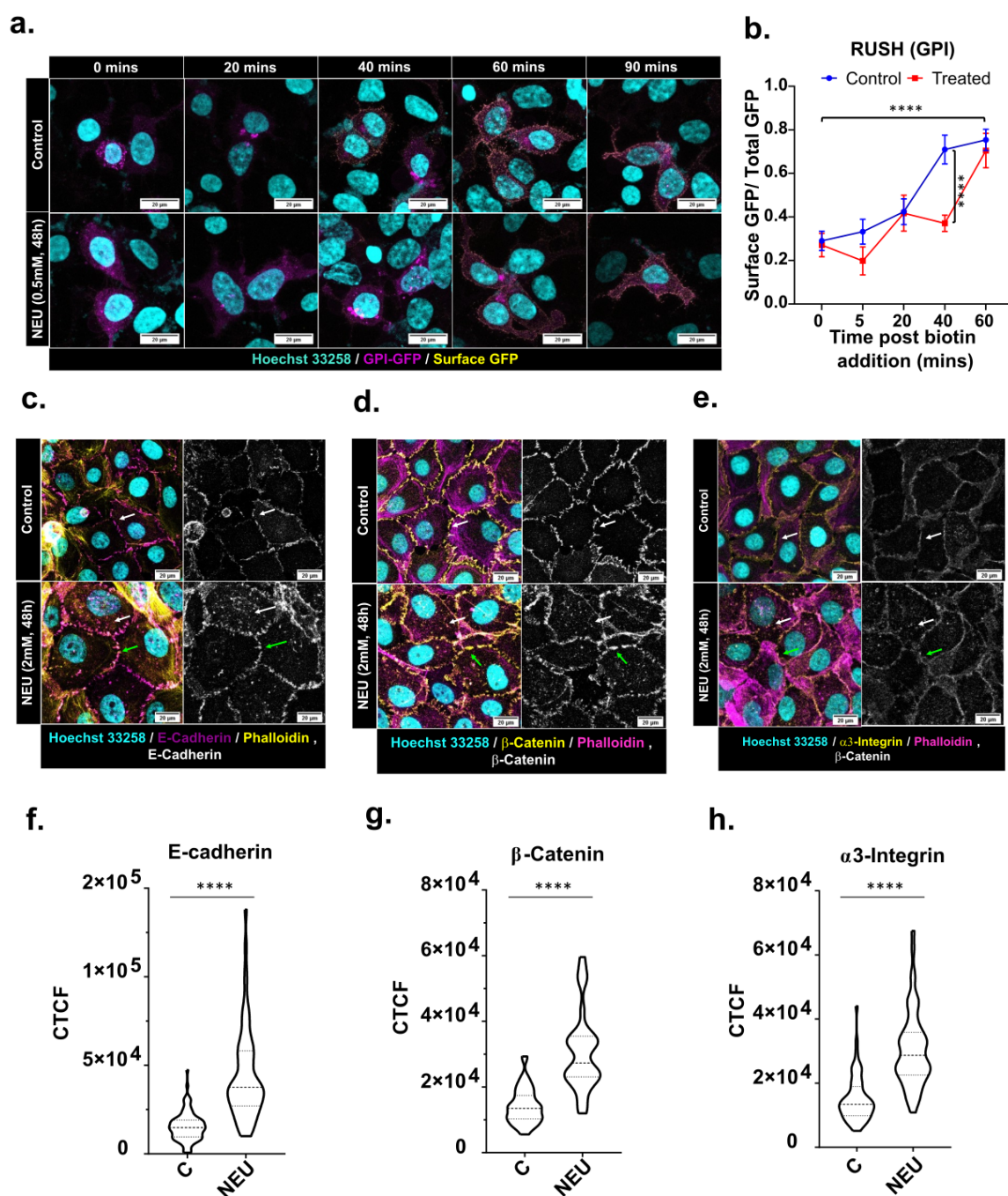


Figure 6: NEU-induced DNA damage led to impaired intracellular trafficking. (a)

Representative images of cells expressing GPI anchored EGFP, fixed at indicated time points post biotin addition. The cells were fixed under non-permeabilising conditions and stained for surface GFP (yellow) with anti-GFP antibody. A delay in the trafficking of GPI-anchored EGFP (magenta) was observed, which was quantified by plotting the ratio of surface GFP to total GFP at different time points (N=3, n=70). Each point in the graph (b) represents mean \pm SEM with the asterisks indicating a two-way ANOVA test significance value of $p < 0.0001$. Immunostaining

NEU-treated cells for (c) E-cadherin (magenta), (d) β -catenin (yellow) and (e) α 3-integrin showed an altered localisation of the cell-cell junction proteins. A pronounced distribution of the proteins in the cytoplasm (white arrow) and a diffused staining (green arrow) at the junctions was observed. The cytoplasmic distribution of the proteins was quantified by measuring the Corrected Total Cell Fluorescence (CTCF) of the cytoplasm. [CTCF = integrated density - (Area of selected cell x Mean fluorescence of background readings)]. The CTCF for (f) E-cadherin (N=3, n=64), (g) β -catenin (N=3, n=40) and (h) α 3-Integrin (N=3, n=56) has been represented as violin plots. Asterisks indicate Mann-Whitney U test significance values; **** p < 0.0001.

Discussion

Previous studies from the lab have highlighted the role of DNA-PK in transforming breast epithelial cells (Anandi et al., 2017). Although these studies were done using 16-day breast acinar cultures, in this study, we observed changes in microtubule dynamics and trafficking as early as 48 hrs.

Changes in microtubule dynamics and dispersal of Golgi have been frequently associated with cancer progression (Bui et al., 2021; Petrosyan, 2015). Despite being thoroughly studied, the exact role of Golgi in cancer progression remains inconclusive. Golgi morphology is often perturbed in cancer cells that have resulted in an altered glycosylation signature and/or accelerated trafficking in cancer cells (Kellokumpu et al., 2002; Schultz et al., 2012; Wang et al., 2001). Cell migration, EMT, cell survival and proliferation, the nodal hallmarks of cancer, have been shown to regulate or be regulated by the Golgi apparatus (Bisel et al., 2008; Bui et al., 2021).

On the other hand, changes in microtubule dynamics have direct implications on cell migration and invasion (Etienne-Manneville, 2013; Lopes and Maiato, 2020; Wattanathamsan and Pongrakhananon, 2021). Microtubules in various cancer cell lines have been shown to have increased acetylation and detyrosination, which mark stable microtubules (Boggs et al., 2015; Mialhe et al., 2001). An increase in microtubule stabilising protein, Tau, has also been observed in metastatic breast cancer cell lines (Lei et al., 2020; Li et al., 2013). These observations have also been seen in breast tumour tissues from patients (Boggs et al., 2015; Whipple et al., 2010).

Invasion and migration require the cell to modulate the microtubule network and its interaction with the Golgi apparatus (Bui et al., 2021; Vinogradova et al., 2012). GDMTs have been linked to polarised trafficking to the cell's leading edge, which is crucial for the initiation of migration and change in direction (Miller et al., 2009; Vinogradova et al., 2009). GDMTs are stable and marked by tubulin acetylation and are essential for maintaining Golgi structure (Vinogradova et al., 2012). Although evident when put together, no study has directly linked GDMTs to cancer progression. Our observations of microtubule stabilisation and GDMTs in MCF10CA1a show that microtubules are more stable and Golgi derived in malignant cell lines when compared to non-tumorigenic cells. Thus, this study is the first to provide an association between GDMTs, genomic instability and cancer progression.

Another aspect of microtubule regulation which is less understood is how the balance of centrosomal and non-centrosomal microtubules is maintained. Maintaining a balance between centrosomal and non-centrosomal microtubules decides the overall arrangement of the microtubule network. Altering this balance has often been seen as a mechanism to reorganise the microtubule network during cellular differentiation (Sanchez and Feldman, 2017). This reorganisation is mainly accomplished by inactivation or loss of centrosomal activity, which tips the balance to a more non-centrosomal array (Muroyama and Lechler, 2017; Nishita et al., 2017). A study by Rosa M Rios's group in 2018 highlighted the plasticity of the interphase microtubule network and showed that centrosome dampens microtubule nucleation at Golgi and cytoplasm. In cells treated with centrinone to inhibit Plk4, the microtubule network was observed to be predominantly Golgi nucleated. It was also reported that cells with multiple centrosomes had little to no MT originating from Golgi (Gavilan et al., 2018). The authors suggest that centrosome-Golgi proximity might regulate the organisation of microtubules from the centrosome and Golgi. Golgi apparatus is associated with the centrosome, and the relevance of this proximity is unknown. A study in 2019 reported that Golgi-centrosome proximity was not essential for its function (Tormanen et al., 2019). Several studies deciphering the functional relevance of GDMTs have reported their importance for maintaining Golgi structure (Kodani and Sutterlin, 2009; Miller et al., 2009; Wu et al., 2016; Zhu and Kaverina, 2013). It is unknown whether the Golgi structure and its proximity to the centrosome regulate non-centrosomal microtubules that arise from Golgi. Our study

provides a clue which hints that Golgi integrity might influence centrosomal control of GDMTs.

Based on findings from this and previous studies, we propose a model reporting a novel response to DNA damage (**Fig.7**). DNA damage leads to the activation of DNA-PK, a DNA damage response protein. As previously reported, activation of DNA-PK leads to Golgi dispersal through the GOLPH3-MYO18A-F-actin axis (Dippold et al., 2009; Farber-Katz et al., 2014). Golgi dispersal leads to an increase in GDMTs through a mechanism yet to be elucidated. The microtubules nucleated at Golgi are stable, marked by enhanced tubulin acetylation, and resistant to nocodazole-induced depolymerisation. Changes in Golgi organisation and microtubule dynamics have been demonstrated to lead to defects in intracellular trafficking that may result in changes in cell polarity.

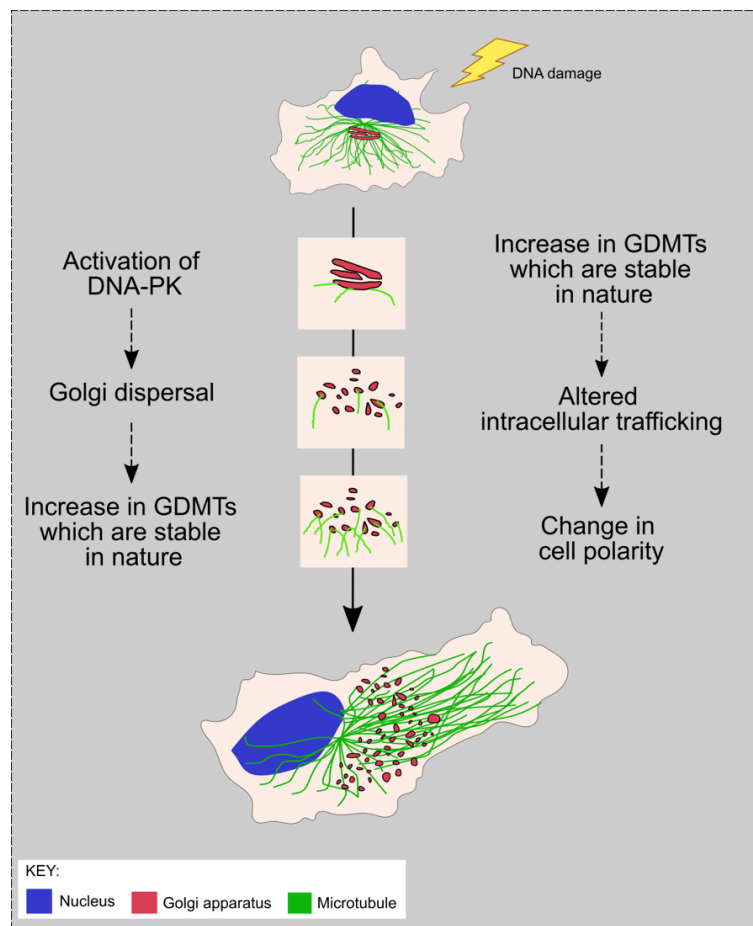


Figure 7: DNA damage leads to Golgi dispersal through the DNA-PK-GOLPH3-MYO18A axis. Golgi dispersal leads to an increase in GDMTs. Due to the difference in dynamics of GDMTs, the trafficking of proteins to the membrane gets altered, leading to mislocalisation of polarity proteins.

Materials and Methods

Cell line and culturing methods

MCF10A cells were a generous gift from Prof. Raymond C. Stevens (The Scripps Research Institute, La Jolla, CA). MCF10A and MCF10CA1a cell lines were cultured in DMEM containing high glucose without sodium pyruvate (Invitrogen) supplemented with 5% horse serum (Invitrogen), 100 units/ml penicillin/streptomycin (Invitrogen) and growth constituents as described in Anandi et al., 2017 (referred to as growth media in later text) (Anandi et al., 2017). HEK293 cells were grown in DMEM containing high glucose and sodium pyruvate (Lonza) supplemented with 10% foetal bovine serum (FBS) (Invitrogen) and 100 units/ml penicillin/streptomycin (Lonza) (referred to as complete DMEM in further text). Cells were cultured in tissue culture-treated 100mm or 60mm dishes (Eppendorf) in a 37°C humidified incubator with 5% CO₂ (Eppendorf).

Immunofluorescence

Cells were seeded at a density of 0.4×10^5 cells onto coverslips (Blue Star) in 24-well petri plates (Eppendorf). After appropriate drug treatment, the cells were fixed with 4% paraformaldehyde. The samples were washed with PBS-T (0.5% Triton-X100) and blocked with 10% FBS. Samples were then incubated in primary antibodies, diluted in 10% FBS, overnight at 4°C. Following incubation in primary antibody, cells were washed with PBS-T (0.5% Triton-X100) and incubated with secondary antibody (1:500) for 1 hour at room temperature. After a few washes with PBS-T (0.5% Triton-X100), the samples were incubated with Hoechst 33258 (Invitrogen) to stain the nucleus. Coverslips were mounted using 90% glycerol mounting media (with 20mM Tris, pH 8.0 and 0.5% propyl gallate). All images were obtained using Leica TCS SP8 X Confocal Microscope (Leica Microsystems). Post imaging, the maximum intensity projection of the stacks was used for analysis and has been represented in the figures.

Microtubule regrowth assay

The cells were grown and treated with 2.5 µg/ml Nocodazole (Sigma) for 3 hrs at 37°C (Zhu and Kaverina, 2011). Following incubation, the cells were washed twice with ice-cold DPBS (Lonza) and supplemented with warm growth media. The microtubules were allowed to repolymerise at 37°C, fixed and stained for microtubule

and Golgi and imaged on the Leica TCS SP8 X Confocal Microscope (Leica Microsystems).

EB3 assay

MCF10A cells were seeded in 8-well chamber cover glass slides (Lab-Tek, Thermo Scientific) at a density of 0.6×10^5 cells and treated with 2 mM NEU (Sigma). After 24 hrs of treatment, the samples were transfected with the EB3-GFP construct. Transfections were performed using Lipofectamine 2000 (Invitrogen) in Opti-MEM (Invitrogen). The cells were then incubated for 4 hrs in the transfected medium, following which the media was changed to MCF10A growth media. The cells were imaged 24hrs after transfection in a live cell imaging chamber on the Leica TCS SP8 X Confocal Microscope (Leica Microsystems). Before imaging, the cells were shifted to L-15 medium (Lonza), and Hoechst 33342 was added to visualise the nucleus. Images were recorded at a frame rate of 1.5s per frame. The EB3 comets were manually tracked using the MTrackJ plugin (developed by E. Meijering, Biomedical Imaging Group, Erasmus Medical Center, Rotterdam) on Fiji/ImageJ (NIH)(Meijering et al., 2012).

RUSH assay

To prepare the coverslips for low-adherent HEK293 cells, Matrigel (Sigma Aldrich) was diluted to 1:50 with DPBS (Lonza) and incubated for 4 hrs at 37°C. Subsequently, the cells were seeded at 0.6×10^5 cells and treated with 2 mM NEU. After 24 hrs of treatment, the cells were transfected with the RUSH constructs using bPEI25 (Sigma) using the protocol described in (Hsu and Uludag, 2012). DMEM (without serum) was used as the transfection medium instead of Opti-MEM to avoid the presence of biotin. The cells were then incubated for 4 hrs in the transfected medium, following which the media was changed to complete DMEM. 16 hrs post-transfection, RUSH assay was performed as described in (Boncompain et al., 2012; Boncompain and Perez, 2014). The cells were stained with Hoechst 33342 (Invitrogen) to mark the nucleus before mounting and visualised on the Leica TCS SP8 X Confocal Microscope (Leica Microsystems).

Statistics

All graphs were plotted and analysed using Graph Pad Prism software (Graph Pad Software, La Jolla, CA, USA). All experimental groups were analysed by non-

parametric methods except quantification of the RUSH assay. The significance of surface GFP/ total GFP in the RUSH assay was tested by two-way ANOVA. The Mann-Whitney test was used to analyse experimental groups with two samples. Groups with more than two samples were analysed using the Kruskal-Wallis test. Asterisks indicate significance values; **** $p < 0.0001$, *** $p < 0.001$, ** $p < 0.01$, * $p < 0.05$ and ns – non-significant. The number of independent experiments performed and the number of cells analysed has been mentioned in the figure legends

Acknowledgements

We would like to thank Dr Aurnab Ghose (IISER Pune, India) for his valuable insights on the project and for also providing us with the EB3 construct and Latrunculin A. We thank Drs. Thomas Pucadyil and Richa Rikhy (IISER Pune, India) for their helpful suggestions. We also thank Dr Franck Perez (Institut Curie, Paris, France) for the RUSH plasmids and Dr Jomon Joseph (NCCS, India) for the K40 acetylated α -tubulin antibody. We thank Dr Libi Anandi and Snehal Bhatia from our laboratory for standardising some experiments. We also would like to acknowledge the IISER Pune Microscopy Facility for access to equipment and infrastructure.

Author contributions

A.V. and M.L. conceived and conceptualised the project. A.V. designed, performed and analysed the experiments. A.V. and M.L. wrote the paper.

Competing Interests

The authors declare no competing or financial interests.

Funding

This study is supported by a grant from the Science and Engineering Research Board (SERB), Government of India (EMR/2016/001974) and partly by the Indian Institute of Science Education and Research Pune Core funding. A.V. was funded through the Council of Scientific and Industrial Research (CSIR)-JRF fellowship.

References

Anandi, L., Chakravarty, V., Ashiq, K.A., Bodakuntla, S., and Lahiri, M. (2017). DNA-dependent protein kinase plays a central role in transformation of breast epithelial cells following alkylation damage. *J Cell Sci* 130, 3749-3763.

- Bershadsky, A.D., and Gelfand, V.I. (1981). ATP-dependent regulation of cytoplasmic microtubule disassembly. *Proceedings of the National Academy of Sciences of the United States of America* 78, 3610-3613.
- Bisel, B., Wang, Y., Wei, J.H., Xiang, Y., Tang, D., Miron-Mendoza, M., Yoshimura, S., Nakamura, N., and Seemann, J. (2008). ERK regulates Golgi and centrosome orientation towards the leading edge through GRASP65. *The Journal of cell biology* 182, 837-843.
- Bodakuntla, S., Libi, A.V., Sural, S., Trivedi, P., and Lahiri, M. (2014). N-nitroso-N-ethylurea activates DNA damage surveillance pathways and induces transformation in mammalian cells. *BMC cancer* 14, 287.
- Boggs, A.E., Vitolo, M.I., Whipple, R.A., Charpentier, M.S., Goloubeva, O.G., Ioffe, O.B., Tuttle, K.C., Slovic, J., Lu, Y., Mills, G.B., *et al.* (2015). alpha-Tubulin acetylation elevated in metastatic and basal-like breast cancer cells promotes microtentacle formation, adhesion, and invasive migration. *Cancer Res* 75, 203-215.
- Boncompain, G., Divoux, S., Gareil, N., de Forges, H., Lescure, A., Latreche, L., Mercanti, V., Jollivet, F., Raposo, G., and Perez, F. (2012). Synchronization of secretory protein traffic in populations of cells. *Nat Methods* 9, 493-498.
- Boncompain, G., and Perez, F. (2014). Synchronization of secretory cargos trafficking in populations of cells. *Methods in molecular biology* 1174, 211-223.
- Bui, S., Mejia, I., Diaz, B., and Wang, Y. (2021). Adaptation of the Golgi Apparatus in Cancer Cell Invasion and Metastasis. *Frontiers in cell and developmental biology* 9, 806482.
- Buschman, M.D., Rahajeng, J., and Field, S.J. (2015). GOLPH3 links the Golgi, DNA damage, and cancer. *Cancer Res* 75, 624-627.
- Chabin-Brion, K., Marceiller, J., Perez, F., Settegrana, C., Drechou, A., Durand, G., and Pous, C. (2001). The Golgi complex is a microtubule-organizing organelle. *Mol Biol Cell* 12, 2047-2060.
- Dippold, H.C., Ng, M.M., Farber-Katz, S.E., Lee, S.K., Kerr, M.L., Peterman, M.C., Sim, R., Wiharto, P.A., Galbraith, K.A., Madhavarapu, S., *et al.* (2009). GOLPH3 bridges phosphatidylinositol-4-phosphate and actomyosin to stretch and shape the Golgi to promote budding. *Cell* 139, 337-351.

Durant, S., and Karran, P. (2003). Vanillins--a novel family of DNA-PK inhibitors. *Nucleic acids research* 31, 5501-5512.

Etienne-Manneville, S. (2013). Microtubules in cell migration. *Annu Rev Cell Dev Biol* 29, 471-499.

Fang, Y.D., Xu, X., Dang, Y.M., Zhang, Y.M., Zhang, J.P., Hu, J.Y., Zhang, Q., Dai, X., Teng, M., Zhang, D.X., *et al.* (2011). MAP4 mechanism that stabilizes mitochondrial permeability transition in hypoxia: microtubule enhancement and DYNLT1 interaction with VDAC1. *PLoS one* 6, e28052.

Farber-Katz, S.E., Dippold, H.C., Buschman, M.D., Peterman, M.C., Xing, M., Noakes, C.J., Tat, J., Ng, M.M., Rahajeng, J., Cowan, D.M., *et al.* (2014). DNA damage triggers Golgi dispersal via DNA-PK and GOLPH3. *Cell* 156, 413-427.

Fong, S., King, F., and Shtivelman, E. (2010). CC3/TIP30 affects DNA damage repair. *BMC cell biology* 11, 23.

Gavilan, M.P., Gandolfo, P., Balestra, F.R., Arias, F., Bornens, M., and Rios, R.M. (2018). The dual role of the centrosome in organizing the microtubule network in interphase. *EMBO reports* 19.

Geeraert, C., Ratier, A., Pfisterer, S.G., Perdiz, D., Cantaloube, I., Rouault, A., Pattingre, S., Proikas-Cezanne, T., Codogno, P., and Pous, C. (2010). Starvation-induced hyperacetylation of tubulin is required for the stimulation of autophagy by nutrient deprivation. *The Journal of biological chemistry* 285, 24184-24194.

Giannakakou, P., Sackett, D.L., Ward, Y., Webster, K.R., Blagosklonny, M.V., and Fojo, T. (2000). p53 is associated with cellular microtubules and is transported to the nucleus by dynein. *Nat Cell Biol* 2, 709-717.

Hsu, C.Y., and Uludag, H. (2012). A simple and rapid nonviral approach to efficiently transfect primary tissue-derived cells using polyethylenimine. *Nature protocols* 7, 935-945.

Hu, J.Y., Chu, Z.G., Han, J., Dang, Y.M., Yan, H., Zhang, Q., Liang, G.P., and Huang, Y.S. (2010). The p38/MAPK pathway regulates microtubule polymerization through phosphorylation of MAP4 and Op18 in hypoxic cells. *Cellular and molecular life sciences : CMLS* 67, 321-333.

Jackson, S.P., and Bartek, J. (2009). The DNA-damage response in human biology and disease. *Nature* 461, 1071-1078.

Kellokumpu, S., Sormunen, R., and Kellokumpu, I. (2002). Abnormal glycosylation and altered Golgi structure in colorectal cancer: dependence on intra-Golgi pH. *FEBS letters* 516, 217-224.

Kodani, A., and Sutterlin, C. (2009). A new function for an old organelle: microtubule nucleation at the Golgi apparatus. *EMBO J* 28, 995-996.

Lei, C., Yang, C., Xia, B., Ji, F., Zhang, Y., Gao, H., Xiong, Q., Lin, Y., Zhuang, X., Zhang, L., *et al.* (2020). Analysis of Tau Protein Expression in Predicting Pathological Complete Response to Neoadjuvant Chemotherapy in Different Molecular Subtypes of Breast Cancer. *Journal of breast cancer* 23, 47-58.

Li, Z.H., Xiong, Q.Y., Tu, J.H., Gong, Y., Qiu, W., Zhang, H.Q., Wei, W.S., Hou, Y.F., and Cui, W.Q. (2013). Tau proteins expressions in advanced breast cancer and its significance in taxane-containing neoadjuvant chemotherapy. *Medical oncology* 30, 591.

Lopes, D., and Maiato, H. (2020). The Tubulin Code in Mitosis and Cancer. *Cells* 9.

Ma, S., Rong, Z., Liu, C., Qin, X., Zhang, X., and Chen, Q. (2021). DNA damage promotes microtubule dynamics through a DNA-PK-AKT axis for enhanced repair. *The Journal of cell biology* 220.

Meijering, E., Dzyubachyk, O., and Smal, I. (2012). Methods for cell and particle tracking. *Methods in enzymology* 504, 183-200.

Mialhe, A., Lafanechere, L., Treilleux, I., Peloux, N., Dumontet, C., Bremond, A., Panh, M.H., Payan, R., Wehland, J., Margolis, R.L., *et al.* (2001). Tubulin detyrosination is a frequent occurrence in breast cancers of poor prognosis. *Cancer Res* 61, 5024-5027.

Miller, P.M., Folkmann, A.W., Maia, A.R., Efimova, N., Efimov, A., and Kaverina, I. (2009). Golgi-derived CLASP-dependent microtubules control Golgi organization and polarized trafficking in motile cells. *Nat Cell Biol* 11, 1069-1080.

Muroyama, A., and Lechler, T. (2017). Microtubule organization, dynamics and functions in differentiated cells. *Development* 144, 3012-3021.

Nakano, A., Kato, H., Watanabe, T., Min, K.D., Yamazaki, S., Asano, Y., Seguchi, O., Higo, S., Shintani, Y., Asanuma, H., *et al.* (2010). AMPK controls the speed of microtubule polymerization and directional cell migration through CLIP-170 phosphorylation. *Nat Cell Biol* 12, 583-590.

Nishita, M., Satake, T., Minami, Y., and Suzuki, A. (2017). Regulatory mechanisms and cellular functions of non-centrosomal microtubules. *Journal of biochemistry* *162*, 1-10.

Parker, A.L., Kavallaris, M., and McCarroll, J.A. (2014). Microtubules and their role in cellular stress in cancer. *Frontiers in oncology* *4*, 153.

Petrosyan, A. (2015). Onco-Golgi: Is Fragmentation a Gate to Cancer Progression? *Biochemistry & molecular biology journal* *1*.

Poruchynsky, M.S., Komlodi-Pasztor, E., Trostel, S., Wilkerson, J., Regairaz, M., Pommier, Y., Zhang, X., Kumar Maity, T., Robey, R., Burotto, M., *et al.* (2015). Microtubule-targeting agents augment the toxicity of DNA-damaging agents by disrupting intracellular trafficking of DNA repair proteins. *Proc Natl Acad Sci U S A* *112*, 1571-1576.

Ryu, N.M., and Kim, J.M. (2020). The role of the alpha-tubulin acetyltransferase alphaTAT1 in the DNA damage response. *J Cell Sci* *133*.

Sanchez, A.D., and Feldman, J.L. (2017). Microtubule-organizing centers: from the centrosome to non-centrosomal sites. *Curr Opin Cell Biol* *44*, 93-101.

Schultz, M.J., Swindall, A.F., and Bellis, S.L. (2012). Regulation of the metastatic cell phenotype by sialylated glycans. *Cancer metastasis reviews* *31*, 501-518.

Skoufias, D.A., Burgess, T.L., and Wilson, L. (1990). Spatial and temporal colocalization of the Golgi apparatus and microtubules rich in deetyrosinated tubulin. *J Cell Biol* *111*, 1929-1937.

Thyberg, J., and Moskalewski, S. (1993). Relationship between the Golgi complex and microtubules enriched in deetyrosinated or acetylated alpha-tubulin: studies on cells recovering from nocodazole and cells in the terminal phase of cytokinesis. *Cell and tissue research* *273*, 457-466.

Tormanen, K., Ton, C., Waring, B.M., Wang, K., and Sutterlin, C. (2019). Function of Golgi-centrosome proximity in RPE-1 cells. *PLoS one* *14*, e0215215.

Vinogradova, T., Miller, P.M., and Kaverina, I. (2009). Microtubule network asymmetry in motile cells: role of Golgi-derived array. *Cell Cycle* *8*, 2168-2174.

Vinogradova, T., Paul, R., Grimaldi, A.D., Loncarek, J., Miller, P.M., Yampolsky, D., Magidson, V., Khodjakov, A., Mogilner, A., and Kaverina, I. (2012). Concerted effort

of centrosomal and Golgi-derived microtubules is required for proper Golgi complex assembly but not for maintenance. *Molecular biology of the cell* 23, 820-833.

Wang, F., Goto, M., Kim, Y.S., Higashi, M., Imai, K., Sato, E., and Yonezawa, S. (2001). Altered GalNAc-alpha-2,6-sialylation compartments for mucin-associated sialyl-Tn antigen in colorectal adenoma and adenocarcinoma. *The journal of histochemistry and cytochemistry : official journal of the Histochemistry Society* 49, 1581-1592.

Wattanathamsan, O., and Pongrakhananon, V. (2021). Post-translational modifications of tubulin: their role in cancers and the regulation of signaling molecules. *Cancer gene therapy*.

Wehland, J., Henkart, M., Klausner, R., and Sandoval, I.V. (1983). Role of microtubules in the distribution of the Golgi apparatus: effect of taxol and microinjected anti-alpha-tubulin antibodies. *Proc Natl Acad Sci U S A* 80, 4286-4290.

Whipple, R.A., Matrone, M.A., Cho, E.H., Balzer, E.M., Vitolo, M.I., Yoon, J.R., Ioffe, O.B., Tuttle, K.C., Yang, J., and Martin, S.S. (2010). Epithelial-to-mesenchymal transition promotes tubulin detyrosination and microtentacles that enhance endothelial engagement. *Cancer research* 70, 8127-8137.

Williams, T., Courchet, J., Viollet, B., Brenman, J.E., and Polleux, F. (2011). AMP-activated protein kinase (AMPK) activity is not required for neuronal development but regulates axogenesis during metabolic stress. *Proceedings of the National Academy of Sciences of the United States of America* 108, 5849-5854.

Wu, J., de Heus, C., Liu, Q., Bouchet, B.P., Noordstra, I., Jiang, K., Hua, S., Martin, M., Yang, C., Grigoriev, I., *et al.* (2016). Molecular Pathway of Microtubule Organization at the Golgi Apparatus. *Dev Cell* 39, 44-60.

Xu, Z., Schaedel, L., Portran, D., Aguilar, A., Gaillard, J., Marinkovich, M.P., They, M., and Nachury, M.V. (2017). Microtubules acquire resistance from mechanical breakage through intraluminal acetylation. *Science* 356, 328-332.

Yoon, S.O., Shin, S., and Mercurio, A.M. (2005). Hypoxia stimulates carcinoma invasion by stabilizing microtubules and promoting the Rab11 trafficking of the alpha6beta4 integrin. *Cancer research* 65, 2761-2769.

Zhu, X., and Kaverina, I. (2011). Quantification of asymmetric microtubule nucleation at subcellular structures. *Methods in molecular biology* 777, 235-244.

Zhu, X., and Kaverina, I. (2013). Golgi as an MTOC: making microtubules for its own good. *Histochemistry and cell biology* 140, 361-367.